A Comparison Study between Coupled and Non-coupled Systems of Poly(3-hexylthiophene) and Fullerene-C_{60} for the Application of Organic Solar Cells

by

Benjamin L. King

A Thesis Presented to the Graduate
Faculty at Middle Tennessee State University
For the Partial Fulfillment of the Requirements
For the Degree of Master of Science in Chemistry

Middle Tennessee State University
May 2014

Thesis Committee:

Dr. Dwight Patterson, Major Professor

Dr. William Ilsley

Dr. Andrienne Friedli

ACKNOWLEDGEMENTS

I would first and foremost like to thank Jesus Christ for the strength and patience he has given me to see the thesis through to the end. Secondly I would like to thank Dr. Dwight Patterson for his patience, guidance, and willingness to take me on as student. I feel confident in my ability as a chemist due to his instruction. Next I would like to thank Dr. Earl Pearson, Dr. Greg Van Patten, and the Department of Chemistry at MTSU for their financial support and understanding while I finished my graduate degree and worked as Laboratory/Safety Manager for the department. I would like to thank my readers, Dr. William Ilsley and Dr. Andrienne Friedli, for their time and expertise. I would also like to thank Jessie Weatherly, Dr. Nathanael Smith, Joyce Miller, and the faculty and staff of the Department of Chemistry for their knowledge, guidance, time, and encouragement for the duration of my degree.

I would also like to thank all my friends and family for their support and encouragement. Last but definitely not least, I would like to thank my wife, Victoria King, for her support, understanding, and encouragement for the duration of my time in graduate school. Without her I would have gone crazy trying to finish this thesis.

ABSTRACT

Organic solar cell technology has become one of the fastest growing areas of polymer science due to the world's need for clean, renewable energy. Some of the highest power efficiencies for organic solar cells have been observed in solar cells where a heterogeneous mixture of poly(3-hexylthiophene) (P3HT) and phenyl-C61-butyric acid methyl ester (PCBM) have been used as the active layer. A process called thermal annealing has been used to give high crystallinity for P3HT, improving light absorption and charge transport, but increasing segregation with the electron acceptor PCBM. In the study, the electron donor P3HT was coupled to fullerene-C_{60}. A blend of P3HT and coupled product was compared to a completely non-coupled system to see if there was improvement in the overall efficiency of the organic solar cells. P3HT was synthesized and successfully coupled to fullerene-C_{60} based on analysis with GC/MS, HPLC, FTIR, and NMR spectroscopy. Synthesized P3HT was found to have only 79% regioregularity and average molecular weights under 3300 Da. The coupled materials were found to have a lower conjugation than the pure P3HT due to disruption to coplanarity by steric hindrance. Through analysis with DSC and TEM, it was discovered that the synthesized coupled material had a negative effect on the P3HT's ability to crystallize in comparison to pure P3HT and the P3HT/C_{60} blend. Based on power efficiency tests, fabricated solar cells containing the P3HT/coupled material blend were exponentially less efficient than the non-coupled blend of P3HT/C_{60}.

TABLE OF CONTENTS

PAGE

SECTION **PAGE**

SECTION **PAGE**

SECTION **PAGE**

LIST OF TABLES

TABLE **PAGE**

LIST OF FIGURES

FIGURE **PAGE**

FIGURE **PAGE**

FIGURE **PAGE**

FIGURE **PAGE**

1 Introduction

1.1 Polymer Chemistry and Its Impact

Polymer Chemistry can be found in almost every facet of our lives, from the plastic bags at the food market, to the tires on our cars, to even the DNA that makes up our genetic coding. Polymers (macromolecules), made up of covalently bonded repeating units, can be found in nature as well as synthetically made materials in devices we use every day. As early as the beginning of the twentieth century, synthetic polymers were being mass-produced and are now one of the biggest areas of industry.[1] Some of the first industrially produced polymers were Bakelite, neoprene, nylon, poly(vinyl chloride), and polystyrene. Applications for the first synthetically made polymers ranged from materials for bowling balls to textiles. Polymers have become some of the most important and practical materials in production today. Polymers are now being used to make rigid plastics, rubbers, fibers, coatings, and adhesives.[2] All the materials mentioned can be made by using different monomer units (the molecule that is repeated in the polymer), by adding side chains to polymers, and using combinations of oligomers (small chains of monomer units) to make copolymers. By changing these components, materials can be made crystalline, glassy, or rubbery as well as having different densities. They can also be coated onto other materials to protect or to provide decoration, such as with polymer-based paints. Polymers can even be made into pressure-sensitive adhesives such as the sticky material on the back of post-it notes. Not only are polymers used in many of today's products, they continue to be researched for

newly created polymers and applications. An area of research that is growing is the application of conductive polymers in optical and electronic devices.

1.2 Organic Conductive Polymers

Conductive polymers have become one of the most exciting and researched areas in polymer chemistry due to the potential impact their applications will have on the world's energy and technology. Unlike other polymers, which are insulators, conductive polymers can transport electrons across their backbone, or main chain. Conductance in a polymer allows for nearly all the components in an electronic device to be fabricated from organic polymer material.[3] Conductive polymers have a wide range of properties that can revolutionize many industries from field-effect transistors to biosensors.[1,3,4] Although organic semiconductors and conductors have made a lot of progress and advancements, they are still not practical replacements for their inorganic counterparts. The history of organic conductive polymers is short in comparison to other polymer materials, but studies in this area are progressing rapidly. As the years progress, more and more publications are being written in the area of organic conductive polymers. With each new article, organic conductive polymers are getting closer and closer to being practical materials in optical and electronic devices.

1.2.1 History of Conductive Polymers

Since the 1950's, certain polymers have been observed to have conductive and semi-conductive properties. Nonmetal polymers, such as poly(sulfur nitride), were the first to be observed with conductivities as high as metals.[1] The most interesting group of

conductive polymers, though, are the synthetic organic conductive polymers. The first organic polymer studied for its electrical properties was polyacetylene. In 1958, G. Natta and coworkers synthesized polyacetylene and found that it had a range of semi-conductivity, "depending upon how the polymer was processed and manipulated".[1] In 1977, Shirakawa, MacDiarmid, and Heeger created a crystalline polyacetylene film with metallic conductivity by a process of p-doping.[1] The same result was found for crystalline polyacetylene film through another process called n-doping.[1] After the initial work on polyacetylene, an explosion of interest and research has been made in organic conductive polymers with some of the most researched being derivatives of polyphenylene, poly(p-phenylene vinylene), polypyrroles, polyanilines, and polythiophenes. Organic conductive polymers however include a variety of different types and systems, which will be discussed in upcoming sections.

1.2.2 Types of Conductive Polymers

As mentioned before, conductive polymer is a term that can be used to describe more than just the homopolymers (polymers of one type of monomer) given in the last section, but can be used to describe any system involving polymer material that shows conductivity. Usually conductive polymers fall into either one of the four categories: conducting polymer composites, redox polymers, ionically conducting polymers, or intrinsically conducting polymers (ICPs).[1] The first category, conducting polymer composites, can only be loosely referred to as a conductive polymer. The polymer used in the composite systems is actually nonconductive, but is blended with a metal or

carbon powder which actually conducts the electricity. The transport of electrons through the composite material, however, is not a continuous path and thus results in a drop of conductivity. A composite material's conductivity can therefore only be as high as the processing conditions allow.

The second type is redox polymers, which contains localized redox sites along the polymer. The main mechanism of electron transport is by "self-exchange between donor and acceptor site".[1] Redox polymers usually fall into four categories of its own: "Saturated organic polymers with pendent transition metal complexes (Figure 1a), electrochemically polymerized transition metal complexes with multiple polymerizable ligands (Figure 1b), saturated organic polymers with pendent electroactive organic moieties (Figure 1c), and ion exchange polymers containing electrostatically bound electroactive ions (Figure 1d)".[1]

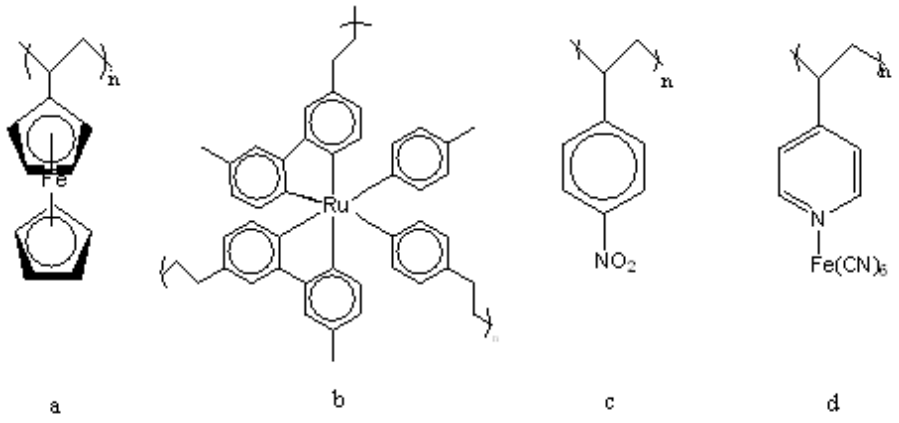

Figure 1. Examples from the four categories of redox polymers.

Each category is an attempt to make a much more efficient path for electron transport. Redox polymers, however, still contain lower conductivities than ICPs due to slow transport along the redox centre.[1]

The third category is different than the other three due to how it transports charge. Ionically conducting polymers conduct ions instead of electrons. The conductivity of ions is much like conductivity of electrons, because either way charge is being transported. Ionically conducting polymers have mainly entered the market in lithium battery applications.[1] Though they have poor conductivities, ionically conducting polymers have built interest in many areas due to their properties and method of charge transport.[1]

The fourth category, however, is the most exciting and promising form of conductive polymers. ICPs (examples shown in Figure 2) contain a variety of properties that are of interest in the field of electrical and optical devices. ICP's can also be controlled by manipulation of many variables to give a variety of products. ICP's show promise in many applications, which will be mentioned in forthcoming sections, and can reach conductivities as high as metals by a process called doping.

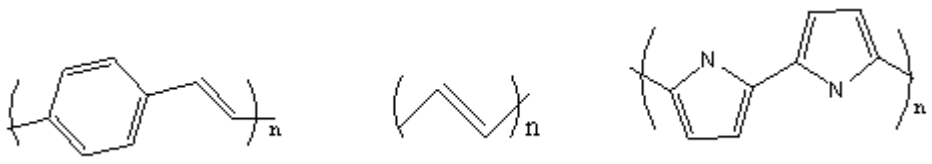

Figure 2. Examples of ICPs: poly(vinyl phenylene), polyacetylene, and polypyrrole.

1.2.3 Doping of Intrinsically Conducting Polymers

Conductive polymers are actually semi-conductive until they are either p-doped (oxidized) or n-doped (reduced). An ICP becomes conductive by a doping process arising from either oxidization of the highest occupied molecular orbital (HOMO) or reduction of the lowest unoccupied molecular orbital (LUMO).[1] The process of doping can be done by three different ways: by adding an oxidizing agent, a reducing agent, or a protonic acid.[1] The result in each case is either a polycation or polyanion, which can carry that charge along its backbone. Doping of ICPs usually requires large amounts of the donor or acceptor material, which will significantly change the structure of the material.[1] Examples of common dopants are iodine (oxidizing agent), sodium amalgam (reducing agent), or sodium naphthalide (reducing agent). In all cases, a material has the potential to move from a semi-conductor to a conductor. Conduction, semi-conduction, and insulation can all be explained by band theory. In band theory, energy levels of atoms form bands when they are closely spaced as in crystal materials.[1,4] The bands are referred as the conduction band (LUMO) and the valence band (HOMO).[1,4,5] The energy difference between the two bands, called the band gap as shown in Figure 3, is what determines whether a material is conductive, semi-conductive, or insulating. At room temperature, if there is no band gap but an overlap of the bands, the material is conductive. If at room temperature the band gap is so small that electrons can be thermally or photonically excited from the valence to the conduction band, the material is semi-conductive.[1]

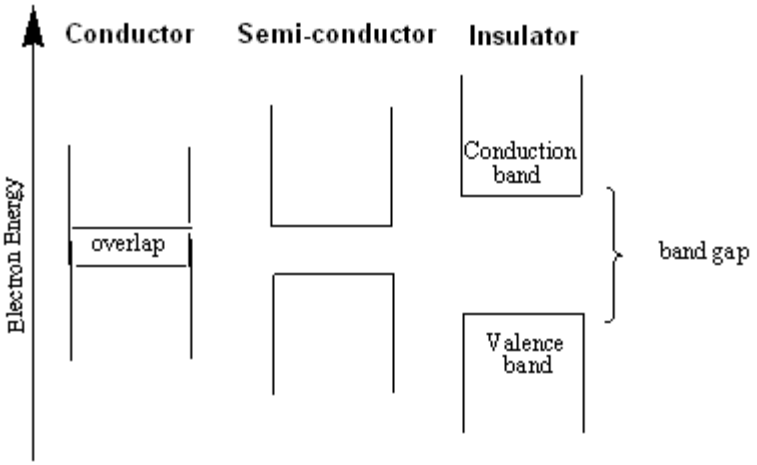

Figure 3. The band gap theory comparing the difference in energy between the valence band and conduction band for conductors (left), semi-conductors (middle), and insulators (right).

But if the band gap is too wide for thermal or photonic excitation of electrons from the valence to the conduction band, the material is an insulator.[1] ICP's are much more complicated than can completely be explained by band theory especially when doped.

1.2.4 Electron Transport in Intrinsically Conducting Polymers

In both p-type and n-type doping, a charge carrier is formed that carries positive or negative charge along the conjugated backbone, while being stabilized by ions of opposite charge between the polymer chain.[1] Charge carriers have different names depending on the degeneracy of the polymer. Polyacetylene is a polymer that has degeneracy in the ground state.[1,6] The charge carrier in this case is referred to as a soliton. In both p and n-doping a soliton is formed, which serves as a boundary (or domain wall) separating "two phases of opposite orientation and identical energy".[1] The

soliton, or domain walls, act like a solitary wave that moves along the backbone. Figure 4 is an example of a positive soliton which has been neutralized by a dopant ion of opposite charge.

Figure 4. A positive soliton with anions countering the positive charge with a change in structure at each domain wall.

A special case soliton is a neutral soliton in which there are an odd number of conjugated carbons and thus an unpaired electron (or radical) along the backbone.[1,3,5] A neutral soliton is spread over several carbons and has an alternation of bond length for double and single bonds along the whole soliton resulting in an equal bond length for double and single bonds at the middle of the soliton. [1,3,5] Neutral charge carriers, such as neutral solitons, will become of more interest later on when discussing optical properties of conductive polymers. In aromatic rings, there is non-degeneracy at the ground states and two charge carriers called polarons (Figure 5a) and bipolarons (Figure 5b).[1] The polaron, unlike the spinless soliton, has a half spin due to its radical cation nature.[1,3,5,6] The radical and cation are coupled together and cause a distortion along several rings resulting in a quinone-type bond sequence.[1,3,5,6] The bipolaron is produced through further doping of the material and is resembles a soliton but for aromatic

systems.[6] Electron transport through ICPs gives researchers insight into the mechanisms that give ICPs their unique optical and electrical properties.

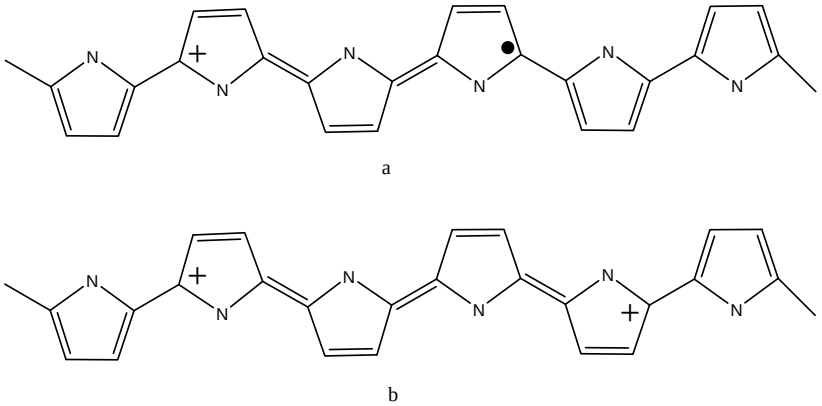

Figure 5. a) A polaron with a cation and a radical. b) A bipolaron with two cations produced after further oxidation.

1.2.5 Properties and Applications of Conductive Polymers

Conductive polymers have a variety of properties that are exciting to researchers and industry for their potential application in optical and electrical devices. The physical properties of organic polymers give them an edge over inorganic polymers and other materials when it comes to mass production and incorporation into devices. Some of the many attractive properties are their solubility in many solvents (including water) depending on their rigidity and substituent groups, their flexibility, their ability to be made into thin films, their thermal stability, their lightweight, and their ability to be easily processed.[1,4] All properties mentioned are important for industrial use in any device but especially in electronic devices. Along with their physical properties,

conductive polymers have a variety of optical and electrical properties that can be applied to electronic devices, such as conductance, fluorescence, electroluminescence, and photovoltaic properties.[3,4] Photovoltaics, the ability for a material to harvest solar energy and convert it into electricity, has become very important recently due to the world's demand for energy.[3] Photovoltaic properties are useful for the development of solar cell materials which provide a renewable source of energy. With the world primary energy demand increasing 1.5% a year, the need for renewable energy technology, like solar cells, has become very prevalent in research.[7]

1.3 Organic Solar Cells

Organic solar cells are the future of energy production and one of the most-exciting areas of research in organic polymers. The possibilities of organic solar cells are endless, from super thin light-harvesting films for small electronic devices, to clean, efficient, large productions of power. Organic solar cells, as seen in Figure 6, show promise that continues to excite scientists and the public due to their possible high efficiency and low cost in comparison to inorganic-based solar cells.[4,8] Organic solar cell actually refers to the light-harvesting material being made of organic material. The material, after harvesting the solar energy, will transport the charge to electron acceptor material and then to storage. Solar cells are measured on their ability to convert light into electricity, which is referred to as energy conversion efficiency or power conversion efficiency. To understand how to make organic solar cells efficient we must understand the mechanism of their photovoltaic property.

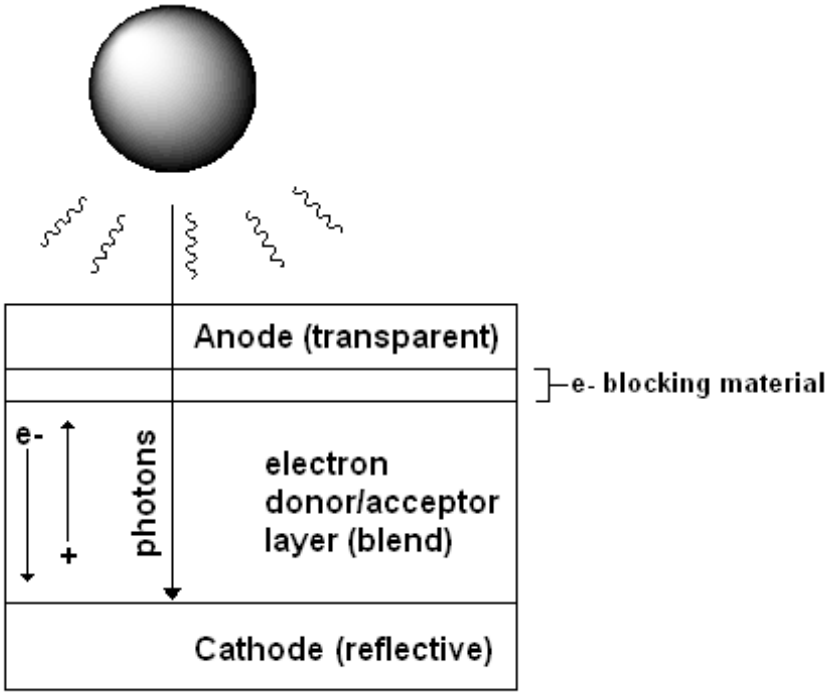

Figure 6. A diagram of the absorption of photons and transportation of electrons in a solar cell device.

1.3.1 Mechanism of Photovoltaics

The mechanism in simple terms is absorption of photons to excite electrons creating charge carriers along the material, which move along in one direction to a node. The process can be broken down into two parts: the photo-generation of charge carriers and the separation of the charge carriers.[4,9] The generation of charge carriers relies on the absorption of a photon that has more energy than the value of the band gap in the semi-conductor. An electron is then excited to the conduction band due to the absorption of energy creating an electron-hole pair or charge carrier. The separation of

the charge carriers can be done in two ways, either by drift of carriers or diffusion of carriers.[9] The first mode, drifting of the carriers, is induced by an electrostatic field. The other mentioned mode, diffusion of the carriers, is induced by zones of high and low concentrations of charge carriers. The following mechanism of transport along the chain follows the description mentioned in Section 1.2.4. Understanding the mechanism is the first step to success, but building organic material that can follow the mechanism perfectly and efficiently while also absorbing a broad spectrum of light is what continues to perplex researchers. Although organic solar cells are in no way ready to replace inorganic-based solar cells they still have shown promise over the history of development of these exciting new materials.

1.3.2 Development of Solar Cells

Organic solar cells have not been the most studied application for conductive polymers due to inefficiencies in power conversion and to widespread use of silicon-based photovoltaic cells. In recent years, however, an organic solar cell of high efficiency has become of great interest to researchers due to two recent developments. The first inspiring development was the success made in the development of organic light-emitting diodes or OLEDs as a viable electronic component. The second inspiration came with the incorporation of electron-accepting fullerene. Development of organic solar cells therefore usually includes an electron-accepting layer of fullerene (C_{60}) with a donating layer of a conjugated polymer or consists of a blend of two organic materials.[8,9] The efficiency of the donor/acceptor systems for the bi-layer and blended

set-ups has increased over the years from 1% or below to energy conversion efficiencies up to 5% or more.[4,9,10,11] This progress can be attributed to the donor/acceptor systems exhibiting narrow band gaps and absorbing a larger range of wavelengths. Fullerene derivatives have been the main acceptor group used due to their exponential increases of the photocurrent, but other acceptor groups have been studied, such as perylene derivatives.[9] The donor layer or components of a solar cell is usually a derivative of one of three polymers: poly(phenyl vinylene), polythiophene, or polyfluorene. Some of the most efficient organic solar cells used polythiophene or polythiophene copolymers as the donor component with efficiencies up to 5% or more.[9,10,11]

1.4 Polythiophene

Polythiophene (PT), a polymer of aromatic thiophene, has been shown to be useful in many areas of polymer technology due to the variety of properties that its derivatives possess. Polythiophene (see Figure 7) has become particularly attractive as a conductive polymer in applications such as transistors, biosensors, LEDs and organic solar cells.[1,4] PT has been shown to be a great donor unit in electronic devices due to the free electrons from the lone pair electrons on the sulfur and the electrons from the pi bonds on its ring. A lot of research in organic conductive polymers for electronic devices has been geared to this multi-functional material. The attraction of polythiophene lies in its semi-conductive properties.

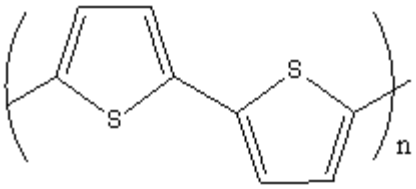

Figure 7. Structure of polythiophene.

1.4.1 Properties of Polythiophene

Polythiophene has many appealing properties to researchers from physical properties to electrochemical properties. Physical properties, such as environmental stability, high solubility of its derivatives in many organic solvents, its possibility of forming highly crystalline compounds, and processability are a few properties that are particularly appealing to industry, but polythiophene's electrochemical and optical properties are some of the most exciting features of polythiophene for research.[1,5] Like other conjugated polymers with aromatic monomer units, a charge carrier, in this case a bipolaron, is the basis for polythiophene's electrochemical properties.[12] When a charge carrier is formed, a domain of eight quinoid isomers long is created, diminishing the band gap.[13] This event takes place when photo-induced, such as when absorbing photons from the sun. Polythiophene derivatives can be made to absorb wide ranges of light from UV to low infrared allowing for a high efficiency of light absorption. PTs high conductivity and ability to create charge carriers through photo-induction make it a very viable active material in organic solar cells.

1.4.2 Polythiophene-Based Polymers for Application to Solar Cells

Polythiophenes have been studied for their application in solar cells since the 1974 when U. Schoeler and others studied thiophene oligomers as a possible active material.[14] Most research with polythiophene derivatives in solar cell applications, however, has been done in the past few years. A study done in 2005, by Jianhai Hou, Chunhe Yang, and Yongfang Li, tested the absorption of solar energy by poly(2,5-dibromo-3-{2-[4-(2-ethylhexyoxy)-phenyl]-vinyl}-thiophene) and found energy conversion efficiency of 0.54% for the polymer.[15] Other studies were done involving derivatives of polythiophene to increase the efficiency of polythiophene based solar cells. Christos L. Chochos and coworkers, synthesized a cyano-substituted polythiophene to be potentially used as the electron acceptor in solar cells. Poly(3-cyano-4-hexylthiophene) was blended with three electron donor derivatives of polythiophene: poly(2-methoxy-5-[3',7'-dimethyloctyloxy]-p-phenylene vinylene), regio-regular poly(3-octylthiophene), and poly(4,4'-dihexylcyclopentadithiophene). Results were low for thiophene electron accepting films, producing maximum power conversion efficiencies of 0.014%.[16] To get better efficiencies an organic polymer/C_{60} or organic polymer/inorganic polymer blend must be made. Yu Huang and coworkers built a photovoltaic device of PEDOT:PSS and poly(3-hexyl-1-enylthiophene) and an electron accepting group of [6,6]-phenyl-C_{61}-butyric acid methyl ester (PCBM). Power conversion efficiency was only 0.28% "due to the lower short circuit current".[17] Recent studies of polythiophene blends, such as the blends of poly(3-hexylthiophene) (P3HT) or

poly(hexylphenanthrenyl-imidazole thiophene) (PHPIT) and [6,6]-phenyl-C_{61}-butyric acid methyl ester (PCBM), have shown power conversion efficiencies of 4-5%.[18,19] Polythiophene may have low power conversions currently, but they show some of the most promise for organic solar cell electron donor material due to their high light absorption and electronic conductivity.

1.5 Thermal Annealing

To increase the efficiency of organic solar cell materials, a process called thermal annealing has been incorporated into the procedure after the active layer has been deposited. Thermal annealing, a thermal treatment in which the material is heated above its glass transition temperature (Tg) held for a period of time then cooled, has shown to increase the power efficiency of the solar cell material. Molecularly, thermal annealing changes the morphology of the polymer material by creating a much higher crystalline material. The creation of a higher crystalline material, both enhances the optical absorption of the material due to a more conjugated system and electron-hole pair mobility as a result of stronger inter-chain interactions. The enhanced optical absorption allows for an increase in charge carriers produced due to the increase of photons absorbed per light energy applied to the material. The stronger inter-chain interactions increase the electron-hole pair mobility by inducing an increase in the free energy of charge separation. The greater separation between the electron and hole, the faster the charges go to their respective electrodes. Both of the enhancements

described allow for greater power efficiency for the whole system. In a study led by Dr. James R. Durrant, thermal annealing was shown to increase short circuit current for a P3HT/PCBM system from 1.35 mA cm^{-2} to 3.9 mA cm^{-2}.[19] The increase in short circuit current was due to the increase in charge carrier collection and mobility in the higher crystalline P3HT. The only reduction of efficiency came at the interface of the P3HT/PCBM. The higher crystallinity of the P3HT resulted in greater separation between the donor and acceptor material. With an increase in segregation between the donor and acceptor material, there is a reduction in exciton transfer, lowering the efficiency of the solar cell material. If a solution can be found for the segregation of the donor and acceptor materials, post-thermal annealed products may give substantial increases in solar cell efficiency.

1.6 Proposed Research

The goal of the proposed research is to determine a solution to the segregation of the donor and acceptor materials after thermal annealing. The solution hypothesized is to couple the fullerene electron acceptors to the poly(3-hexylthiophene) electron donors while still allowing for increased crystallinity of the donor. A study will be done between two systems: a non-coupled system and coupled system. The non-coupled system will resemble previous studies, where there is a heterogeneous mixture of fullerenes and the poly(3-hexylthiophene) for the active layer. The coupled system will have all the fullerenes coupled to poly(3-hexylthiophene) while still adding non-coupled poly(3-

hexylthiophene) to aid in increasing crystallinity. The hope is that the coupled material will solve the problem of segregation between donor and acceptor while still allowing for increased crystallinity thus raising the power conversion efficiency for the organic solar cell. Since beginning the study described, two papers have been published with similar goals. One merely developed fullerene-terminated P3HT, without studying its power efficiency,[20] while the other study developed C_{60}-end capped P3HT to be used as a compatibilizer in a P3HT/PCBM system and studied its power efficiency.[21] Unlike the previous mentioned studies, the C_{60}-end capped P3HT in this work will be used as a compatibilizer and electron acceptor. Both this study and the latter study described, show comparisons between a non-coupled system and coupled system. By comparing to a non-coupled control, the studies remove variables dependent on the fabrication of the solar cells between the two systems. The goal is to have an accurate study between two systems, to determine the effectiveness of coupling the donor and acceptor materials.

2 Experimental Section

2.1 Materials

The following chemical reagents were purchased through Sigma-Aldrich: 2-bromo-3-hexylthiophene, poly(3-hexylthiophene) (MM of 87,000 Daltons), fullerene-C_{60}, iodine, iodobenzene diacetate, anhydrous THF (sure seal), isopropyl magnesium chloride (2.0 M solution in THF), [1,3-Bis(diphenylphosphino)propane]dichloronickel(II) (Ni(dppp)Cl_2), copper powder (425 microns), copper (I) bromide, 2,2'-bipyridyl, ITO-glass plates, and a solution of poly(ethylenedioxythiophene)/poly(sulfonatedstyrene) in water. Electrical connection legs and epoxy resin were purchased from the photovoltaic company Ossila. The chromatography columns used in filtration (Wilmad-Labglass) have a 300 mL reservoir and a 24/40 joint. The platinum foil (0.025 mm thick) used as the working electrode in the electrosynthesis coupling (STREM Chemicals, Inc.) was cut into strips (6 mm x 25 mm). The silver chloride electrode (Ag/AgCl in sat'd KCl solution, single junction) used as the reference electrode was purchased through Pine Research Instrumentation. The glassy carbon disk electrode (1 mm diameter glassy carbon disk) used as the counter electrode was purchased through eDAQ Products.

Glassware was oven-dried for at least two hours at 110°C before use. For most of the work, Schlenkware was used due to the need for argon or nitrogen atmosphere. A glove box was used when air and moisture-sensitive reagents were prepared. The electrolyte solution for the electrosynthesis was 0.1 M ammonium acetate in methanol. The

platinum working electrode was drop-casted into a solution of dissolved fullerene-C_{60} in CH_2Cl_2. The procedure was done in a glove box under nitrogen atmosphere. The fullerene-C_{60} was dissolved into the solvent overnight and drop-casted the next day by lowering the electrode in the solution for 30 seconds and then raising it to dry for several minutes. The voltage applied for the electrochemical cell was supplied by an EG&G Princeton Applied Research Potentiostat/Galvanostat Model 273A.

2.2 Syntheses

2.2.1 Preparation of 2-bromo-3-hexyl-5-iodothiophene.[22,23]

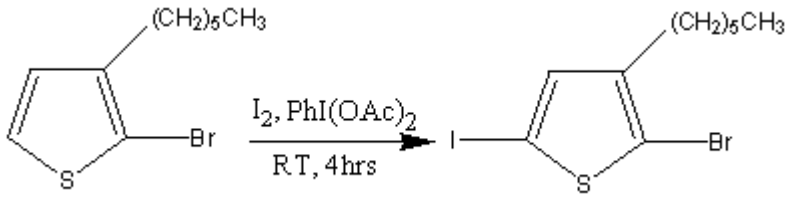

Into a dried round bottom flask was added dichloromethane (50 mL), 2-bromo-3-hexylthiophene (5g), and a stir bar. The flask was placed in a sodium chloride (NaCl)/ice bath to bring the solution down to 0 °C. While the solution was at 0 °C and being stirred, iodine (2.84 g, 11.2 mmol) and iodobenzene diacetate (3.93 g, 12.2 mmol) was added. The mixture was warmed up to room temperature and then left to stir for four hours. Every hour a sample was taken and run on the GC/MS to follow the extent of the

reaction. After the starting product, 2-bromo-3-hexylthiophene, was consumed, the reaction was terminated by adding 10% aqueous sodium thiosulfate, and the mixture was extracted with anhydrous diethyl ether. Using a separatory funnel, the organic layer was washed two more times with 10% aqueous sodium thiosulfate. The organic layer was then transferred to an Erlenmeyer flask and dried with magnesium sulfate. The solution was filtered and the solvent was evaporated using a rotary evaporator. Further purification was done by using two Wilmad chromatography columns in a series (one being set above the other). Both were built using glass wool, sand, and silca gel (200-400 mesh) that had been dried overnight as shown in Figure 8.

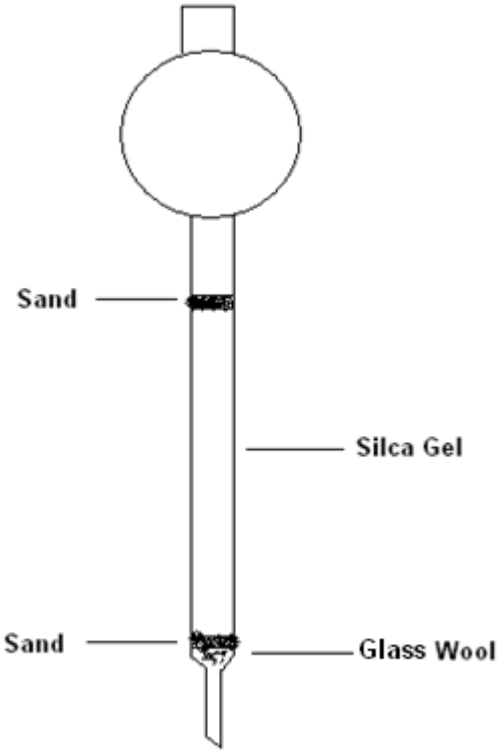

Figure 8. Chromatography column for monomer purification.

Hexane was used as the eluent or mobile phase. With the stopcock open both columns were wetted and filled with hexane to the top of the sand/silica gel immediately before the purification. The product was added to the top column and the stopcock was opened until the product was just to the top of the sand/silica gel. The reservoir for the top column was then filled with hexane. The stopcocks for both columns were opened so that each dripped at the same rate. After the product reached the bottom column fractions were taken 20 mL at a time until there was visibly (product has yellow color) no more product in the column. The fractions were tested on the GC/MS for pure 2-bromo-3-hexyl-5-iodothiophene and the pure monomer fractions were added together. The solvent was then evaporated using rotary evaporation.

2.2.2 Synthesis of Poly(3-hexylthiophene) (P3HT).[23]

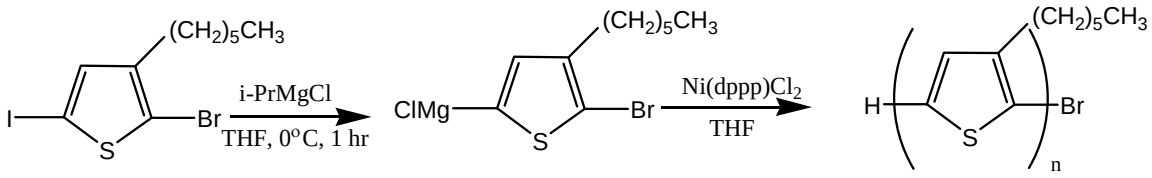

A dried three-neck round bottom flask was quickly assembled for an inert gas system with the left neck fitted to a hose that ran to a gas manifold, the middle neck connected

to a condenser and bubbler, and the right neck plugged by a septum as seen in Figure 9. The flask was then further dried under vacuum in an oil bath and cooled to room temperature using a stream of argon.

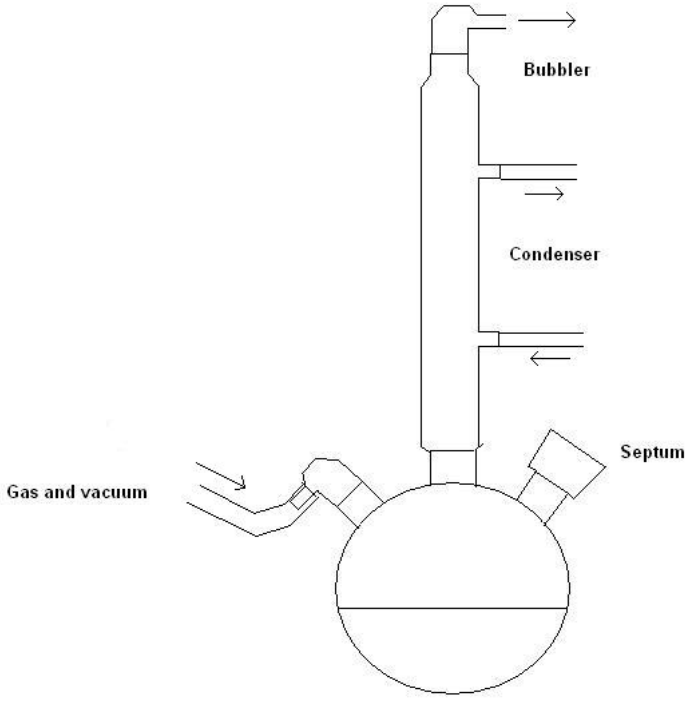

Figure 9. Set up for synthesis of poly(3-hexylthiophene).

To obtain a larger amount of product, the mass or volume of each reactant used in the procedure was quadrupled and the time was doubled from the literature procedure.[23] The monomer, 2-bromo-3-hexyl-5-iodothiophene (4 mmol, 864 µL) was added along

with a stir bar into the flask and the atmosphere was replaced by argon gas. Using a syringe, dry THF (20 mL) was added into the flask. The mixture was then stirred and cooled down to 0 °C using a NaCl/ice bath. Isopropyl magnesium chloride (2.0 M in THF, 4 mmol, 2 mL) was added to the flask via syringe and left to react for one hour at 0 °C. During the one hour, a solution of Ni(dppp)Cl_2 (21.6 mg) in dry THF (20 mL) was prepared in a glove box and put into a syringe. At the end of the one hour, the nickel catalyst solution was added to the flask and the mixture was brought to room temperature. The reaction was left to react for two days at room temperature in an argon atmosphere.

The reaction was stopped by the addition of de-ionized water and the mixture was extracted with chloroform. The organic layer was washed with water several times through a separatory funnel and collected into an Erlenmeyer flask after the wash was finished. The mixture was dried over anhydrous magnesium sulfate and filtered. After filtration, the mixture was poured into a one-neck round bottom flask and the solvent was evaporated using a rotary evaporator. The product was then washed several times with methanol to remove lower molecular mass product. The higher molecular mass fraction P3HT was re-dissolved with a small amount of chloroform and put into a pre-weighed vial. The solvent was then evaporated off again using a vacuum oven to give Coupling Method 1 product (CP1).

2.2.3 Coupling of P3HT and Fullerene-C_{60} : Method 1.[24]

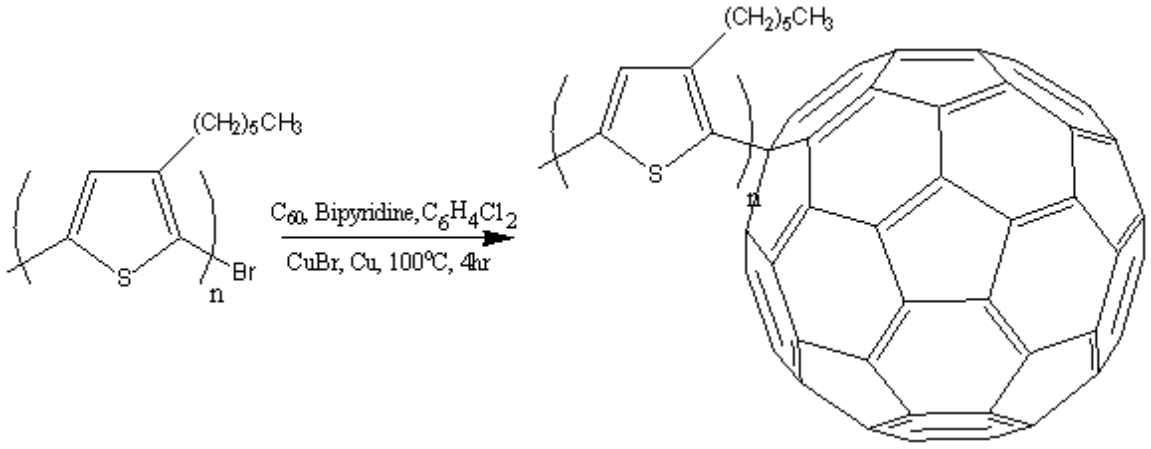

The following procedure for coupling P3HT and fullerene-C_{60} is a variation of the procedure used for the coupling of poly(hexylthiophene)-graft-poly(styrene-co-chloromethylstyrene) to fullerene-C_{60}.[24] The coupling of the polymer to the fullerene-C_{60} is a synthesis technique called atom transfer radical addition.[24] In the procedure, copper (I) bromide initiates the coupling by complexing with bipyridine and abstracting the halogen from the polymer by homolytic cleavage.[25,26] The homolytic cleavage of the carbon-halogen bond "generates a primary organic radical that adds across the carbon-carbon double bond"[25] of the fullerene-C_{60}. The fullerene-C_{60} is then reduced by the copper which forms a copper halide after abstracting the halogen from the copper (I) complex. In the article, chlorine was the halogen group displaced, but in coupling the

poly(3-hexylthiophene) to fullerene-$C_{60,}$ the end group bromine was the leaving group. The vial with the P3HT was re-weighed to get an accurate weight for the polymer material. Depending on the molar amount of P3HT (average molecular mass was used to determine molar amount), copper powder (1 equiv.), copper (I) bromide (0.3 equiv.), 2,2'-bipyridyl (1.2 equiv.), and fullerene-C_{60} (1 equiv.) were weighed out and placed into the flask. The mixture was dissolved into 1,2-dichlorobenzene (50 mL) and stirred for several minutes. The flask was then assembled similar to Figure 9 except at the gas inlet, where the stop-cock was replaced by a glass pipette put through a septum and connected to the hose running to the gas manifold. The other end was placed into the mixture, which was degassed by bubbling nitrogen through it for 20 minutes. Nitrogen continued to be bubbled through while the mixture was stirred at 100 °C for 4 hours. After 4 hours, the flask was taken out of the oil bath to cool down. The mixture was filtered through a fritted disk funnel and the filtrate washed with toluene. It was then poured into a one-neck flask and the solvents were evaporated as much as possible by the rotary evaporator. The product mixture was poured into a vial and the solvents were evaporated further in a vacuum oven. After the solvents were evaporated, the product was dissolved in THF to separate the soluble high molecular mass P3HT coupled to fullerene from any uncoupled fullerenes or fullerenes coupled to low molecular mass P3HT. The solution was decanted and dried in a vacuum oven to remove the THF.

2.2.4 Coupling of P3HT and Fullerene-C_{60} : Method 2

2.2.4.1 Synthesis of P3HT

Polymerization was carried out according to the procedures in Section 2.2.2, but after two days the reaction was not ended.

2.2.4.2 Bromination of Fullerene-C_{60}

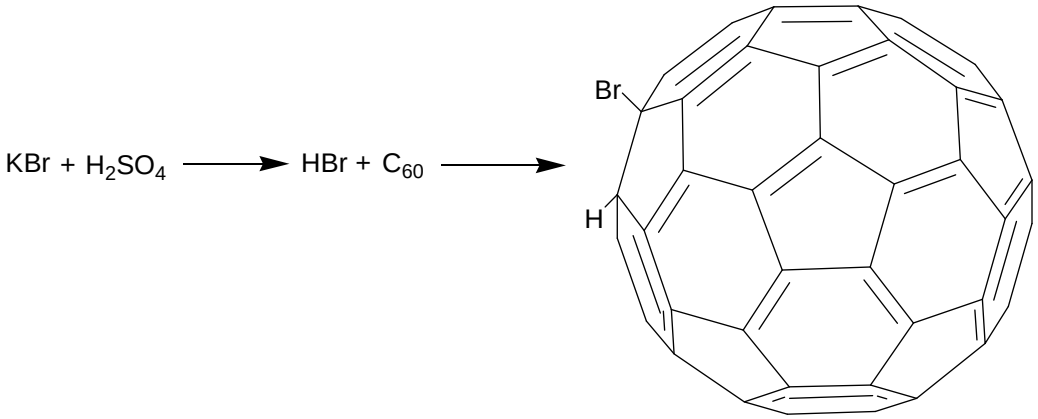

Into a single-neck flask was added fullerene-C_{60} (0.5 mmol, 0.360 g) in 1,2-dichlorobenzene. It was then stirred and connected to a three-neck flask via a tube with a stopcock. In the three-neck flask was added KBr dissolved in water. A separatory funnel containing dilute sulfuric acid was connected to the left neck of the three-neck flask as seen in Figure 10. The dilute sulfuric acid was added to the KBr solution and the mixture was stirred at 85 °C overnight, generating HBr. The HBr formed from the reaction bubbled into the single-neck flask containing the dissolved fullerene-C_{60}.

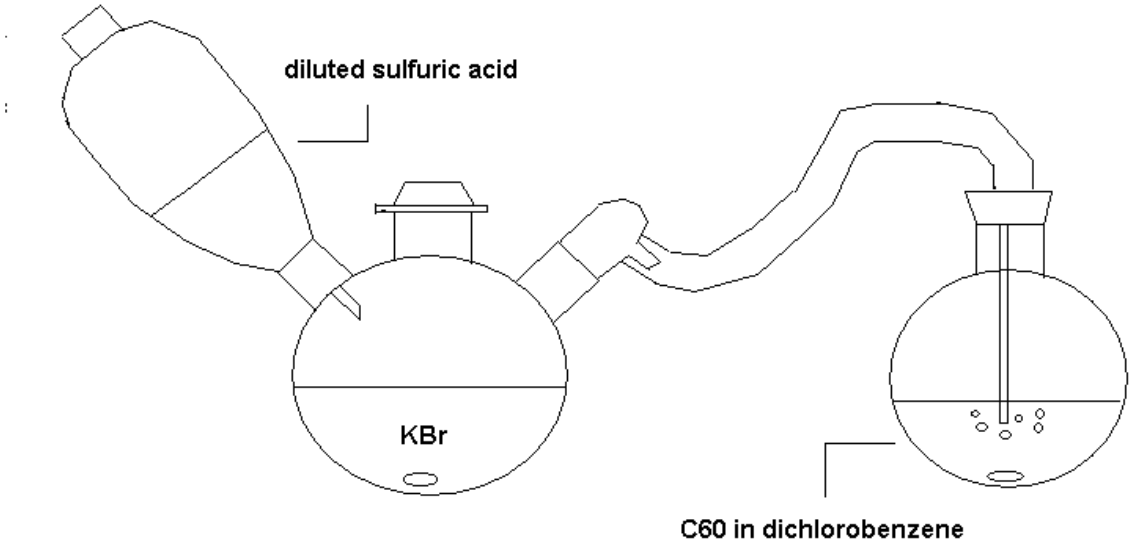

Figure 10. Apparatus for the synthesis of $HBrC_{60}$.

2.2.4.3 Coupling of P3HT/Fullerene-C_{60}

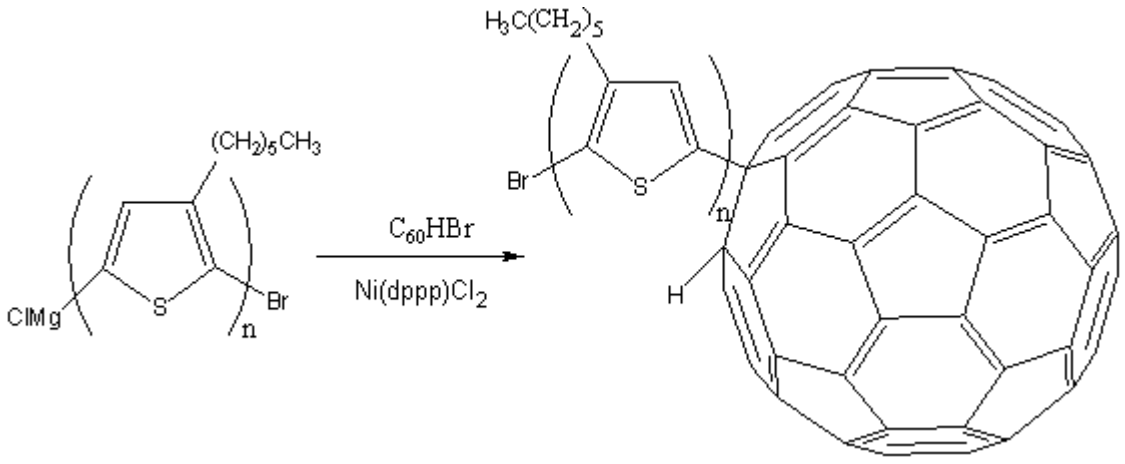

At the end of the two days, the brominated fullerene (178 mg, 0.25 mmol) was dissolved into 1,2-dichlorobenzene and added into the three-neck flask via syringe. The mixture was stirred at 100 °C overnight. The product was then purified through the same process found in 2.2.2. As in Coupling Method 1, the product was dissolved in THF to separate the soluble high molecular mass P3HT coupled to fullerene from any uncoupled fullerenes or fullerenes coupled to low molecular mass P3HT. The THF was then evaporated off again in a vacuum oven to give Coupling Method 2 product (CP2).

2.2.5 Coupling of P3HT and Fullerene-C_{60} : Method 3.[27]

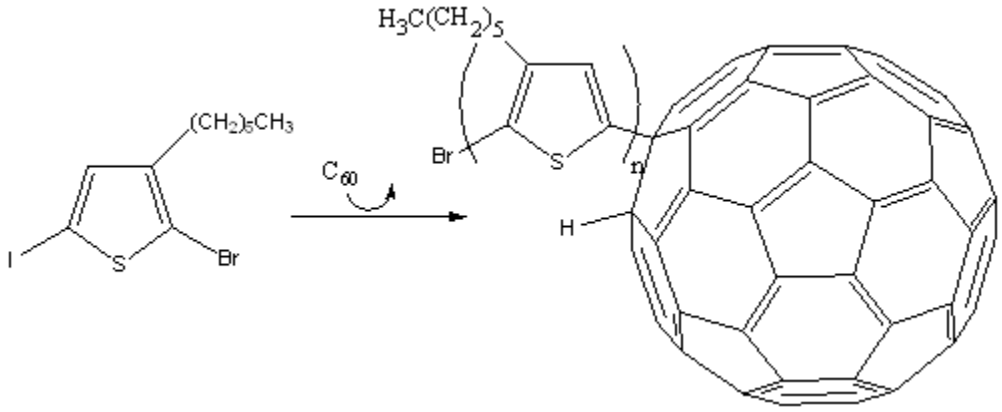

An electrosynthesis procedure for the synthesis of poly(phenylene vinylene) and its coupling to fullerene-C_{60}, was adapted for the synthesis of poly(3-hexylthiophene) and coupling to fullerene-C_{60}.[27] Instead of using tetraethylammonium tetrafluoroborate as

the electrolyte in the solution, ammonium acetate dissolved in methanol was the electrolyte chosen to carry the charge between electrodes. Into an electrochemical cell was poured 0.1 M ammonium acetate in methanol. 2-Bromo-3-hexyl-5-iodothiophene (1 µL) was added to the cell. The electrodes were set-up as shown in Figure 11.

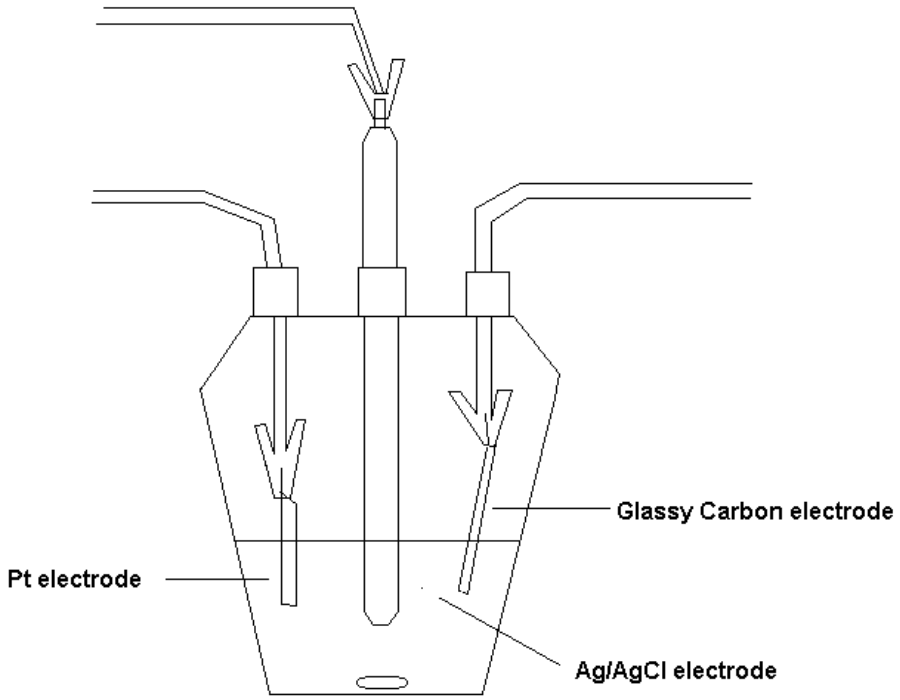

Figure 11. Set-up for electrochemical synthesis of P3HT and its coupling to C_{60}.

The solution was stirred with a small stir bar for several minutes. The potentiostat was turned on and the software PowerSuite was opened. Cyclic Voltametry-Ramp-Linear

Scan was used for the first step, run with 50 mV/s and a voltage range of -0.415 V to -2.715 V. The voltage, at which signs of reaction were shown, was written down and another experiment was started in Chronoamerometry. The second experiment was held at the voltage of reaction for 120 seconds. The experiment was ended and the working electrode checked for deposited P3HT/fullerened-C_{60} coupled material. After four trials of the electrosynthesis, signs of polymerization and coupling were never found so Coupling Method 3 was not pursued further.

2.3 Fabrication of Organic Solar Cells.[28, 29]

Optimum conditions for fabrication of organic solar cells were determined from published works studying optimal conditions of each step.[28, 29] The fabrication of the organic solar cells was mostly carried out in a glove box under an inert atmosphere. Before the procedures were begun, two solutions were made for the application of the active layer at 1% by mass concentrations.[28] The first solution was a mixture of poly(3-hexylthiophene) and fullerene-C_{60} in dichlorobenzene at ratio of 1:0.7 P3HT: fullerene-C_{60}.[29] The second solution was a mixture of poly(3-hexylthiophene) and poly(3-hexylthiophene)/fullerene-C_{60} coupled product in dichlorobenzene with a ratio of 0.7:1 P3HT:coupled product. The ratio was switched for the second solution due to part of the coupled product mass attributed to the P3HT. The solutions were left to dissolve for 48 hours and then heated up to 45 °C and cooled for 30 minutes right before the

fabrication of the solar cell.[29] The ITO-glass plates purchased from Sigma-Aldrich were pre-cleaned and in individual packages so further cleaning was not necessary.

The ITO-glass plates were tested by a multi-meter, set for resistance, to determine which side was the coated side. After the plates were tested, the non-coated side was either marked or placed down so that the correct side would be coated with the other layers. The plates were then transported to a spin-coater. The purchased solution of PEDOT:PSS was spin-coated on the coated side of each ITO-glass plate at 5000 rpm for 60 seconds.[28] The plates were transported to a glove box and then thermally annealed on a hot plate for 10 minutes at 150 °C.[28] For the next step, the plates were divided equally so that half were spin-coated with the first solution and the other half were spin-coated with the second solution. The spin-coating was done at 500 rpm for 90-120 seconds to form a roughly 70-100 nm thick film.[28,29]

The coated slides were then quickly transported to the Edwards AUTO 306 vacuum coater where they were placed on a shadow mask face down. The shadow mask was placed inside the instrument. Aluminum was placed into a metal coil basket, which was connected to the electrical connection points and then moved into the correct position. The chamber was closed and the air was evacuated. The voltage was increased until 100 nm of aluminum was deposited onto the plates. The plates were removed and transported to the glove box where they were thermally annealed at 150 °C for 60 minutes.[29] The electrical connection legs were then placed on the cathode of the cells and the cells were sealed with glass slides and an UV curable epoxy resin.

2.4 Analysis

2.4.1 Gas Chromatography/ Mass Spectroscopy (GC/MS)

GC/MS analysis was run on the monomer material during the synthesis and after the purification on a Agilent 5890/5970 GC/MS. Hexane was used as the solvent for the sample using helium as the carrier gas. The solvent delay was 3 minutes and the starting temperature, 50 °C, was held for four minutes. There was a ramp of 25 °C/min with a final temperature of 310 °C. The final temperature was held for another 2 to 5 minutes for residual material.

2.4.2 High Pressure Liquid Chromatography (HPLC)

HPLC analysis was done on different fractions of a synthesized P3HT sample, as well as, samples of both the Method 1 and Method 2 coupled products (CP1, CP2). P3HT fractions were produced through a series of washes, first with methanol and then with acetone. The residual material left from the two washes was kept as the third fraction. Polystyrene standards, the fractions of the synthesized P3HT, and both coupled materials were run on a Dionex U300 with a Corona Aerosol Detector. A guard column and two Mix D columns were used for all the runs. HPLC grade THF was used as the only eluent in the analysis at a rate of 1 mL/min. The method ran for 25 minutes total. The two polystyrene standards were used to calculate the molecular masses of the polymer fractions by graphing the standard molecular masses versus their retention times and

creating an equation from the calibration curve. The calibration curve along with the equation created can be seen in Section 3.1.2.

2.4.3 Fourier Transform Infrared (FTIR) Spectroscopy

FTIR analysis was run on the monomer, synthesized P3HT, purchased P3HT (used in solar cell), $HBrC_{60}$, CP1, and CP2 using a Varian 7000 FTIR spectrometer. An ATR attachment was used to give immediate spectra. To generate clean spectra, a KBr pellet was made with each sample, except the monomer, at a mass ratio of 20:1 KBr to sample. A pellet of pure KBr was also made and used to give a good background. The system was evacuated of moisture and CO_2 before each sample was run with 256 scans.

2.4.4 ^{1}H Nuclear Magnetic Resonance (NMR) Spectroscopy

^{1}H NMR analysis was carried out on the monomer, synthesized P3HT, purchased P3HT (used in solar cell), $HBrC_{60}$, CP1, and CP2 with a JEOL ECA-500 MHz NMR spectrometer. Deuterated chloroform was used as the solvent for the monomer while deuterated 1,1,2,2-tetrachloroethane was used for all other samples. The method used was an automated experiment with no changes to the set up except the number of scans, depending on the complexity of the material. The highest number of scans used was 256 scans for CP1 and CP2.

2.4.5 ^{13}C NMR Spectroscopy

^{13}C NMR analysis was also carried out on all products with a JEOL ECA-500 MHz NMR spectrometer. The solvent choice was the same as described in Section 2.4.4. An experiment was developed for the analysis of the products. A 90 degree pulse was used with a 11 ms pulse width and a 2 or 4 second relaxation delay between pulses. There was a 1000:1 signal to noise ratio and scans were not specified. The analysis was usually run overnight with some extended further into the next day.

2.4.6 Thermogravimetric Analysis (TGA)

Thermogravimetric analysis was carried out on a sample of the P3HT used in the solar cells, fullerene-C_{60}, CP1, and CP2. The analysis was done on a TA Instruments TGA Q500. Each run started at room temperature and had a ramp of 10 °C/min. At 600 °C the gas was switched from nitrogen to air. The final temperature of all runs was 1000 °C. After observing the thermogram for CP2, the product was dissolved in THF overnight and the solution was pipetted into another vial. Both vials were put into a vacuum oven overnight to dry the products. Both the THF soluble and insoluble CP2 were run on the TGA using the same parameters as the other coupled products.

2.4.7 Differential Scanning Calorimetry (DSC)

Three mixtures were made by dissolving P3HT with either fullerene-C_{60}, CP1, or CP2. The mixtures were made up to the specifications described in Section 2.3 for the preparation

of the two active layer solutions. The three solutions were mixed overnight and then dried in a vacuum oven. The dried samples along with pure P3HT were analyzed on a TA Instruments DSC 2920 to determine the heat energy of fusions, the onset of the melting point temperatures, and the maximum melting point temperature. Each material was run two times to a temperature of 275 °C with a ramp of 10°C per minute and cooled back down. Each material then underwent an isothermal annealing at 150°C for 60 minutes to mimic the thermal-annealing process during fabrication of the solar cell. Two runs were carried out afterward using the same procedure as before the isothermal run.

2.4.8 Transmission Electron Microscopy

Transmission Electron Microscopy was used to produce images of the morphology of coupled and non-coupled, annealed and non-annealed products. A 1% by mass solution was made for both the coupled and non-coupled systems similar to description in Section 2.3. Two glass slides were spin-coated with the two different solutions. The films on the glass slides were floated off using a tray full of de-ionized water and tweezers. As the films were floated off, several copper grids were laid on the floating film and Parafilm was pushed down on the film and brought up at an angle. A copper grid from both films was cut out and thermally annealed at 150°C for 60 minutes. The copper grids and film were transported to the TEM where images of the morphology of all four systems were taken at magnifications of 4000, 5000, and more if possible.

2.4.9 Power Efficiency Analysis

After fabrication of the solar cells, they were tested for their power efficiency using the set up shown below in Figure 12.

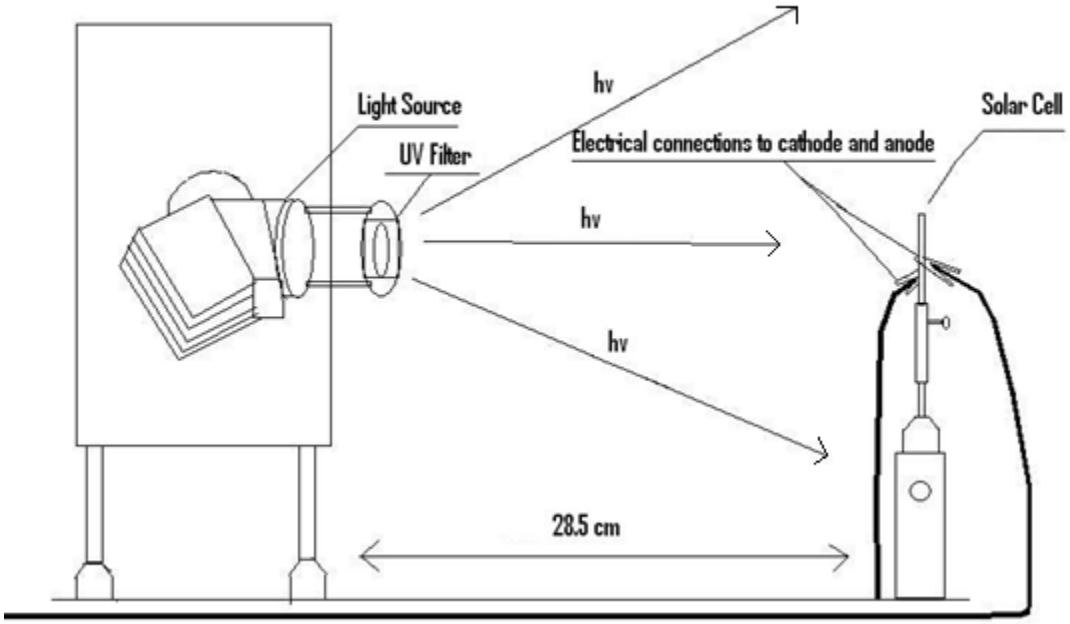

Figure 12. Set-up for testing solar cells.

A source light representing the light of one Sun was used to represent real applications. The current generated was measured by a Keithley 2400 Source Meter, which generated an I-V curve in a software program called MATLAB. Each fabricated solar cell was tested and the results were saved under a name indicating which system it represented.

3 Results and Discussion

A coupled product of poly(3-hexylthiophene) and fullerene-C_{60} was synthesized through a series of steps and studied by different methods of characterization. The coupled product was then incorporated into an organic solar cell as the active layer and compared to an organic solar cell with a non-coupled active layer to determine if there was an increase in power efficiency.

3.1 Characterization of Synthetic Routes

3.1.1 Gas Chromatography/Mass Spectrometry

Gas Chromatography/Mass Spectrometry (GC/MS) was used in the analysis of the monomer, 2-bromo-3-hexyl-5-iodothiophene. After purification, the product was run on the GC/MS resulting in a major peak at a retention time of 12.1 minutes and a minor peak at a retention time around 11.5 minutes as seen in Figure 13. The mass of the product, correlated to the major peak, was 373 Daltons (Da), which is the formula weight of 2-bromo-3-hexyl-5-iodothiophene. The mass of the product, correlated to the minor peak, was 326 Da, which is the formula weight of 2,5-bromo-3-hexylthiophene. Both products can be used in the polymerization of poly(3-hexylthiophene) so the mixture was not purified further. After confirmation through other characterization techniques, the monomer was used in the synthesis of poly(3-hexylthiophene).

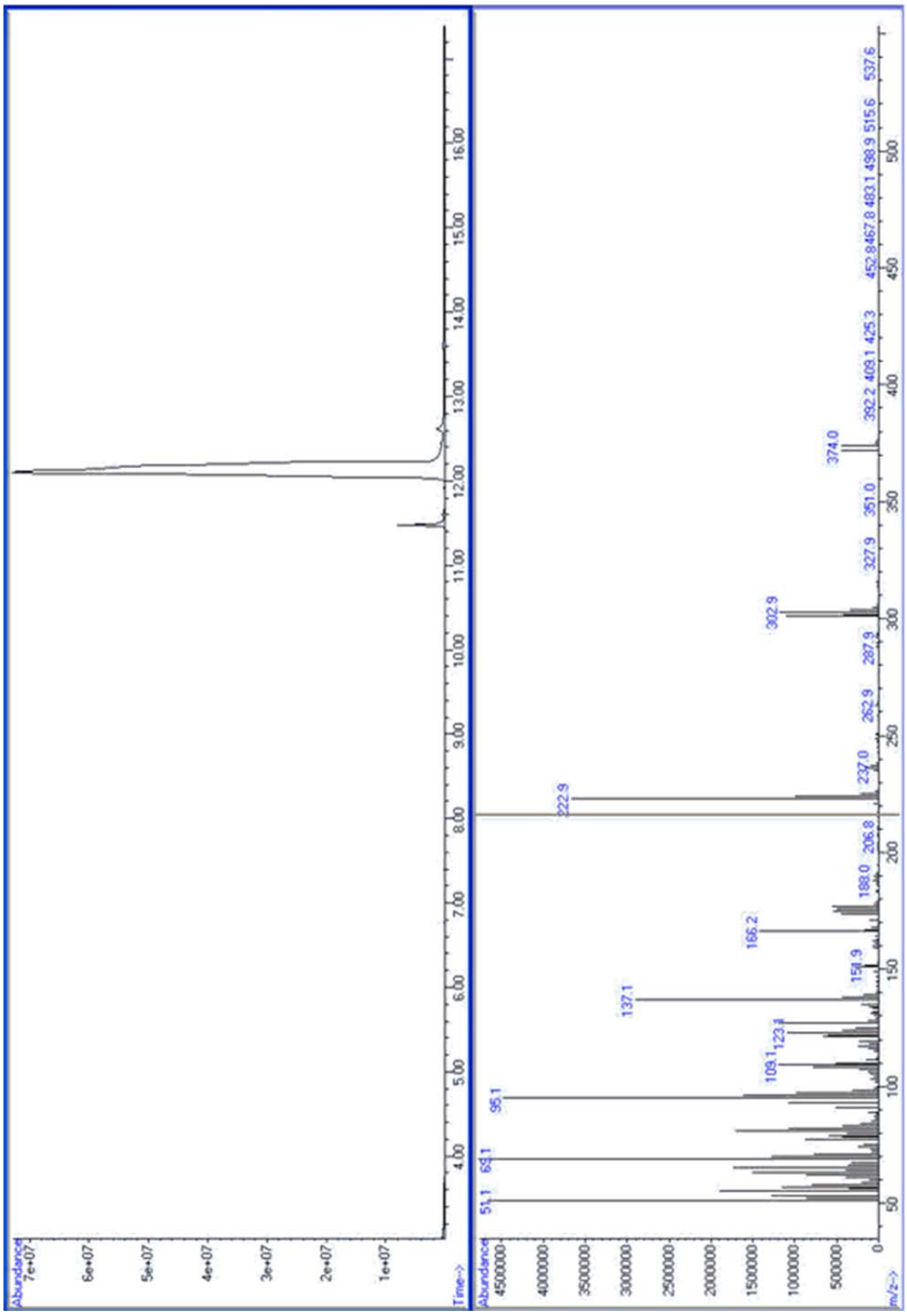

Figure 13. GC/MS chromatogram for monomer.

3.1.2 High Pressure Liquid Chromatography (HPLC)

Polystyrene standards, fractions of synthesized P3HT, CP1, and CP2 were analyzed using HPLC as seen in Figures 15 through 21. Figure 14 shows a calibration curve that was developed from the runs of the polystyrene standards, seen in Figures 15 and 16.

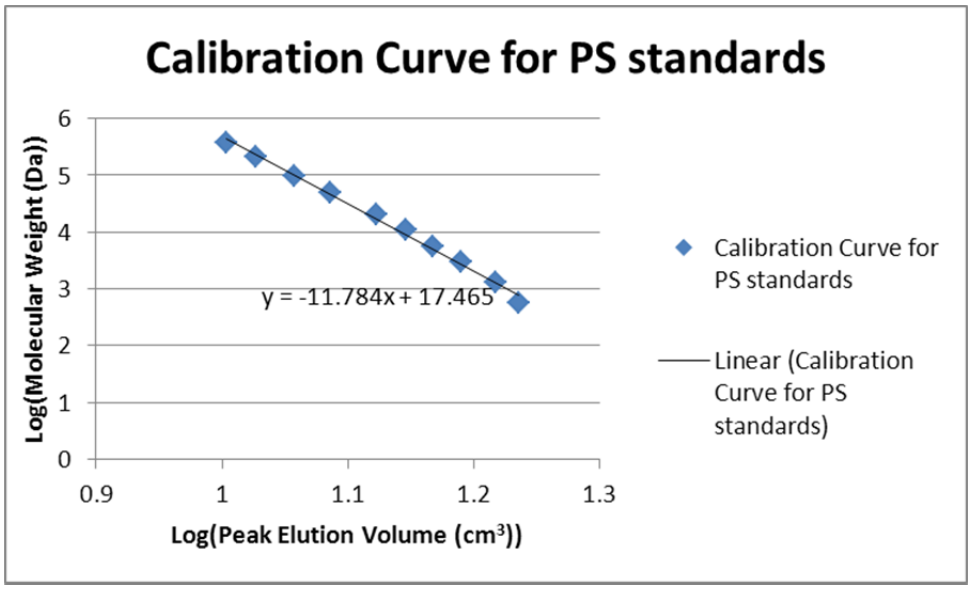

Figure 14. Calibration curve and equation (y= -11.784x + 17.465) for the molecular mass determination of synthesized P3HT fractions, CP1, and CP2. R^2 = 0.995.

From the calibration curve, an equation was obtained to calculate the molecular mass of each P3HT from the fractions. Origin 8.1 software was used to give the best curve fit for each spectra and provide accurate peak positions and areas under the peaks.[30] Using

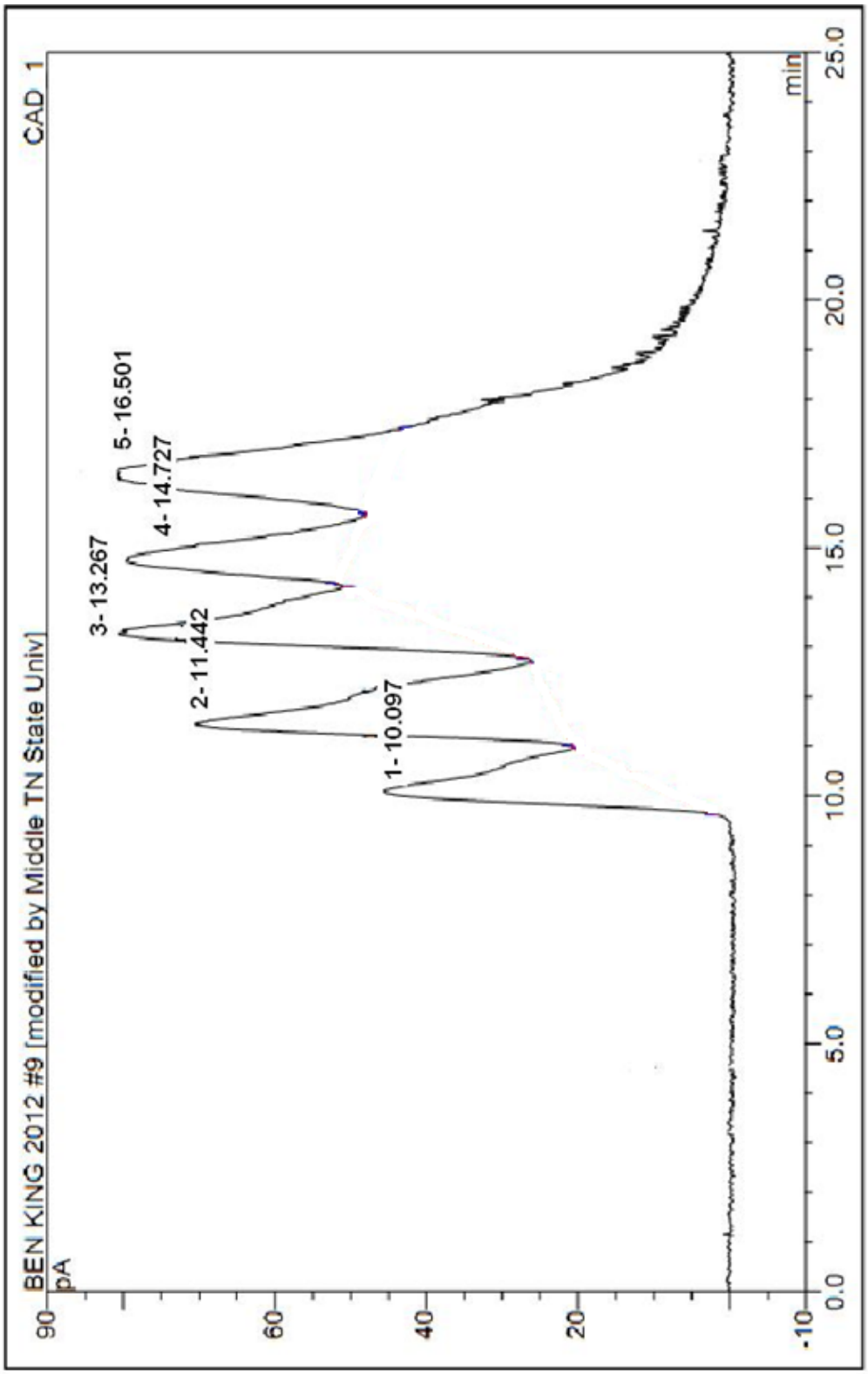

Figure 15. HPLC chromatogram of polystyrene standard A. Molecular masses are as followed: 1-377,400 Da, 2-96,000 Da, 3-20,650 Da, 4-5,460 Da, and 5-1,300 Da.

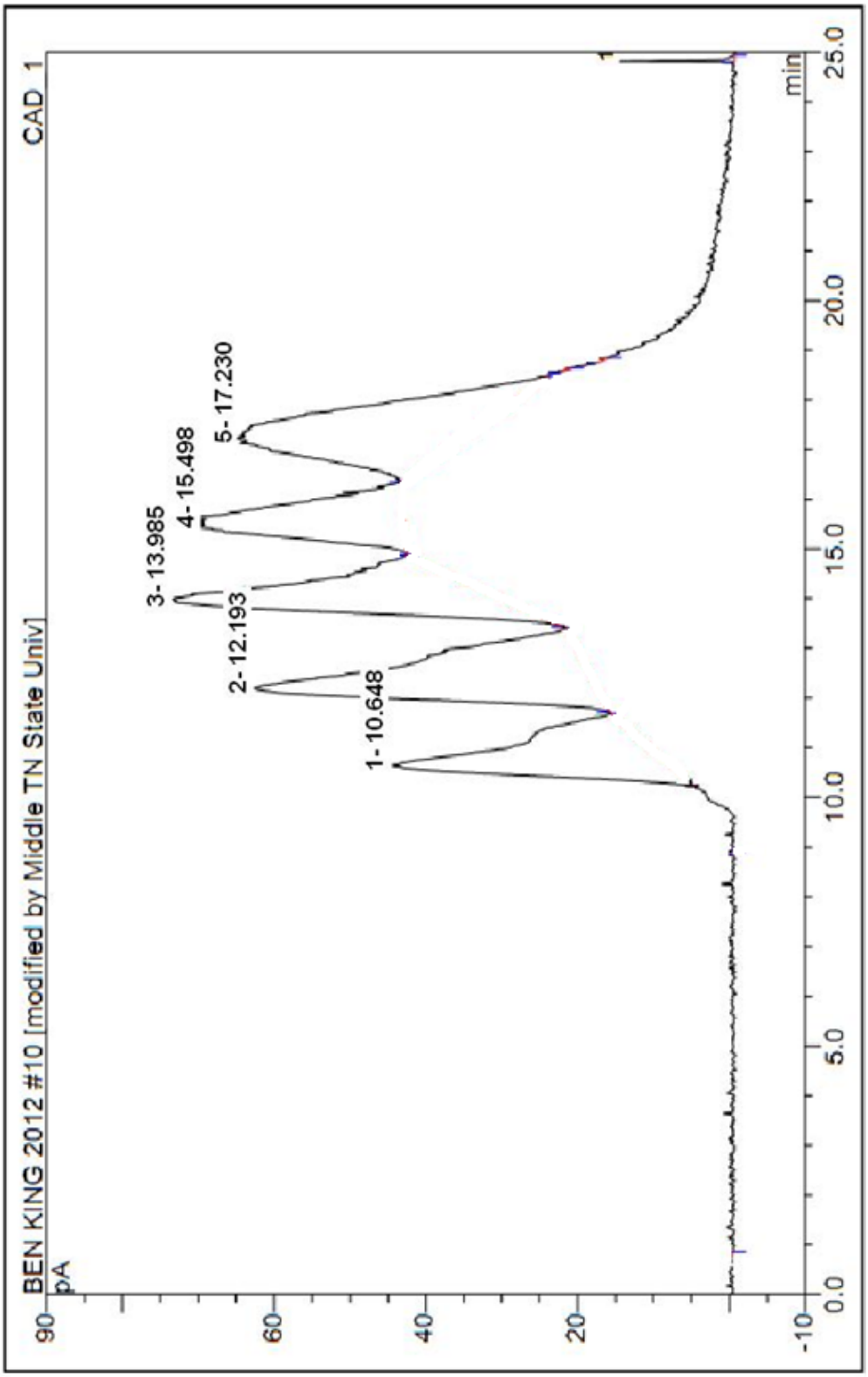

Figure 16. HPLC chromatogram of polystyrene standard B. Molecular masses are as followed: 1-210,500 Da, 2-50,400 Da, 3-10,850 Da, 4-2,930 Da, and 5-580 Da.

the equation from the calibration curve and peak positions from the Origin software, the molecular mass for each peak was calculated, as seen in Table 1. Using the area under the curves provided from the Origin software, the percentages of each molecular mass species for the high molecular mass P3HT, CP1, and CP2 were calculated and added under their respective molecular masses.

Table 1.
HPLC Data for P3HT Fractions

Peak #	Methanol P3HT Fraction	Acetone P3HT Fraction	High MM P3HT Fraction	CP1	CP2
1st	830 Da	5670 Da	60780 Da 4%	109800 Da 3%	2410 Da 92%
2nd	530 Da	1050 Da	3250 Da 69%	23200 Da 21%	140 Da 8%
3rd	380 Da	870 Da	650 Da 27%	2650 Da 42%	N/A
4th	190 Da	480 Da	N/A	1000 Da 34%	N/A
5th	90 Da	130 Da	N/A	N/A	N/A

The chromatogram for the methanol fraction, Figure 17, appeared to have five peaks. The first three peaks were from oligomeric molecules with molecular masses between 380 Da and 830 Da. The fourth and fifth peaks are most likely the result of foreign material in the columns or byproducts within the sample because there molecular

masses are too low to be thiophene. The chromatogram of the acetone fraction, Figure 18, had five identifiable peaks as well. The first peak contained species with a molecular mass of 5670 Da, much higher than that found in the methanol fraction. The rest of the peaks were similar to what was found in the methanol fraction, probably residual low molecular mass material trapped in the matrix of the high molecular mass P3HT. As seen in Figure 19, the high molecular mass fraction had three peaks of very different molecular masses. The first peak was the result of very long chain P3HT with a molecular mass of 60780 Da, but accounted for only 4% of the product. The second peak was the result of P3HT with a molecular mass of 3250 Da similar to the high molecular mass material found in the acetone fraction. The P3HT with a molecular mass of 3250 Daltons made up 69% of the product as seen in Table 1. The third and final peak was from oligomeric material not removed from the previous two washes. Based on percentages of each molecular mass for the high molecular mass P3HT, most of the synthesized P3HT appears to have molecular masses less than 3300 Da, too low to produce high crystallinity.[31] The P3HT synthesized was still used for the production of the coupled products, but due to potential low crystallinity, would be insufficient for any other use in the active layer. Characterization methods of FTIR and NMR were still done on the synthesized P3HT to compare it to the coupled materials.

CP1 had four observable peaks as seen in Figure 20. The first peak represented the largest molecular mass at 109800 Da which appears to be only 3% of the total mass. The next peak was the result of a species with a molecular mass of 23200 Da and made up

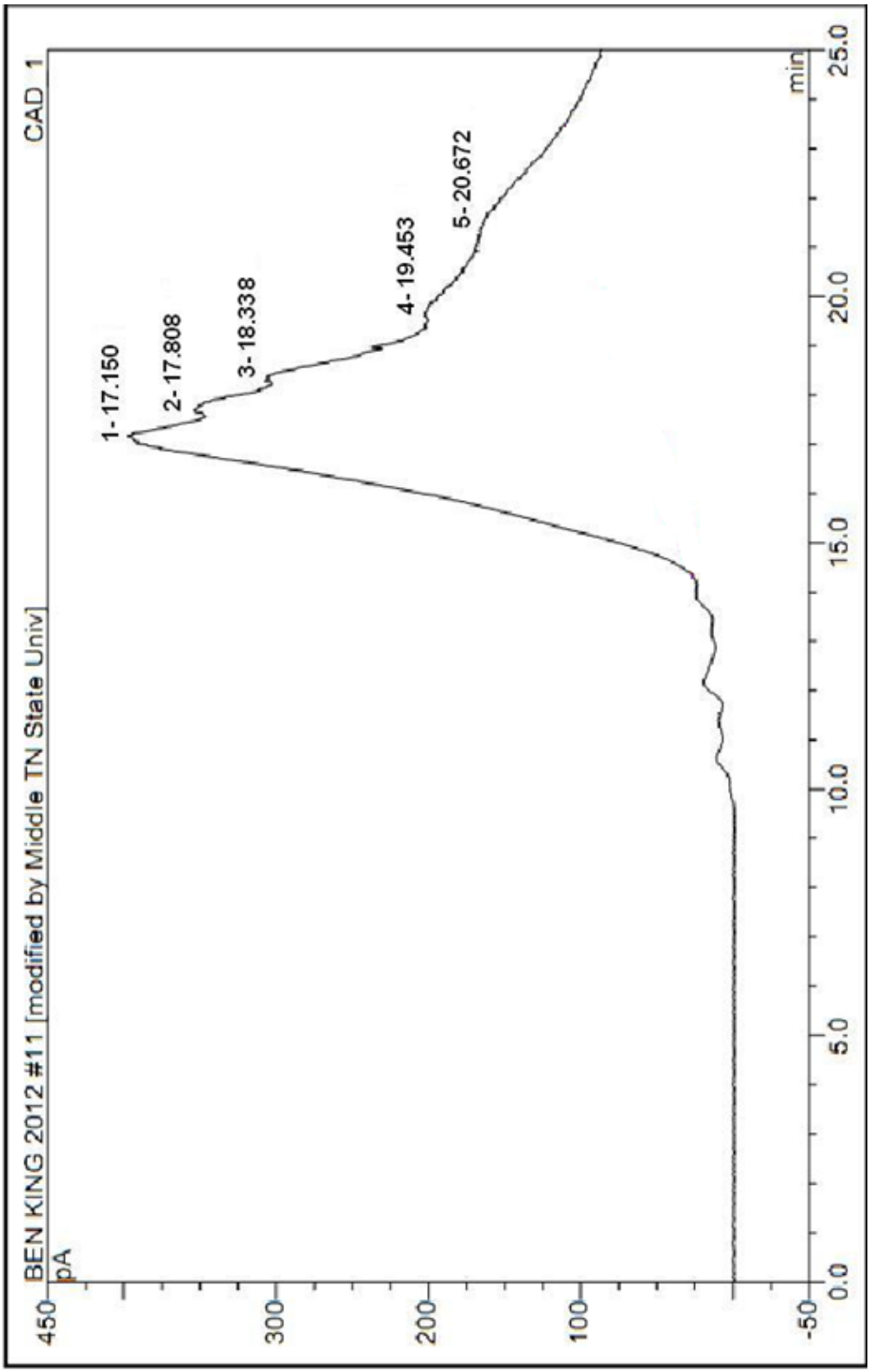

Figure 17. HPLC chromatogram of the methanol fraction for synthesized P3HT. Molecular masses are as followed: 1-832 Da, 2-5340 Da, 3-378 Da, 4-189 Da, and 5-92 Da.

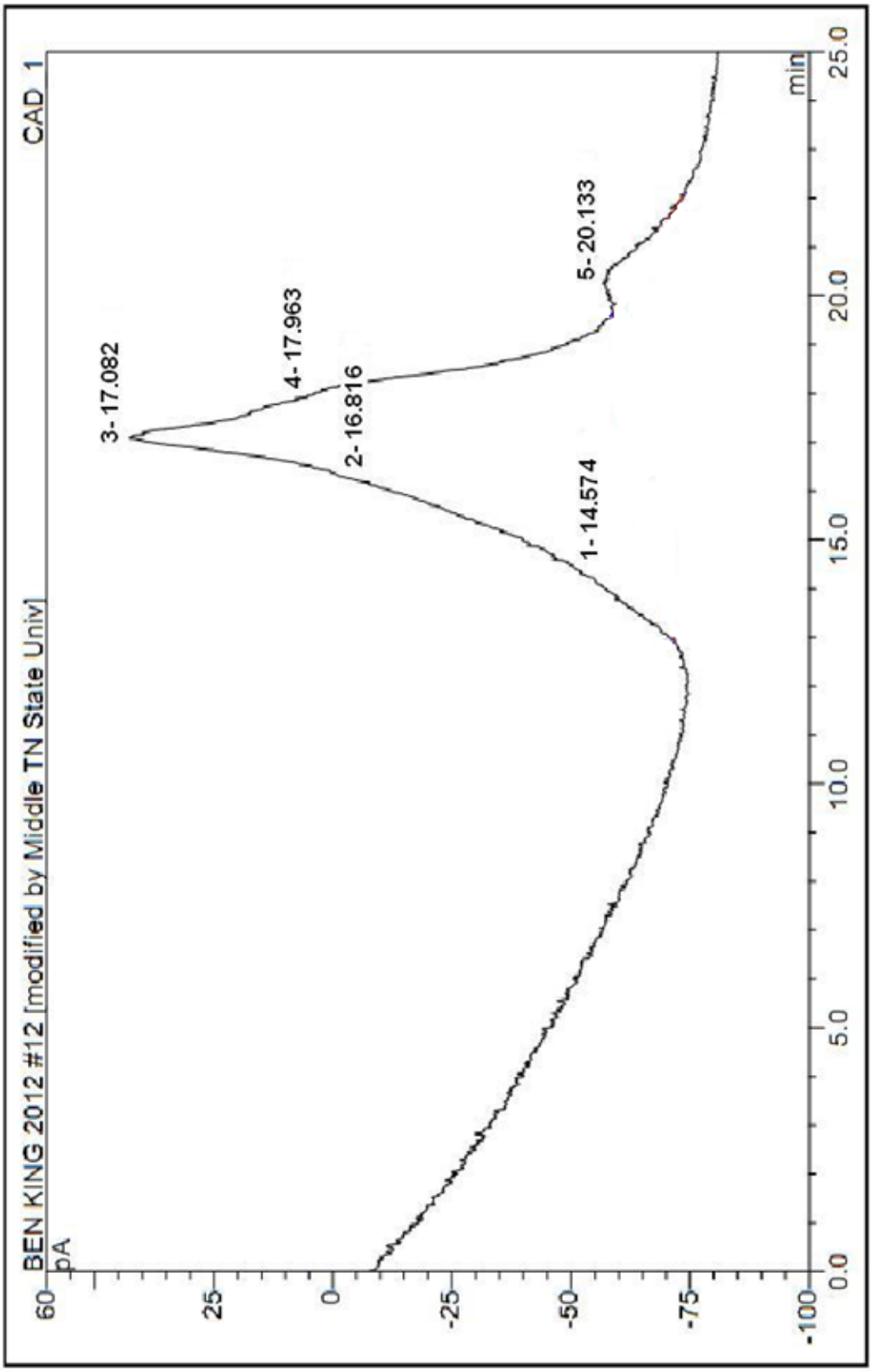

Figure 18. HPLC chromatogram of the acetone fraction for synthesized P3HT. Molecular masses are as followed: 1-5,668 Da, 2-1,050 Da, 3-872 Da, 4-482 Da, and 5-126 Da.

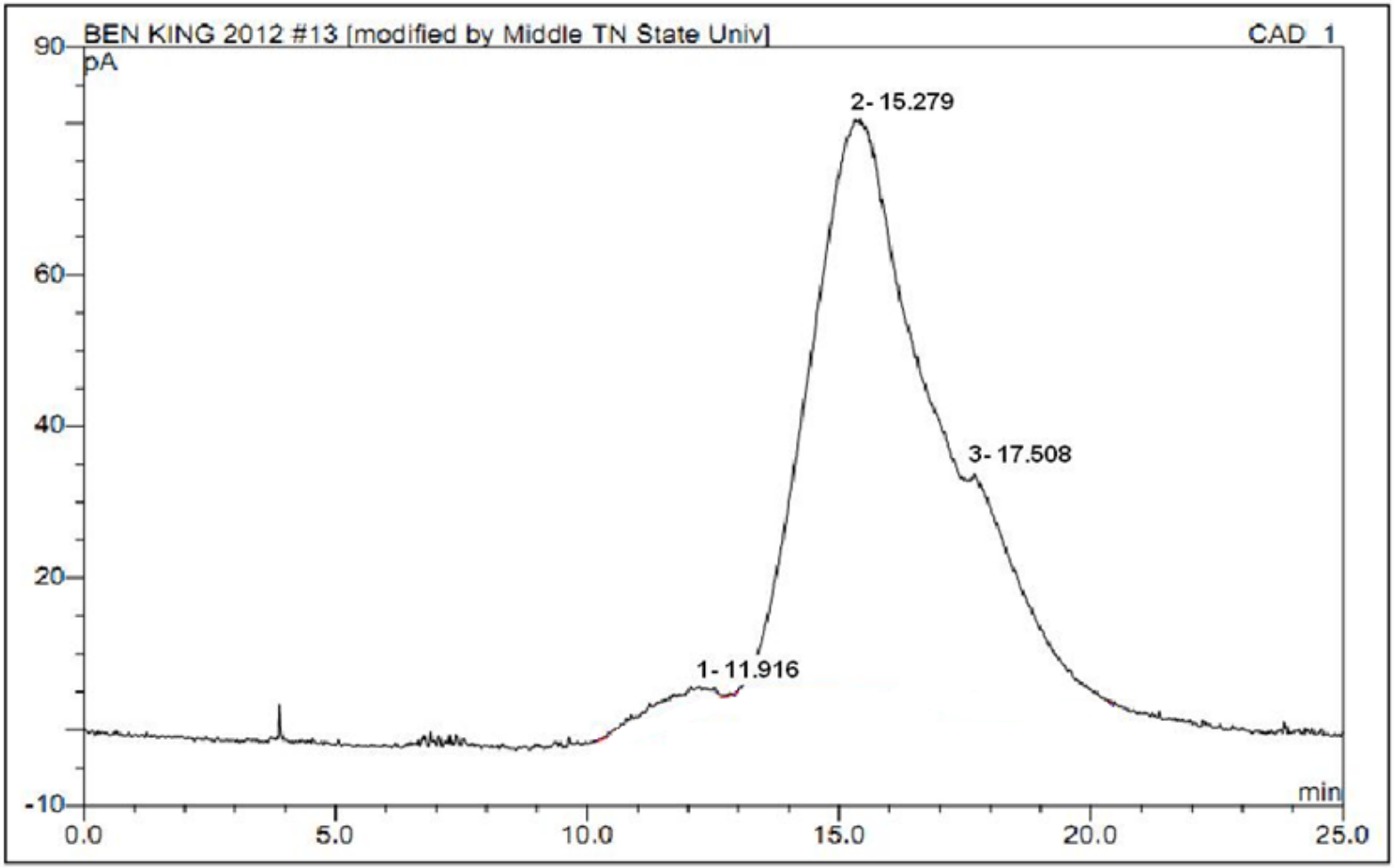

Figure 19. HPLC chromatogram of the high molecular mass fraction for synthesized P3HT. Molecular masses are as followed: 1-60,781 Da, 2-3,247 Da, and 3-652 Da.

21% of the total mass of the CP1 product. The third and largest peak was the result of coupled product with a molecular mass of 2650 Da and made up 42% of the total mass of the product. The fourth peak represented 34% of the CP1 product, but only had a molecular mass of 1000 Da. As seen in Figure 21, CP2 had only two peaks with the second one being the result of foreign material in the columns or byproducts within the sample. The first and largest peak was the result of coupled material with a molecular mass of 2410 Da and represented 92% of the total CP2 product. Both coupled materials had over 75% of their total mass due to species with molecular masses below 3000 Da with 24% of the CP1 having a large molecular mass.

Based on the molecular mass of the coupled products and the mass of fullerene-C_{60}, most of the P3HT chains coupled to the fullerene-C_{60} are too short to crystallize independently. The short P3HT chains of the coupled material will need to be incorporated into the crystalline material of the non-coupled P3HT without disruption to the crystals. In sections 3.2.3 and 3.2.4, the effect of the short chain coupled P3HT/C_{60} material is studied to determine its effect on the crystallinity of the non-coupled P3HT. Based on analysis in the two later sections, coupled material with long P3HT chains seem necessary to avoid crystal disruption and aid in high crystalline P3HT production in the active layer of the solar cell.

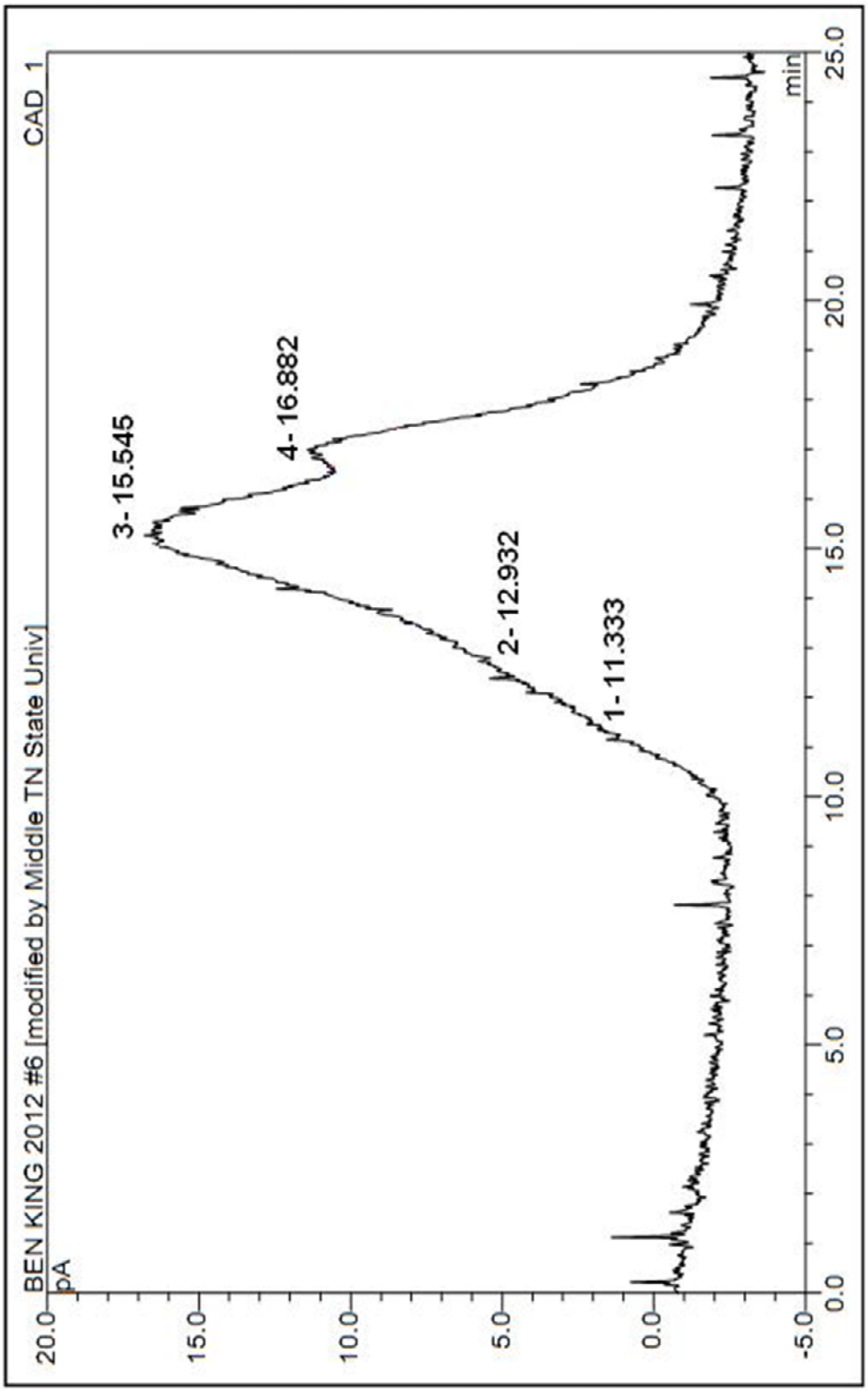

Figure 20. HPLC chromatogram of CP1. Molecular masses are as followed: 1-109,837 Da, 2-23,175 Da, 3-2,650 Da, and 4-1,002 Da.

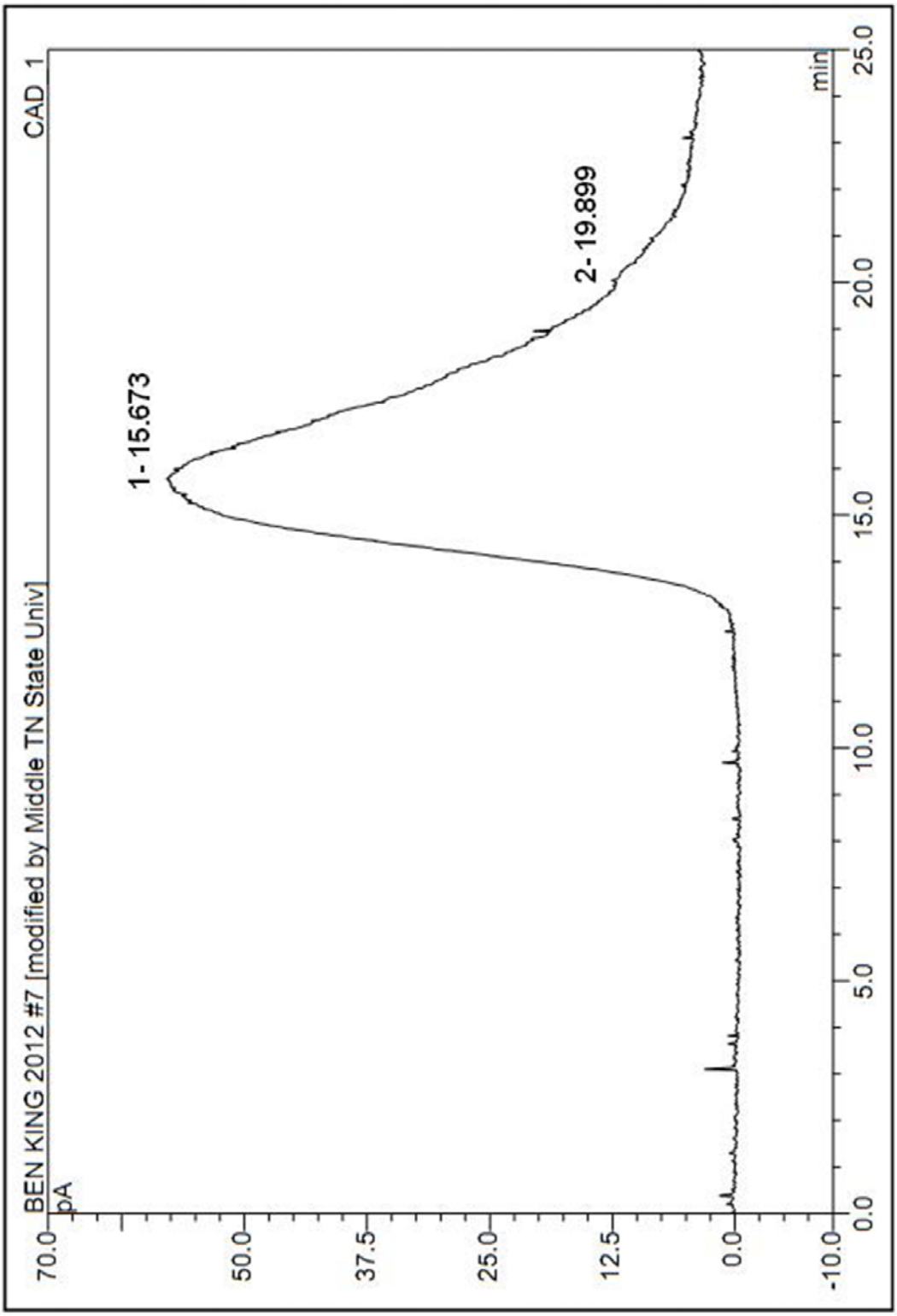

Figure 21. HPLC chromatogram of CP2. Molecular masses are as followed: 1-2,406 Da and 2-144 Da.

3.1.3 Fourier Transform Infrared (FTIR) Spectroscopy

The monomer, synthesized P3HT, solar cell P3HT, $HBrC_{60}$, CP1 and CP2 were analyzed using FTIR. In Figure 22 and Table 2, the monomer, synthesized P3HT, CP1, and CP2 were compared to show the progression of the material through the series of syntheses. Seen in Table 2, the area just above 3000 cm^{-1} shows a very weak absorption in all spectra, except for $HBrC_{60}$, due to the aromatic C-H stretching of the carbon and hydrogen at the C-4 position of the thiophene. One difference above 3000 cm^{-1} is the broad peak between 3300 cm^{-1} and 3600 cm^{-1} which is the result of the KBr pellets. This peak is not seen in the spectrum of the monomer since it was acquired using the ATR-attachment. Three strong peaks, between 2800 and 3000 cm^{-1}, are present in the spectra of all four materials. The peaks are the result of aliphatic C-H stretching on the hexyl group coming off the C-3 position on the thiophene. Below 1800 cm^{-1} there are many apparent differences between materials. One peak consistent amongst all four spectra is the peak around 1460 cm^{-1}, which is due to the C-H bending of the hexyl group. When comparing spectra of the monomer and synthesized P3HT, most of the peaks are similar with only a few additional peaks or replacement peaks. Two absorption peaks that can be found in the spectrum of the polymer, but not the monomer, 1631 cm^{-1} and 1680 cm^{-1}, are not easily identified. The peaks appear to be a result of unsymmetrical C=C stretching in a conjugated system.[32] In Figure 23, the synthesized P3HT and Solar Cell P3HT (purchased P3HT) are compared and shown to have nearly identical spectra. The main difference is how the peaks are shifted or

Table 2.
Comparison between Infrared Absorption Peaks of Six Materials

Monomer	Synth. P3HT	Solar Cell P3HT	HBrFullerene-C_{60}	CP1	CP2
Wavelengths (cm^{-1})	Wavelengths (cm^{-1})	Wavelengths (cm^{-1})	Wavelengths (cm^{-1})	Wavelengths (cm^{-1})	Wavelengths (cm^{-1})
3081	3054	3058		3065	3051
2953	2954	2953		2954	2950
2925	2924	2926	2918	2921	2921
2855	2854	2855	2850	2853	2852
1712	1768	1718			
	1679	1676			1665
	1631		1635		
1535	1538	1516	1538		
1462	1458	1458		1457	1458
			1428	1427	1428
	1419				
1404					
1377	1376	1376			1375
1356		1338			
	1261	1270		1260	
1217					
1192	1197	1185			
			1181	1180	1181
		1114			
1095	1094			1097	1097
996	1019			1019	
910	923		908		
828	831	834		801	838
725	725	725			726
	616			622	636

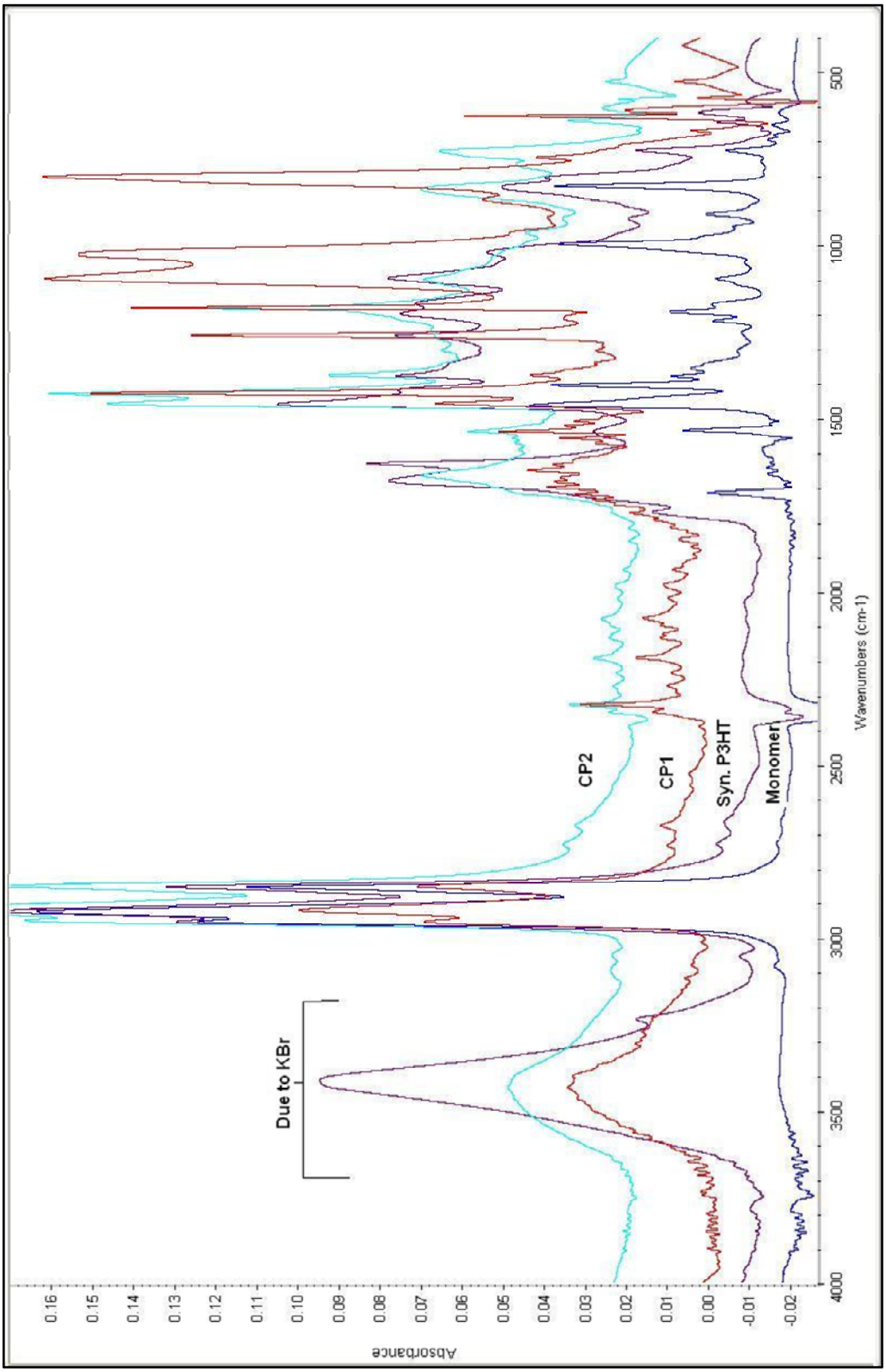

Figure 22. Infrared absorption spectra comparison for monomer, synthesized P3HT, CP1, and CP2.

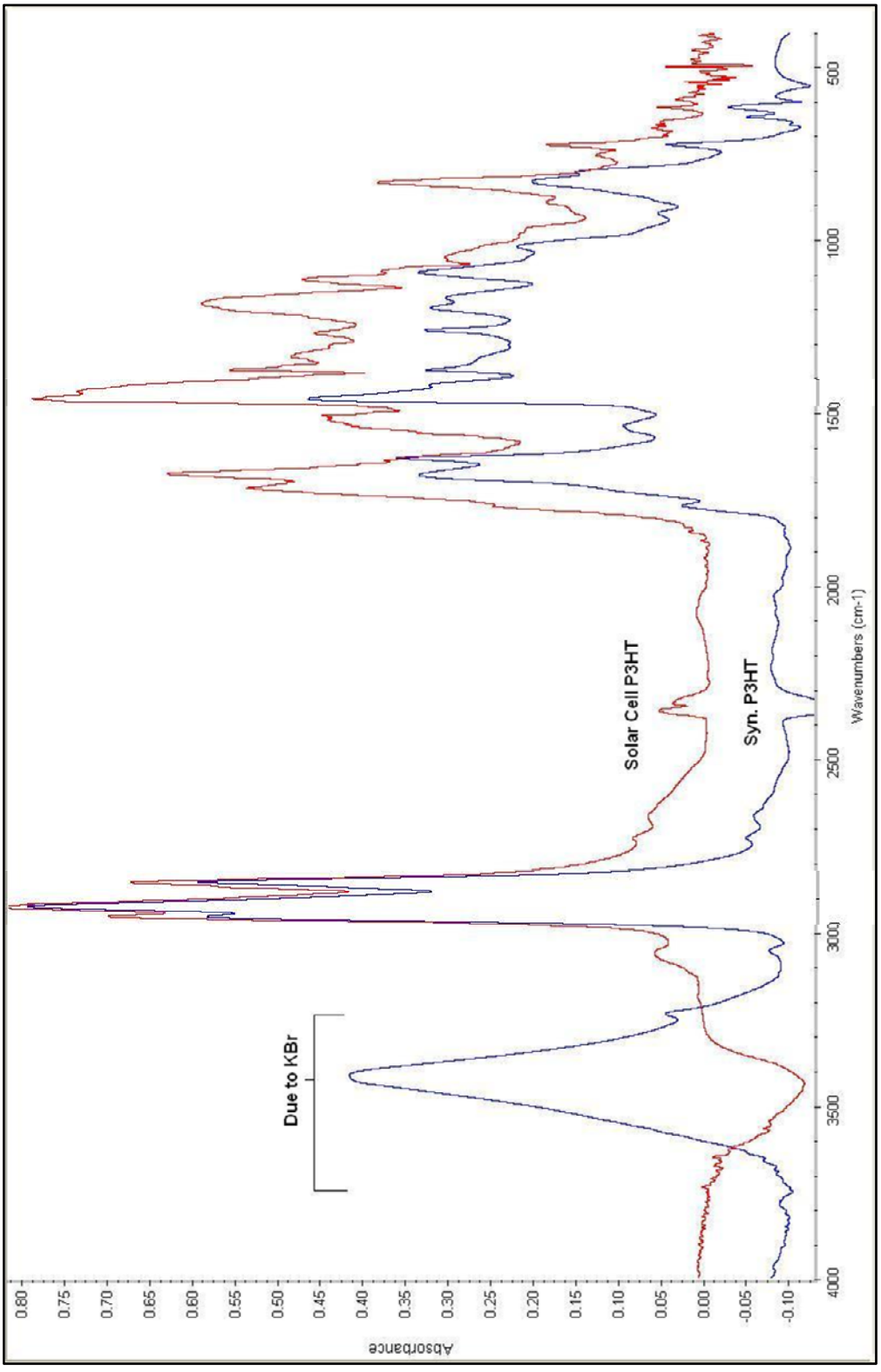

Figure 23. Comparison between synthesized and solar cell P3HT (purchased) IR absorption spectra.

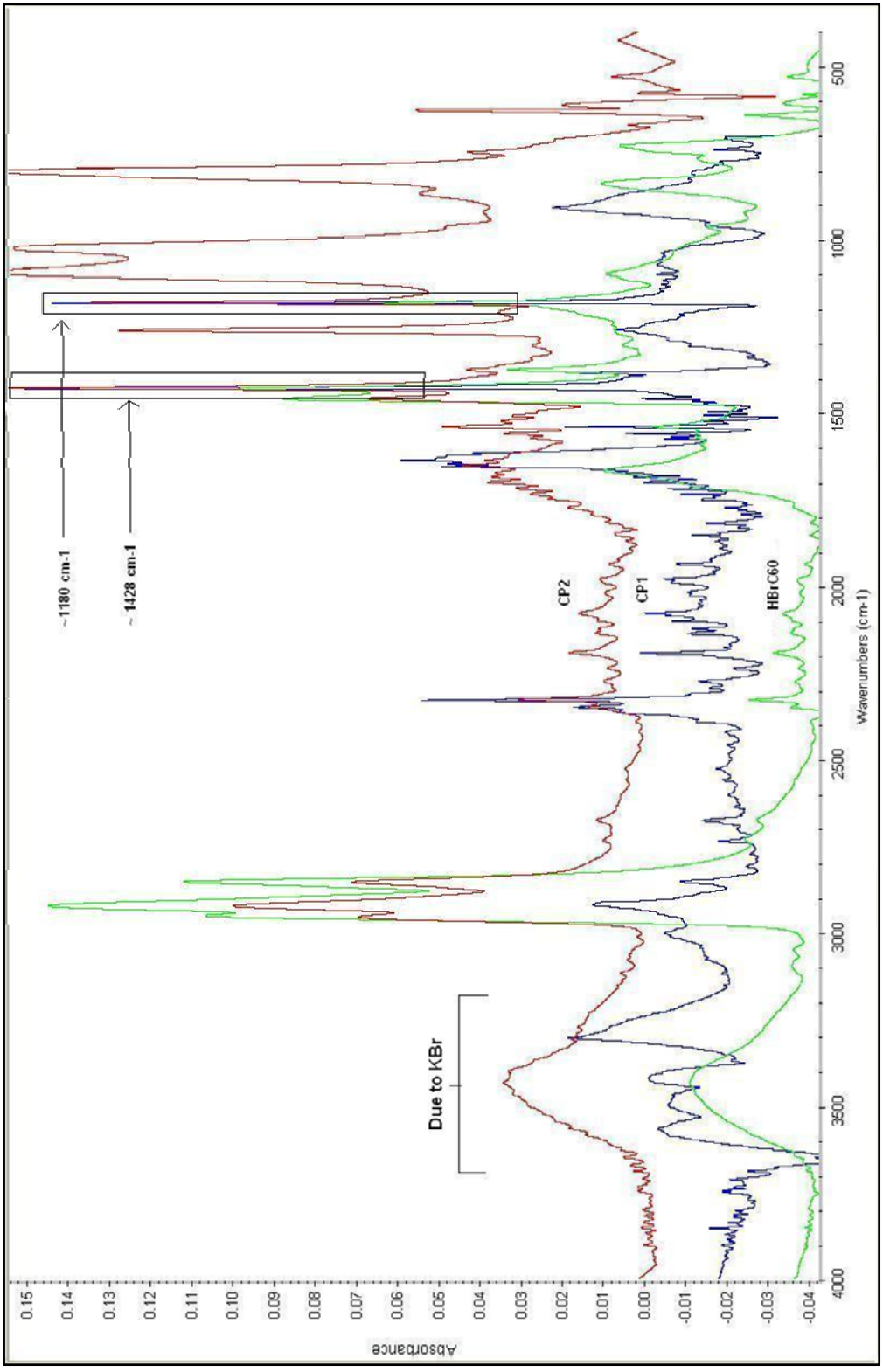

Figure 24. Comparison between IR absorption spectra of CP1, CP2 and fullerene-C_{60}.

sharpened when the purchased polymer was analyzed, possibly a result of increased conjugation. The most important comparison, though, is between the synthesized P3HT and the coupled materials, seen in Figure 24 and Table 2. Though CP1 and CP2 have similarities with the synthesized P3HT, one main difference is the strong peaks at around 1180 cm^{-1} and 1428 cm^{-1}. As seen in Figure 24, the peaks at those two positions are distinct peaks found in the spectrum of $HBrC_{60}$ as a result of the fullerene C_{60}.[33] Appearance of the two mentioned peaks in the coupled materials lead to the assumption that both Coupling Methods were successful.

3.1.4 ^{1}H NMR Spectroscopy

All materials stated in Section 3.1.4 were analyzed by ^{1}H NMR spectroscopy after each step and compared to the other products. The NMR tubes were cleaned with a series of solvent washes, the last being with methanol. As seen in Figures 26 through 29, there is a peak around 3.5 ppm, which is a result of residual methanol from the cleaning process. The spectrum of the monomer, seen in Figure 25 and Table 3, shows peaks from 0.8 ppm to 2.5 ppm, which were the result of the aliphatic hydrogens on the hexyl group. There was also a single peak at 6.9 ppm, which was the result of the lone hydrogen on the C-4 position of the thiophene. The ^{1}H NMR spectrum for the synthesized P3HT, seen in Figure 26, differs from the monomer in the aliphatic region. There are now multiple broad peaks in the aliphatic region which are also a result of the hexyl group as seen in Table 3. These peaks are broaden due to effects seen for

Table 3.
^{1}HNMR Peak Comparison between Six Materials

Carbon Position	Monomer Peaks (ppm)	Syn. P3HT Peaks (ppm)	Purch. P3HT Peaks (ppm)	$HBrC_{60}$ Peaks (ppm)	CP1 Peaks (ppm)	CP2 Peaks (ppm)
a	0.89 (t, 3H)	0.87 (s, 3H)	0.89 (s, 3H) 0.97 (s, 3H)		0.86 (s, 3H)	0.82 (s, 3H)
b	1.30 (sept., 6H)	1.31 (s, 6H) 1.41 (s, 6H)	1.33 (s, 6H) 1.42 (s, 6H)		1.27 (s, 6H)	1.23 (s, 6H)
c	1.54 (quint., 2H)	1.52 (s, 2H) 1.67 (s, 2H)	1.60 (s, 2H) 1.68 (s, 2H)		1.59 (s, 2H)	1.54 (s, 2H)
i				1.63 (s, 1H)		
d	2.51 (t, 2H)	2.52 (s, 2H) 2.78 (s, 2H)	2.57 (s, 2H) 2.78 (s, 2H)		2.49 (s, 2H)	2.46 (s, 2H) 2.72 (s, 2H)
e	6.96 (s, 1H)	6.95 (s, 1H)	6.97 (s, 1H)		7.20 (d, 1H) 7.45 (d, 1H)	6.92 (s, 1H) 7.16 (t, 1H) 7.39 (t, 1H)

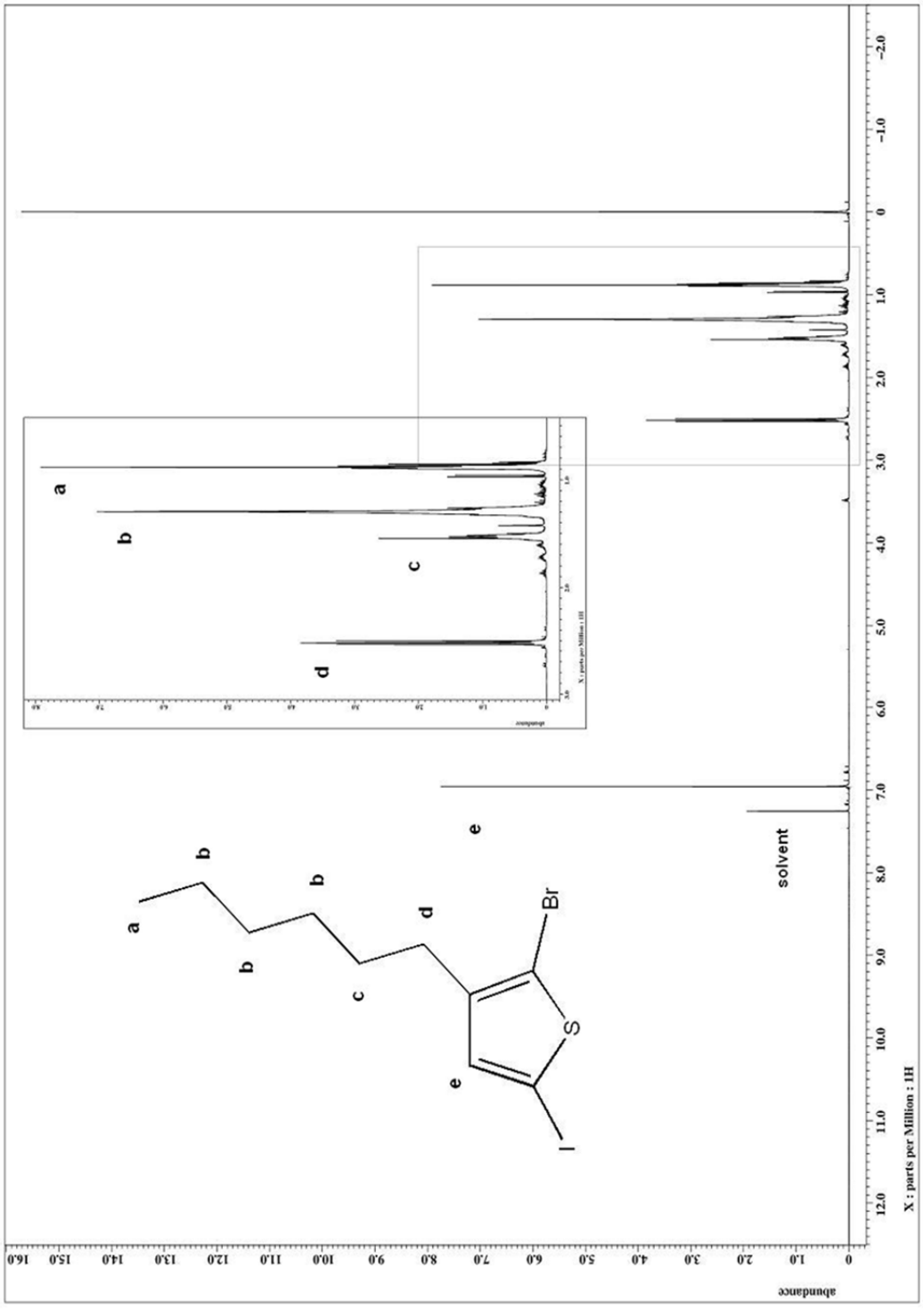

Figure 25. ^{1}H NMR spectrum of the monomer, 2-bromo-3-hexyl-5-iodothiophene.

macromolecules. Polymers exhibit anisotropic tumbling instead of the isotropic tumbling seen for smaller molecules. As a result, there is not a clear average for the protons along the chain, giving less resolution and broad peaks. The appearance of extra peaks is the result of areas of regioregular or highly conjugated material causing further delocalization of electrons and greater de-shielding of hydrogens on the hexyl group. Between 2.5 ppm and 3.0 ppm, we see two broad peaks which are a result of an aliphatic hydrogen adjacent to a regioregular or highly conjugated P3HT backbone (2.7 ppm) and an aliphatic hydrogen adjacent to a regiorandom or lowly conjugated P3HT backbone (2.5 ppm). The ratio of the area between the two can be used to determine the percentage of regioregular material, the desired product for high crystallinity.[34] Based on the spectra there is 79.6% regioregular species for the synthesized material. In comparison, the purchased P3HT has around 91.0% regioregularity, as seen in Figure 27. In the aromatic region, there was no difference between the synthesized P3HT and bought P3HT, and only a broadening of the one aromatic peak between the P3HT products and the monomer, due to same effects seen in the aliphatic region.

The ^{1}H NMR spectrum of $HBrC_{60}$ is shown in Figure 28. There is one peak in the aliphatic region at 1.6 ppm shown in the spectrum, which is the result of a substituted hydrogen atom on the fullerene-C_{60}. The peak is not split leading to the belief that either there is only one hydrogen atom substituted on the fullerene or there are no hydrogens in close proximity of each other.

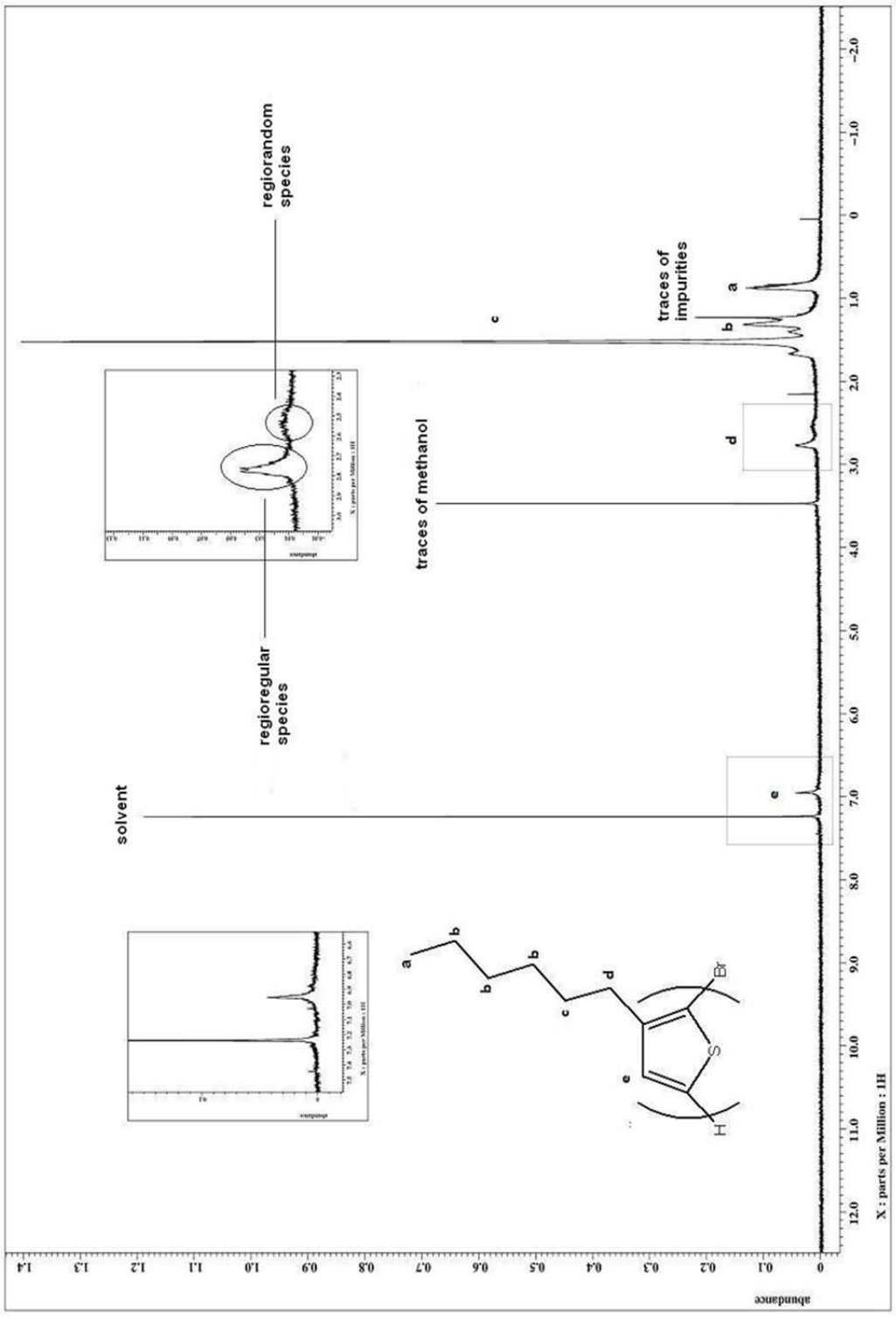

Figure 26. ^{1}H NMR spectrum of the synthesized P3HT.

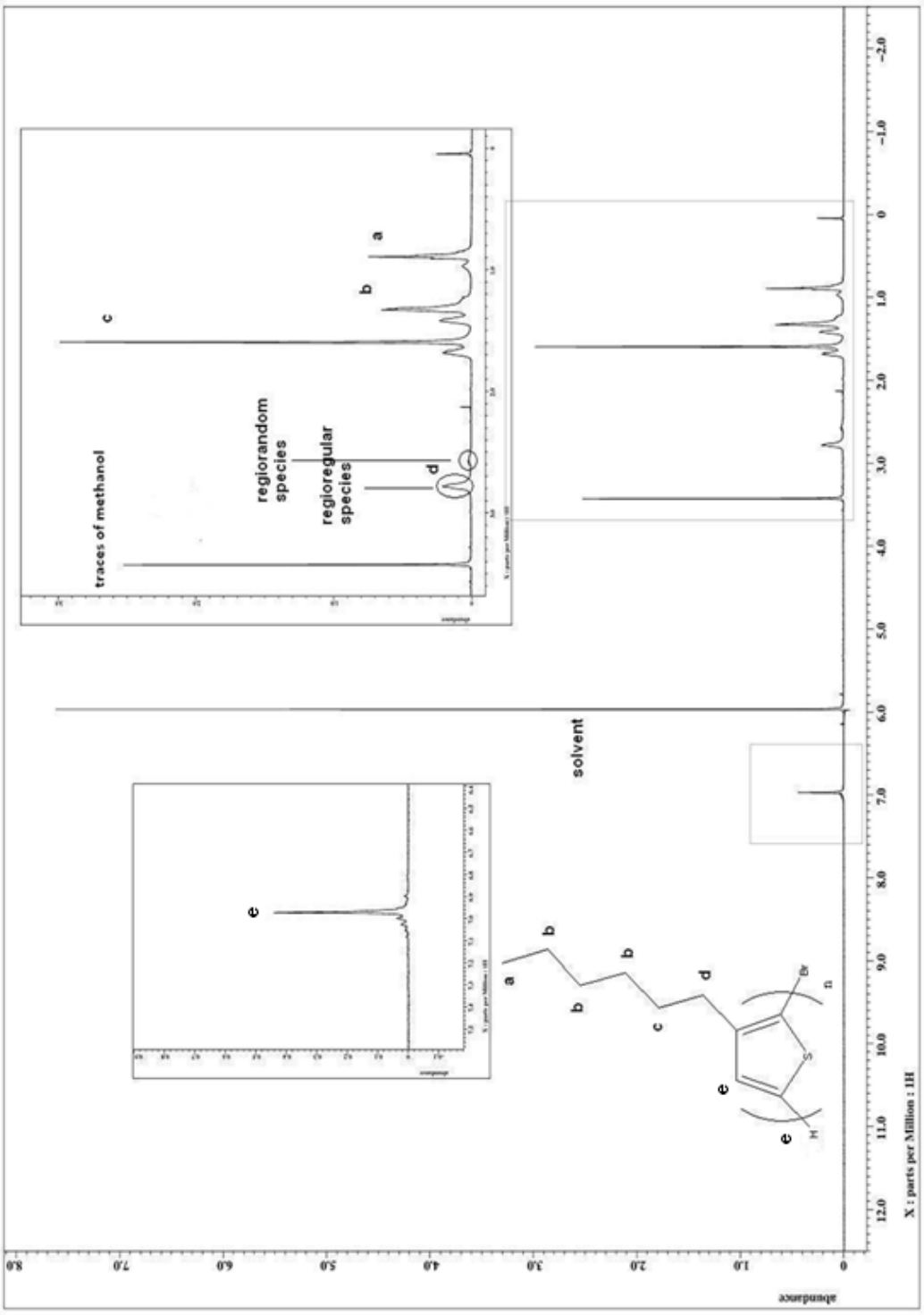

Figure 27. ^{1}H NMR spectrum of the purchased P3HT (solar cell P3HT).

The ^{1}H NMR spectra of CP1 and CP2 were compared to the spectra for the synthesized P3HT and the $HBrC_{60}$. As seen in Figures 29 and 30, the coupled materials have similar spectra to the synthesized P3HT in aliphatic region below 2.0 ppm. The aliphatic peak at 1.5 ppm in the $HBrC_{60}$ spectra could not be distinguished from the peaks associated with P3HT. Above 2.0 ppm in the aliphatic region, there is only one peak for the CP1 product which is at the same chemical shift as the regiorandom or lowly conjugated species of the synthesized P3HT. Based on the disappearance of the peak at 2.7 ppm, the CP1 product must have low conjugation due to both steric hindrance of the fullerene-C_{60} and the hexyl group's proximity to the fullerene-C_{60}. The CP2 product has peaks at both 2.5 and 2.7 ppm, but the highly conjugated material only makes up 37% of the product based on the ratio between the areas of the peaks. Steric hindrance is reduced in the CP2 product compared to the CP1 product, but the fullerene-C_{60} still decreases the co-planarity of the P3HT chains. When comparing the aromatic peaks of the coupled products to the synthesized P3HT there are many differences. Seen in Table 3, there are two doublet peaks found at 7.20 ppm and 7.45 ppm for the CP1 product instead of one singlet peak at 6.96 ppm seen for the synthesized P3HT. The two shifted peaks are the result of two types of low conjugated species which are further de-shielded by the very electron withdrawing fullerene-C_{60}. Splitting of peaks is due to interactions between hydrogens, but there are no adjacent carbons with substituted hydrogens close to the aromatic hydrogen on the thiophene. Due to twisting of the P3HT backbone from steric hindrance there could be interactions between aromatic hydrogens on other thiophenes

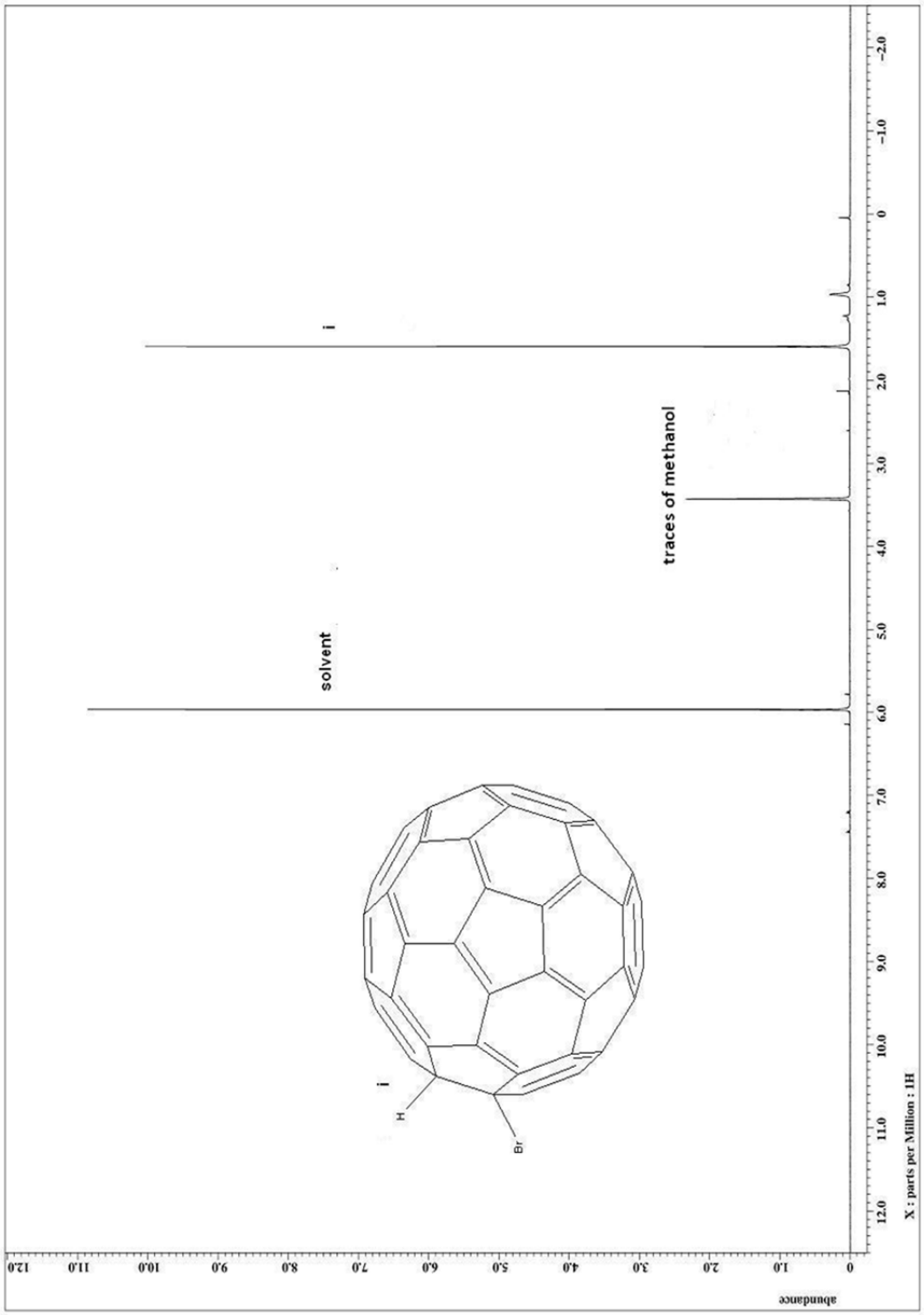

Figure 28. ^{1}H NMR spectrum of the $HBrC_{60}$.

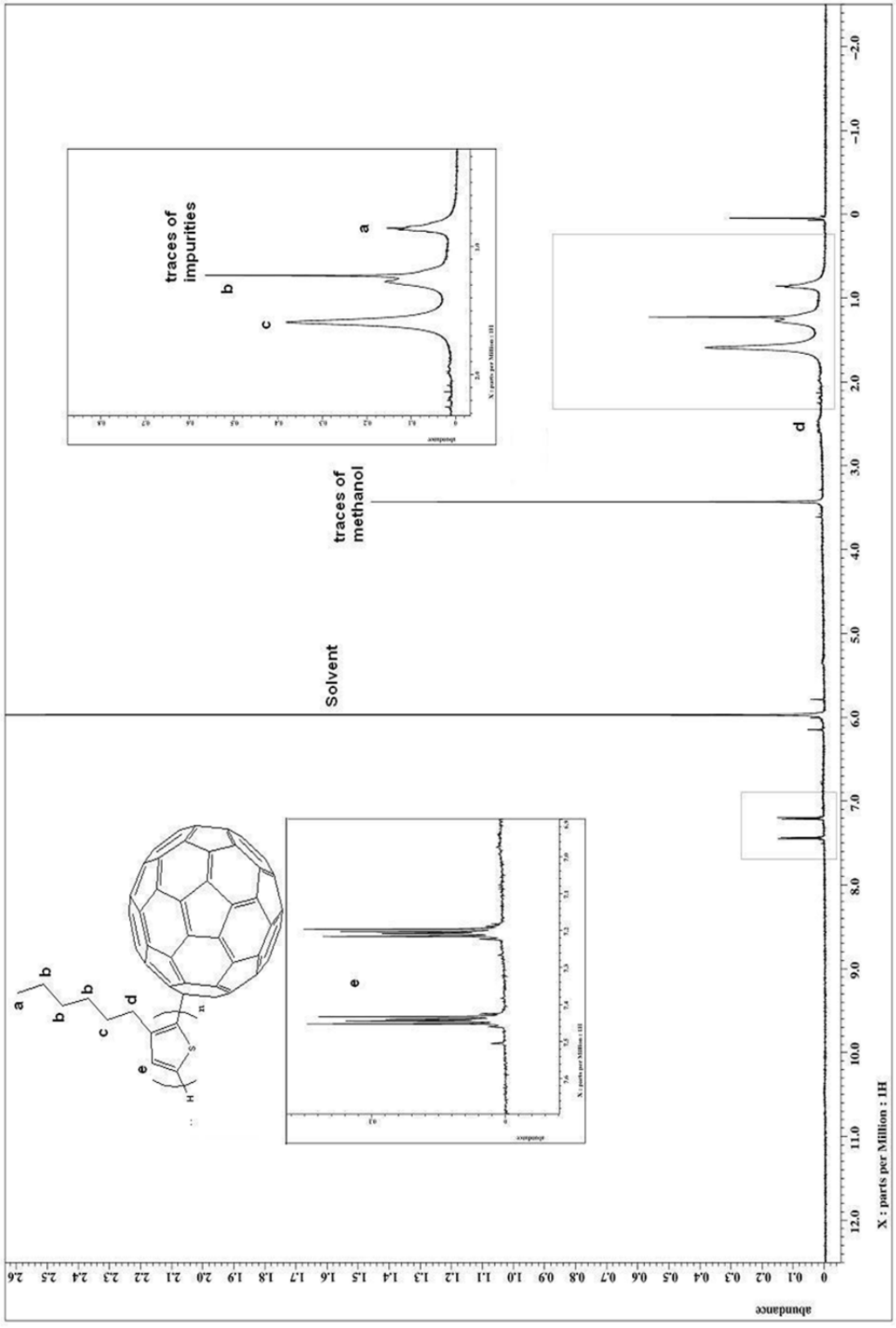

Figure 29. ^{1}H NMR spectrum of the CP1.

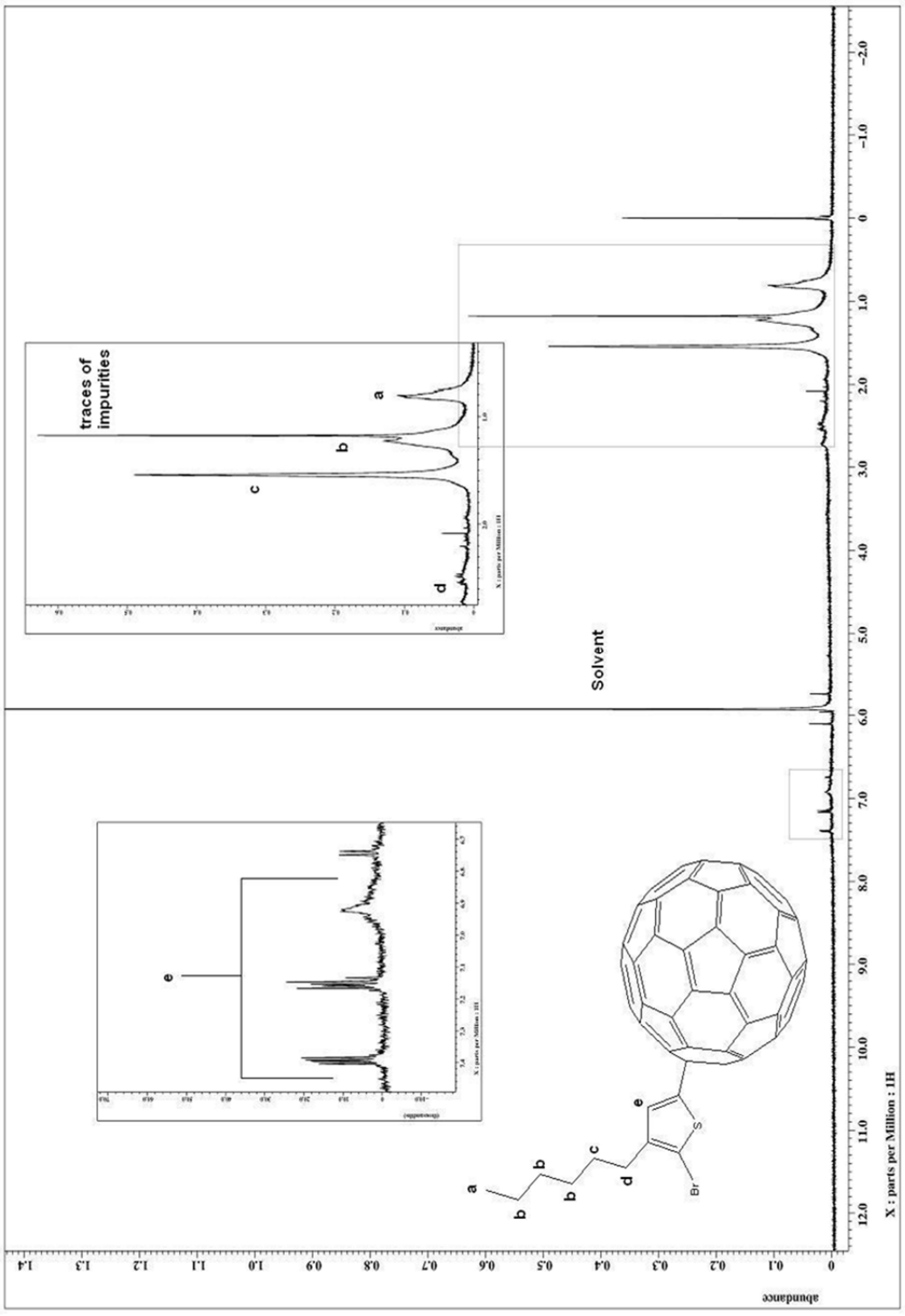

Figure 30. ^{1}H NMR spectrum of the CP2.

or aliphatic hydrogens on the hexyl group undergoing long-range coupling with the aromatic hydrogen. The CP2 product has three aromatic peaks: a singlet at 6.92 ppm, a triplet at 7.16 ppm, and a triplet at 7.39 ppm. The peak at 6.92 ppm is the result of coplanar, highly conjugated areas along the P3HT backbone. The peaks at 7.16 ppm and 7.39 ppm are a result of the same effects seen for the CP1 product.

Based on the ^{1}H NMR results, the synthesized P3HT has a lower regioregularity than the purchased P3HT. Due to a higher molecular mass and regioregularity, the purchased P3HT would give higher crystallinity and would be more ideal for uses in the solar cell active layer. The coupled materials showed a decrease in conjugation of the P3HT chain, which could result in either a disruption in the P3HT crystals or the coupled material still being segregated from the crystal material. One positive result could be increased charge separation due to the observed electron affinity of the fullerene-C_{60} seen by the de-shielding of the aromatic hydrogen atoms. Further analysis was done to determine the effect of the coupled material on the crystallinity of P3HT.

3.1.5 ^{13}C NMR Spectroscopy

All samples from Section 3.1.5 were also run overnight for ^{13}C NMR Spectroscopy and the peaks were tabulated, as seen in Table 4. The ^{13}C NMR spectrum for the monomer, seen in Figure 31, has several peaks in the aliphatic region due to the carbons of the hexyl group. There are two peaks in the aromatic region between 135 ppm and 145 ppm that correlate with the carbons at the C-3 and C-4 position of the thiophene. The peak

Table 4.
^{13}CNMR Peak Comparison between Six Materials

Carbon Position	Monomer Peaks (ppm)	Syn. P3HT Peaks (ppm)	Purch. P3HT Peaks (ppm)	HBrC60 Peaks (ppm)	CP1 Peaks (ppm)	CP2 Peaks (ppm)
a	14.1	14.1	14.4		14.2	14.2
b	22.6	22.6	22.9		22.7	23.0
c	28.8	28.8	29.3		29.1	
d	29.2	29.2	29.7		29.5	29.7
e	29.6	29.6	30.6		30.5	
f	31.6	31.6	31.9		31.8	31.8
i				31.3		
ii				120.5		
g	71.0	128.2	130.4		128.7	
h	111.7	108.8	133.7		130.6	
j	137.9	125.1	128.5		127.8	
k	144.2	142.0	140.2			
iii				143.2	143.2	143.2

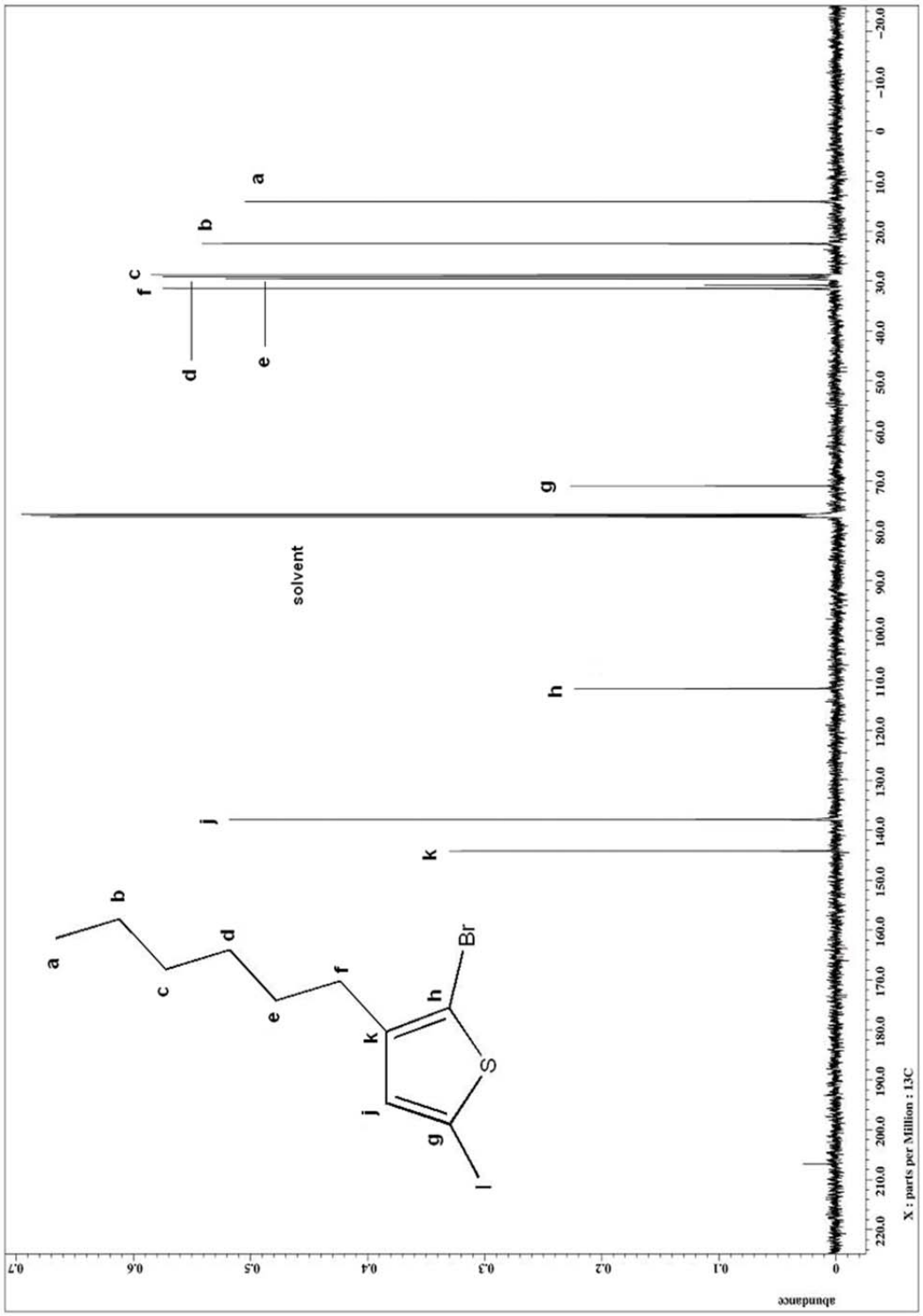

Figure 31. ^{13}C NMR spectrum of the monomer.

found at around 112 ppm is due to the carbon adjacent to the bromine and the peak found at 71 ppm is a result of the carbon adjacent to the iodine, seen in Figure 31. The bromine and iodine on the thiophene cause the aromatic carbon signals to shift up field due to an increase of shielding of the carbon nuclei by the halogen atoms. The ^{13}C NMR spectrum for the synthesized P3HT, seen in Figure 32, is similar to the monomer at the aliphatic region, but has shifting in aromatic region. There are four aromatic peaks which are the result of the four aromatic carbons. The peak at 71 ppm is no longer there due to the iodine being removed during the polymerization, but a peak at 108 ppm is present in the spectrum which is a result of the bromine remaining as an end group. The spectrum for the purchased P3HT, Figure 33, is nearly identical to the synthesized P3HT except for the peak around 110 ppm, which is shifted downfield due to the absence of a bromine end group.

The ^{13}C NMR spectrum of the $HBrC_{60}$, seen in Figure 34, shows three peaks, two in the aromatic region and one in the aliphatic region. The aromatic peaks are due to the vinyl carbons of the fullerene-C_{60} and the aliphatic peak is a result of the carbon with a substituted hydrogen. A peak for the bromine substituted aliphatic carbon is not observed either due to poor signal or because the signal shifted beyond -20 ppm.[32] The ^{13}C NMR spectra of CP1 (Figure 35) and CP2 (Figure 36) products are compared to the spectrum of the synthesized P3HT (Figure 32). All three spectra have peaks in the aliphatic region that correlate to aliphatic carbons. All three also have peaks in the aromatic region, but with differences between all three. CP1 has several aromatic

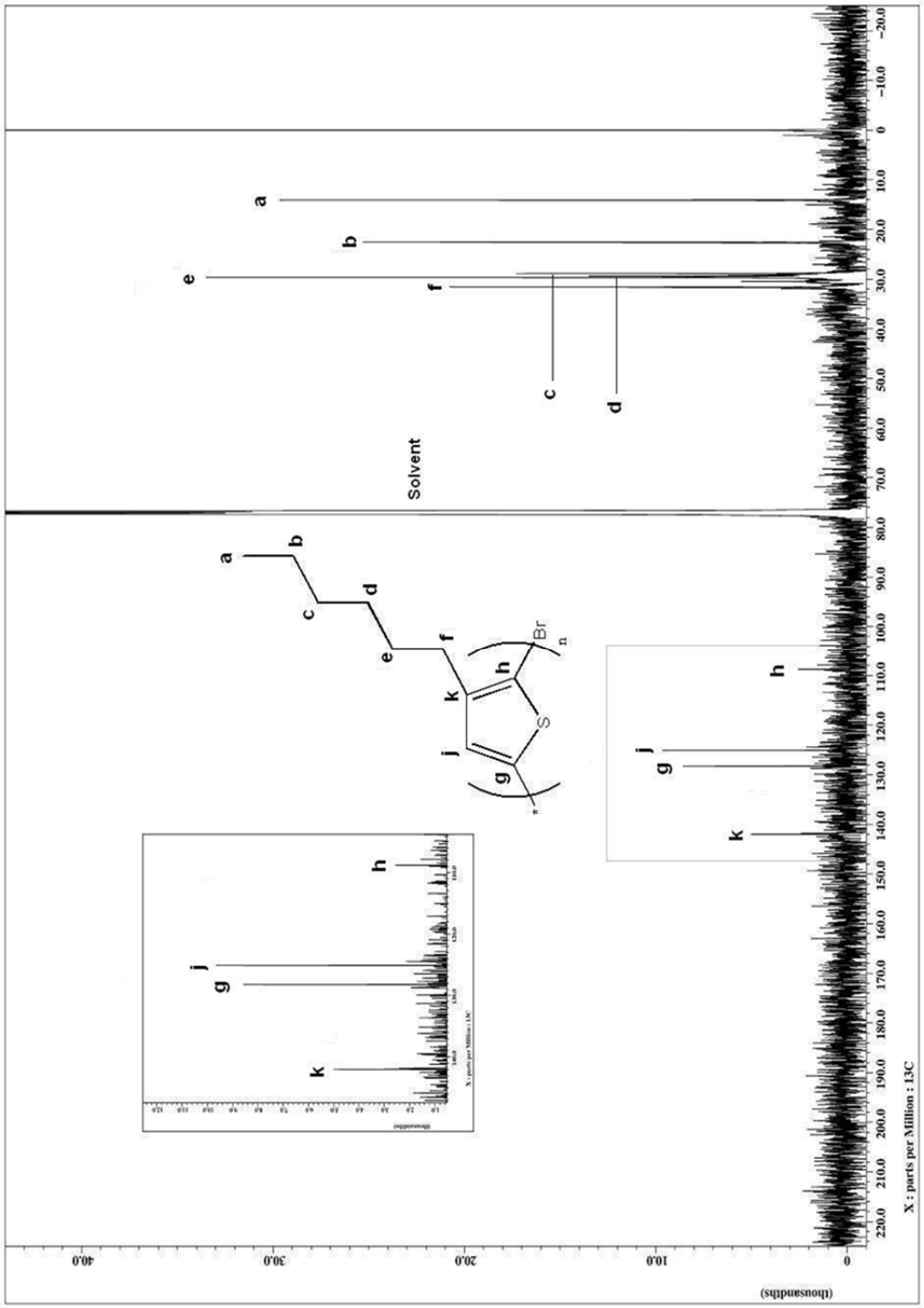

Figure 32. ^{13}C NMR spectrum of the synthesized P3HT.

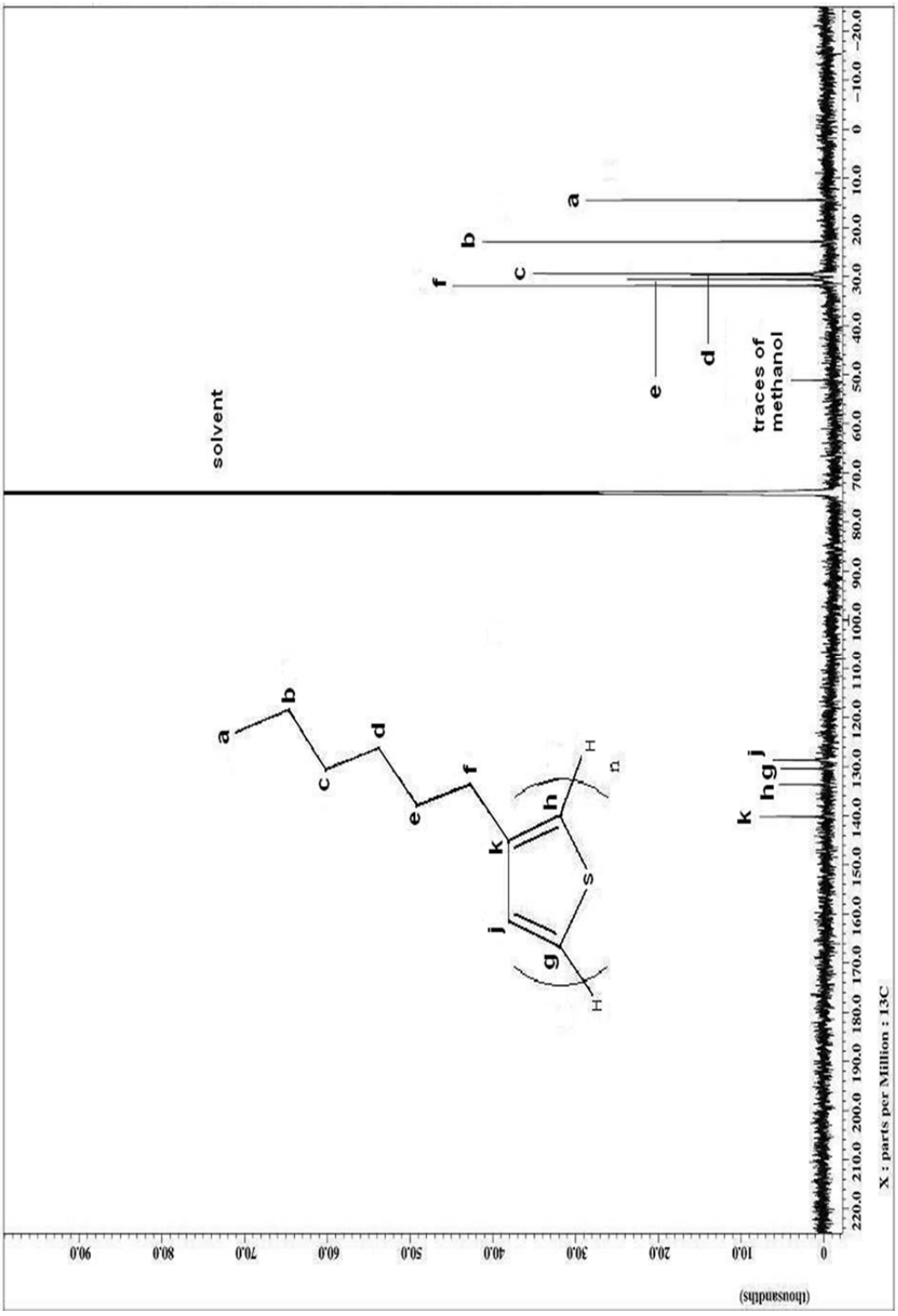

Figure 33. ^{13}C NMR spectrum of the purchased P3HT (solar cell P3HT).

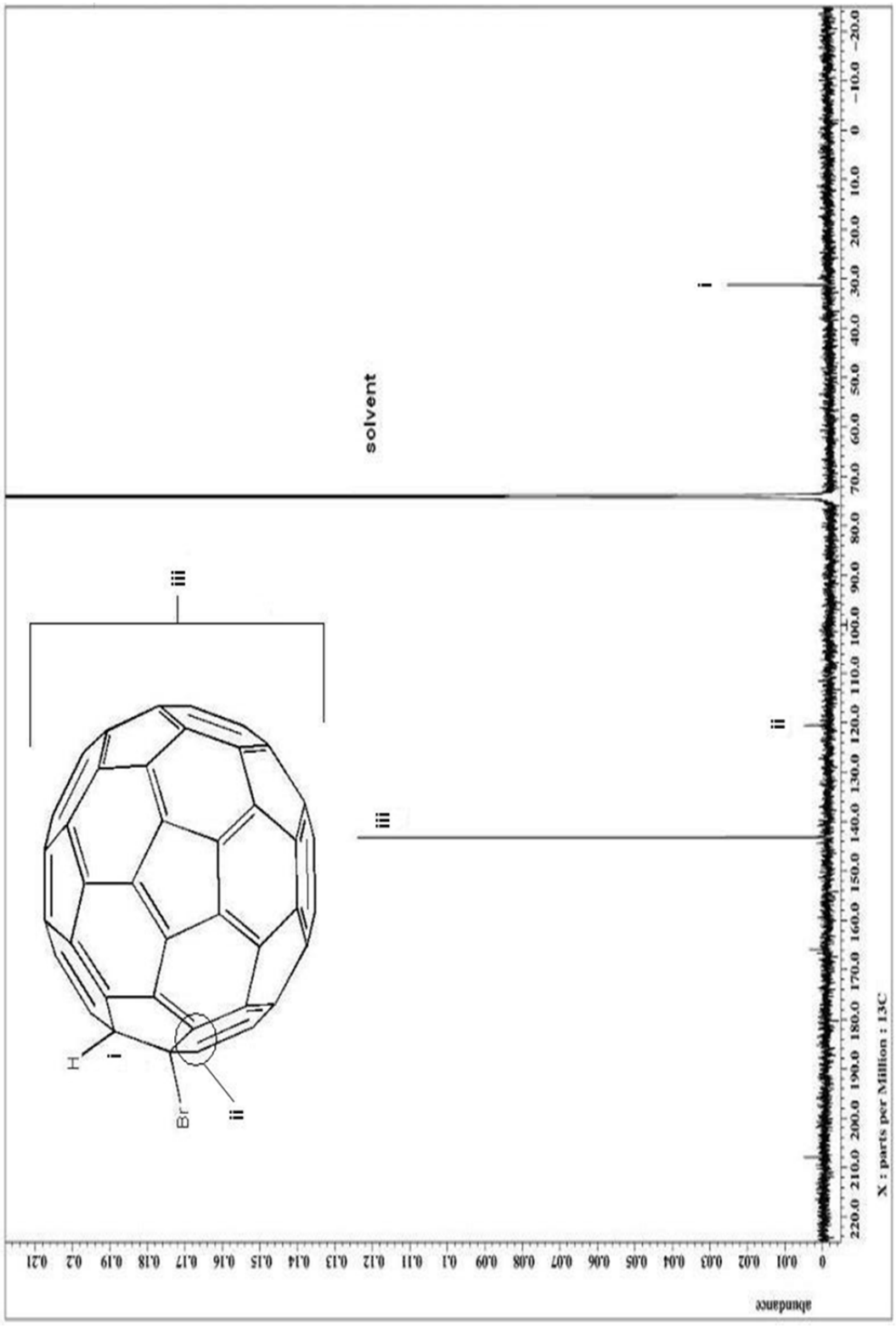

Figure 34. 13C NMR spectrum of the $HBrC_{60}$.

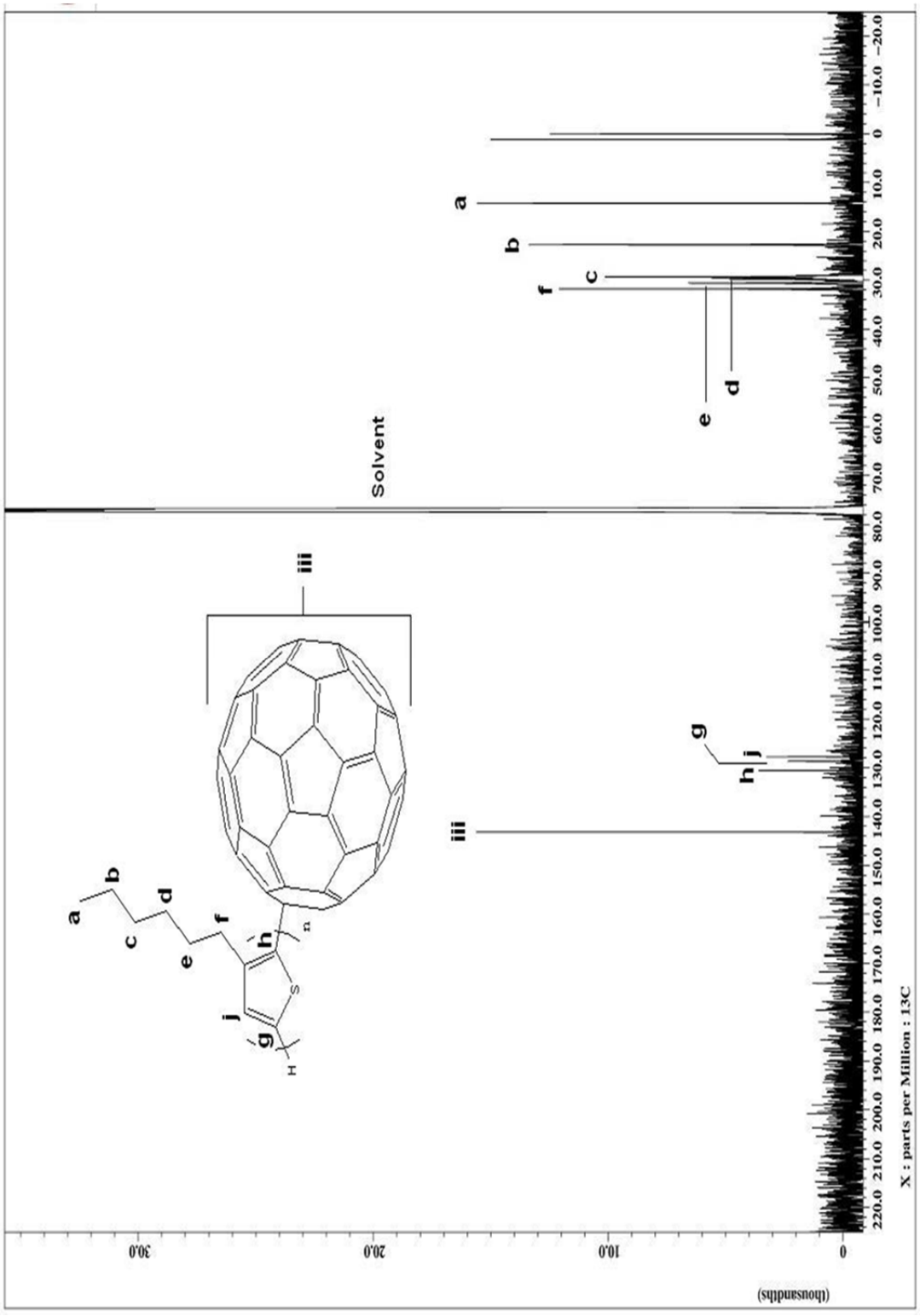

Figure 35. ^{13}C NMR spectrum of the CP1.

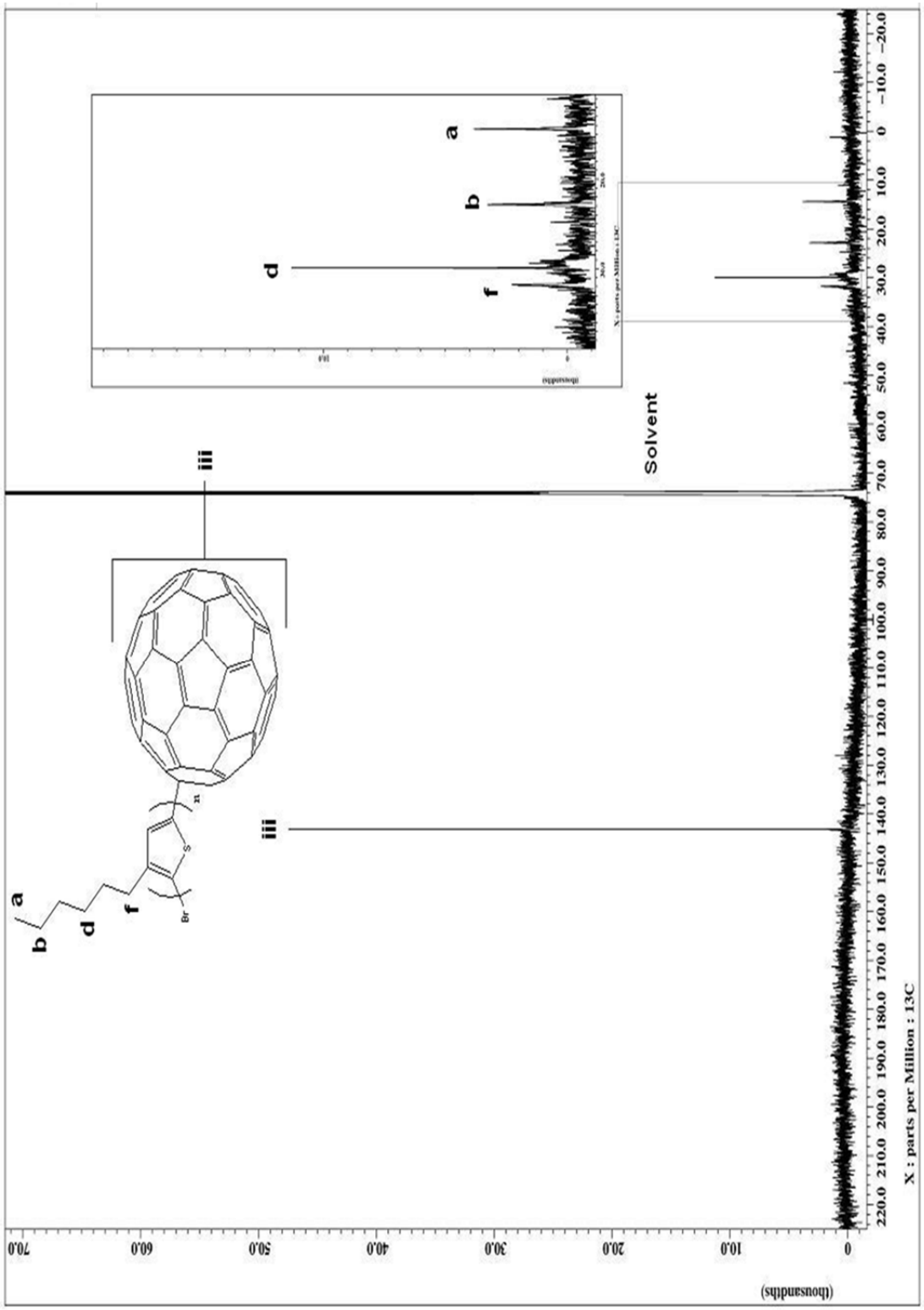

Figure 36. ^{13}C NMR spectrum of the CP2.

signals, three weaker signals that are very similar to the synthesized P3HT and a strong peak above 140 ppm resembling the peak found in the spectrum of $HBrC_{60}$. The synthesized P3HT also has a peak just above 140 ppm, but the signal is weaker. CP2, like CP1, has a strong peak above 140 ppm resembling the $HBrC_{60}$, but there are no other peaks in the aromatic region. Also the aliphatic peaks resulting from the hexyl group are very weak in comparison to the synthesized P3HT and CP1. Discovered and described in a later section, Section 3.2.2, it is found that CP2 has high fullerene-C_{60} content, before separating the desired THF-soluble material from the insoluble, because of low molecular mass P3HT coupled to the fullerene-C_{60}. The pre-separated CP2 analyzed through NMR spectroscopy has a higher fullerene-C_{60} content resulting in weaker P3HT carbon peaks. The presence of the strong signal above 140 ppm in both coupled materials confirms the materials were coupled. Based on analysis from Sections 3.1.2 through 3.1.6, the procedures from both Coupling Methods were successful, but the synthesized P3HT would be insufficient for use in the solar cells. In further analysis only materials used within the solar cell would be tested.

3.2 Characterization of Solar Cell Materials

3.2.1 Thermogravimetric Analysis

Thermogravimetric Analysis (TGA) was performed on the purchased (solar cell) P3HT, fullerene- C_{60}, CP1, and CP2, as well as the THF soluble and insoluble CP2 products. From

Figures 37 through 42, decomposition temperatures and percentage mass losses were obtained and tabulated, as seen in Table 5.

Table 5
TGA Thermograms of Solar Cell Materials

Decomposition	Temperature / % Weight Loss	Solar Cell P3HT	Fullerene-C_{60}	CP1	CP2	CP1 Insoluble	CP2 Soluble
1st	Temperature	400 - 570 °C	200 - 550 °C	140 -200 °C	50 - 85 °C	330 - 550 °C	180 - 290 °C
	% Weight Loss	69.15%	4.86%	0.65%	1.90%	9.25%	6.06%
2nd	Temperature	590 - 740 °C	610 - 780 °C	200 - 375 °C	200 - 550 °C	600 - 690 °C	290 - 400 °C
	% Weight Loss	30.07%	94.69%	24.31%	20.20%	85.56%	10.20%
3rd	Temperature	N/A	N/A	375 - 525 °C	600 - 650 °C	N/A	400 - 600 °C
	% Weight Loss			13.58%	50.79%		25.17%
4th	Temperature	N/A	N/A	605 - 670 °C	650 - 705 °C	N/A	600 - 760 °C
	% Weight Loss			49.96%	17.64%		56.13%
5th	Temperature	N/A	N/A	805 - 900 °C	800 - 900 °C	N/A	N/A
	% Weight Loss			2.96%	1.33%		

The results were used to determine the upper temperature limits for the analysis by Differential Scanning Calorimetry (DSC) and to further determine the composition of the material. As seen in Figure 37 and Table 5, the solar cell P3HT decomposed sharply between 400 °C and 570 °C with a loss of 69.15% of its total mass. Just before 600 °C, when the gas was changed to compressed air, the solar cell P3HT began to decompose further. Except for a very small percentage, the remaining P3HT decomposed by 740 °C. In Figure 38, fullerene- C_{60} is shown to have small decompositions between 200 °C and

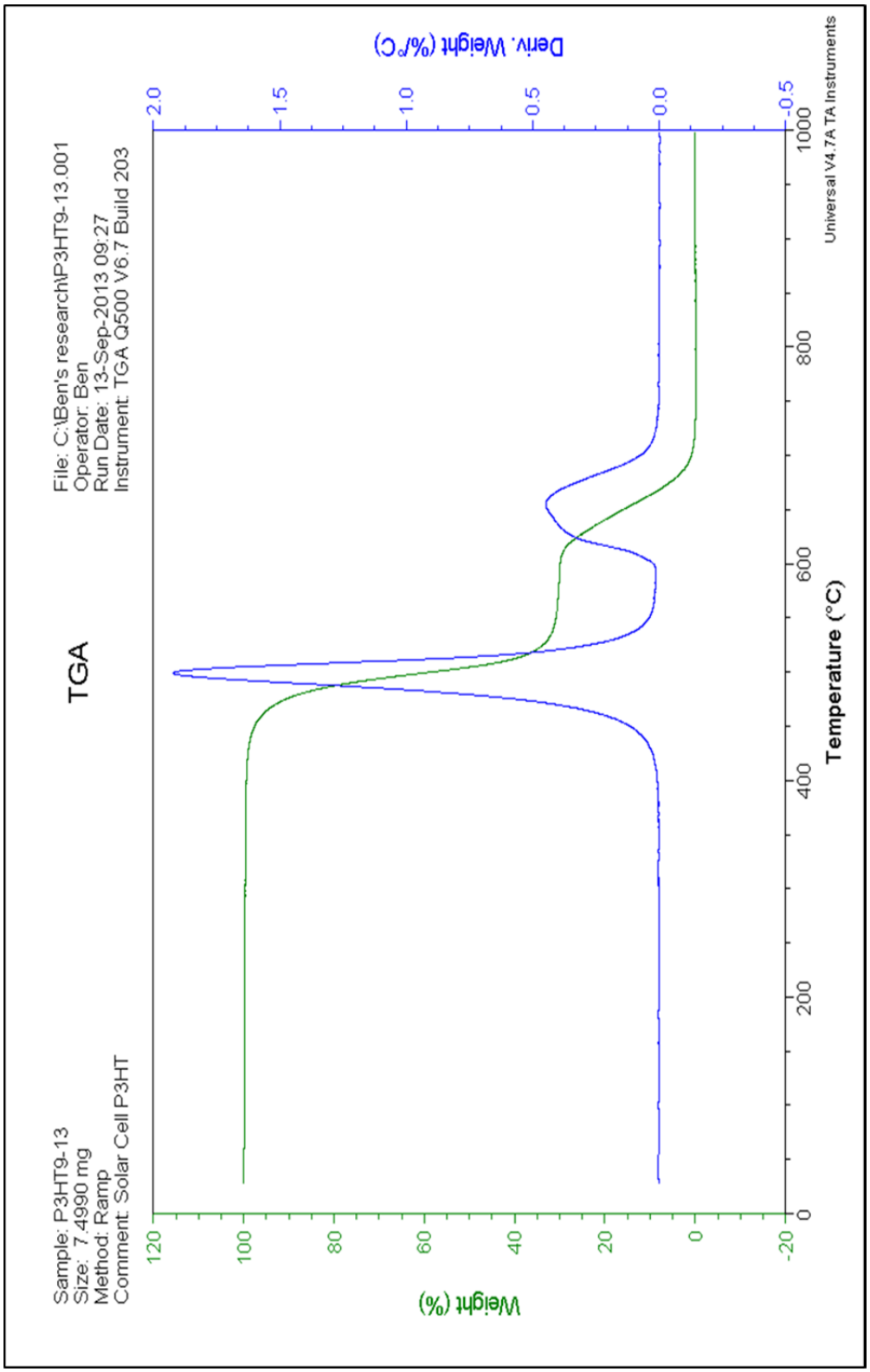

Figure 37. TGA thermogram of purchased P3HT (solar cell P3HT) along with its derivative to better observe mass loss vs. temperature.

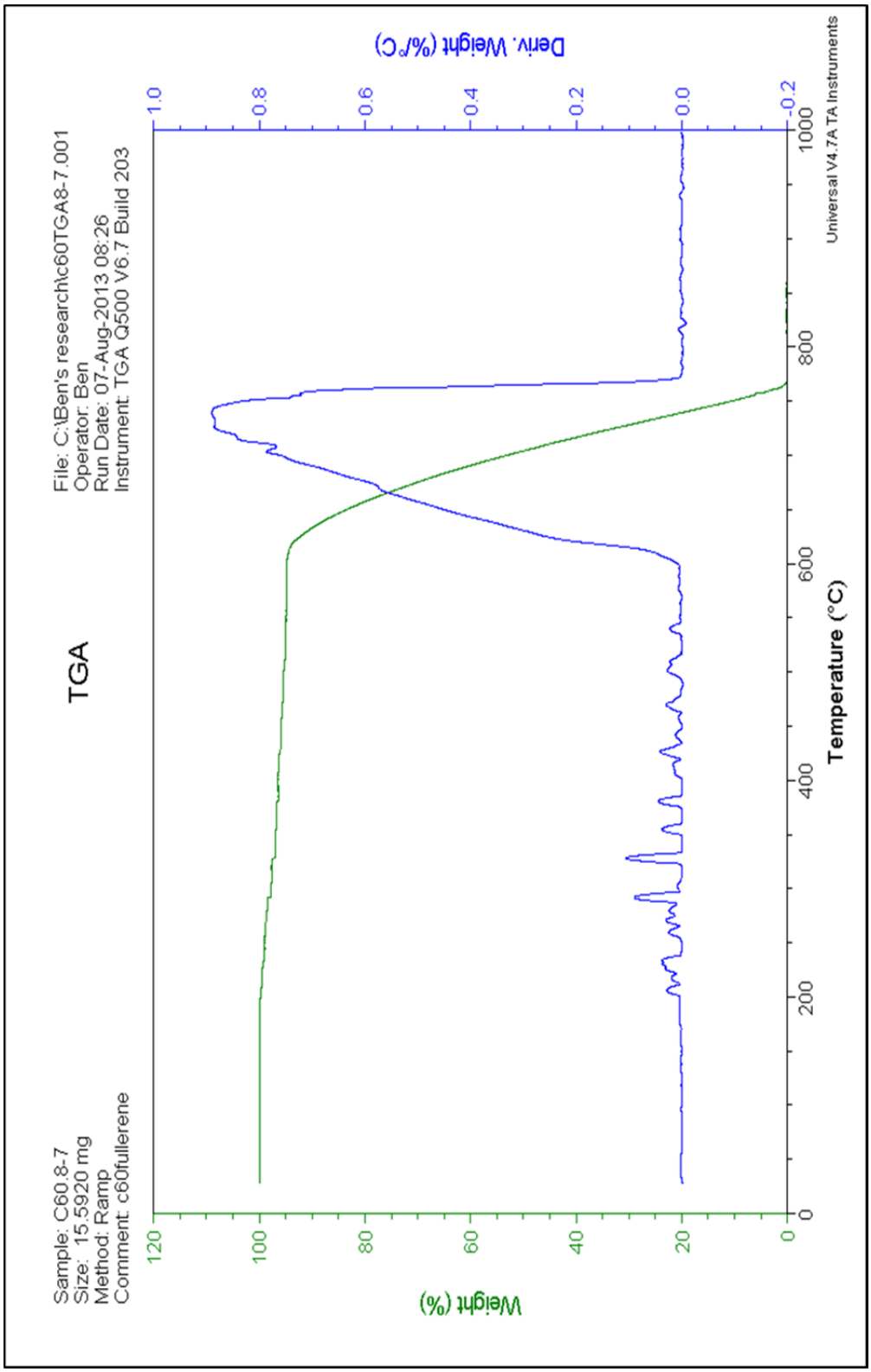

Figure 38. TGA thermogram of fullerene-C_{60} along with its derivative to better observe mass loss vs. temperature.

550 °C with only 4.86% mass loss. The fullerene- C_{60} does not have a drastic decomposition until after the gas change over from nitrogen to air. Between 610 °C and 780 °C, the fullerene- C_{60} loses 94.69% of its mass.

CP1 has five steps of decomposition, seen in Figure 39, with the first three happening in a nitrogen atmosphere and the last two in air. The total decomposition before 600 °C is a mass loss of 38.54% and after is a mass loss of 52.92%. If the decomposition of both the P3HT and fullerene- C_{60} of the coupled material resembled degradation of the pure materials, P3HT would make up 49% of the mass of the material. CP2 also had five decompositions, but only two were in nitrogen atmosphere, as seen in Figure 40. After adding the first two steps of decomposition of the CP2, seen in Table 5, there is a total mass loss of just over 22%. Three steps of decomposition follow when the gas is changed to air, giving a combined mass loss of just under 70%. CP2 material appears to have a lower percentage of its mass attributed to P3HT in comparison to CP1. The material was dissolved in THF and the soluble and insoluble materials were separated to both be run for TGA analysis. The insoluble and soluble materials' spectra are seen in Figures 41 and 42. Based on the figures and the data in Table 5, it is determined that during the Coupling Method 2 procedure, low molecular mass P3HT chains are also coupled to the fullerene- C_{60}. The low molecular mass coupled products are not removed through the methanol and acetone washes because of the low solubility of the fullerene- C_{60}. As seen in Figure 41, most of the mass of the THF insoluble material is due to the fullerene- C_{60}. The THF soluble material, however, has a composition similar

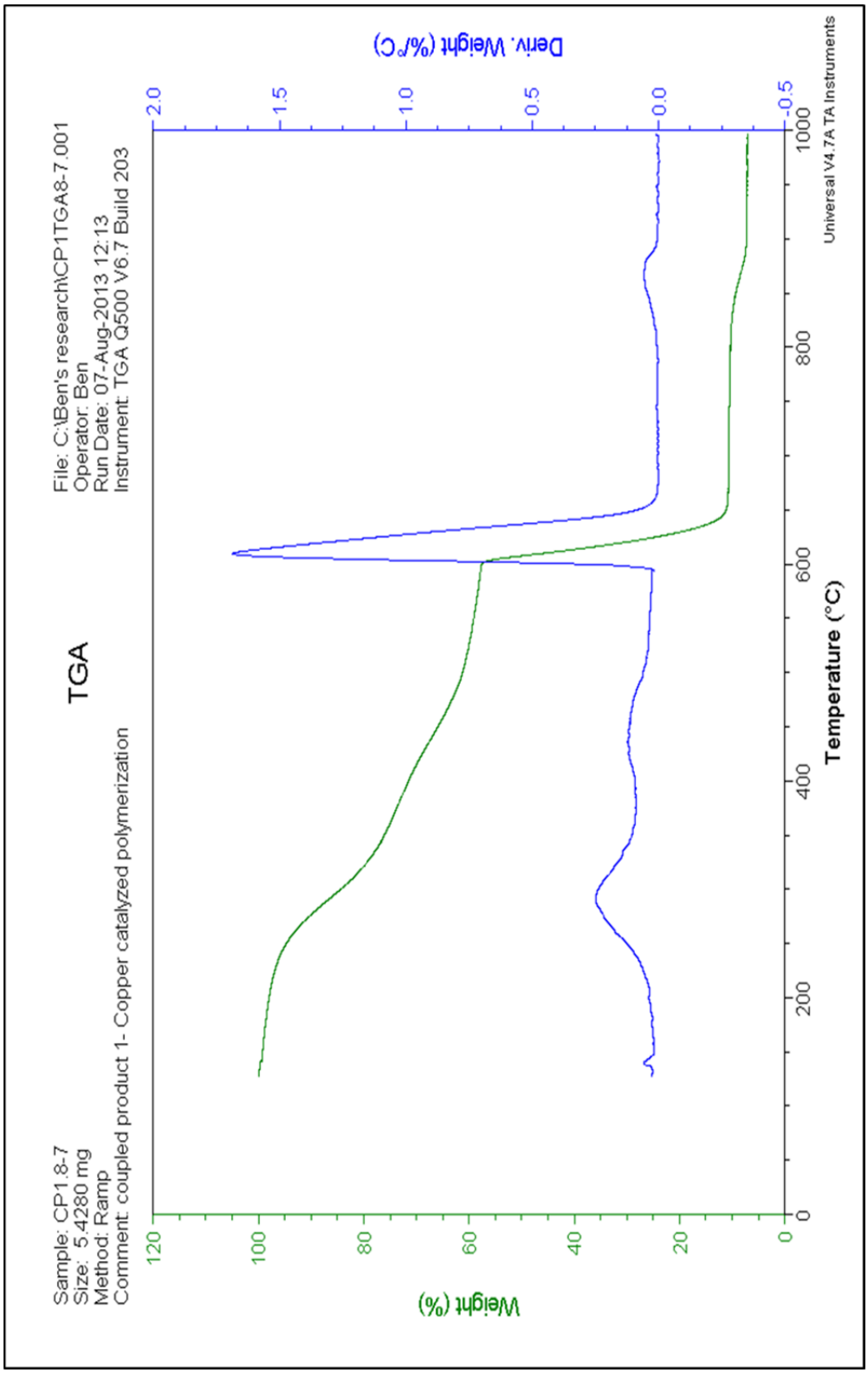

Figure 39. TGA thermogram of CP1 along with its derivative to better observe mass loss vs. temperature.

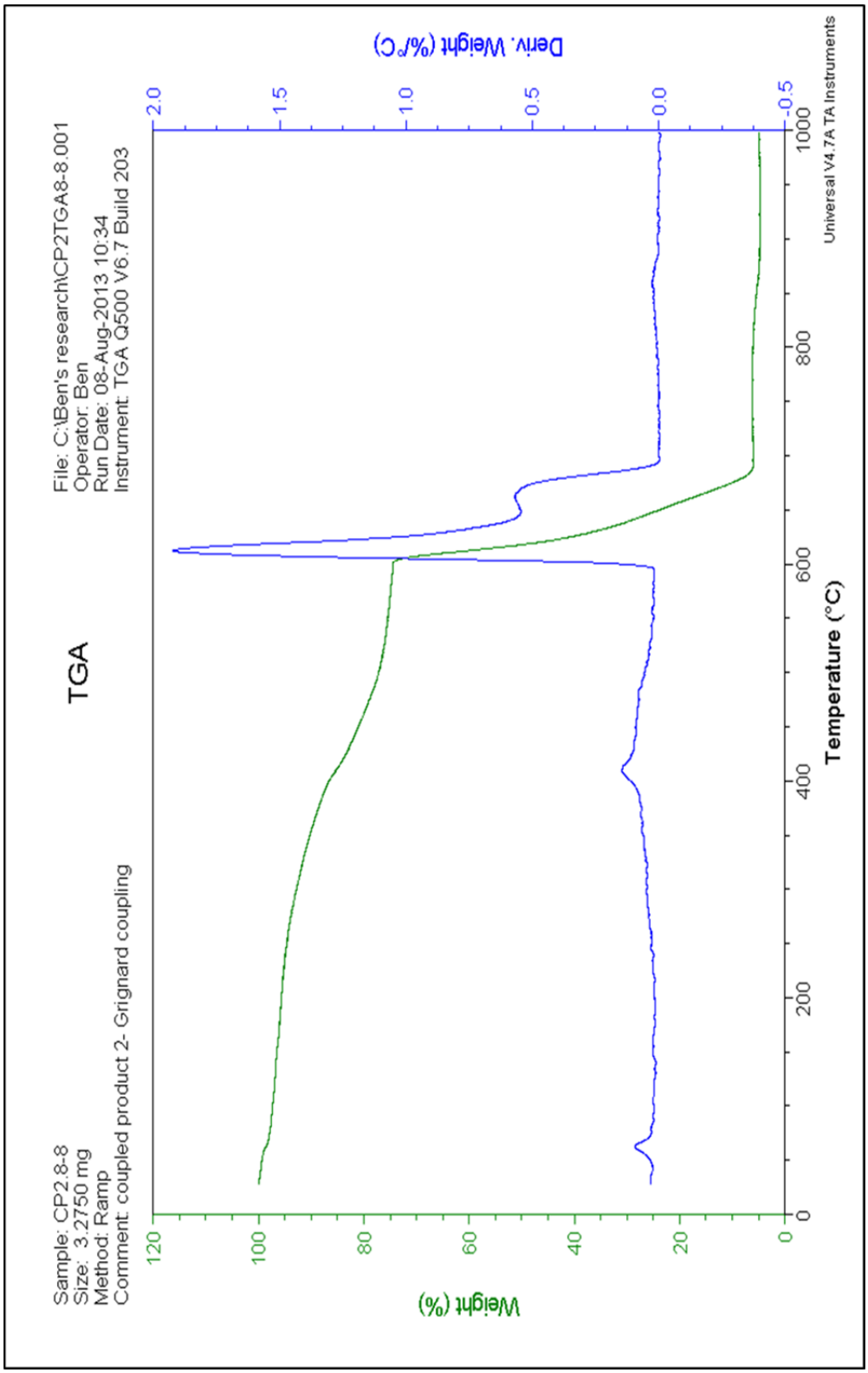

Figure 40. TGA thermogram of CP2 along with its derivative to better observe mass loss vs. temperature.

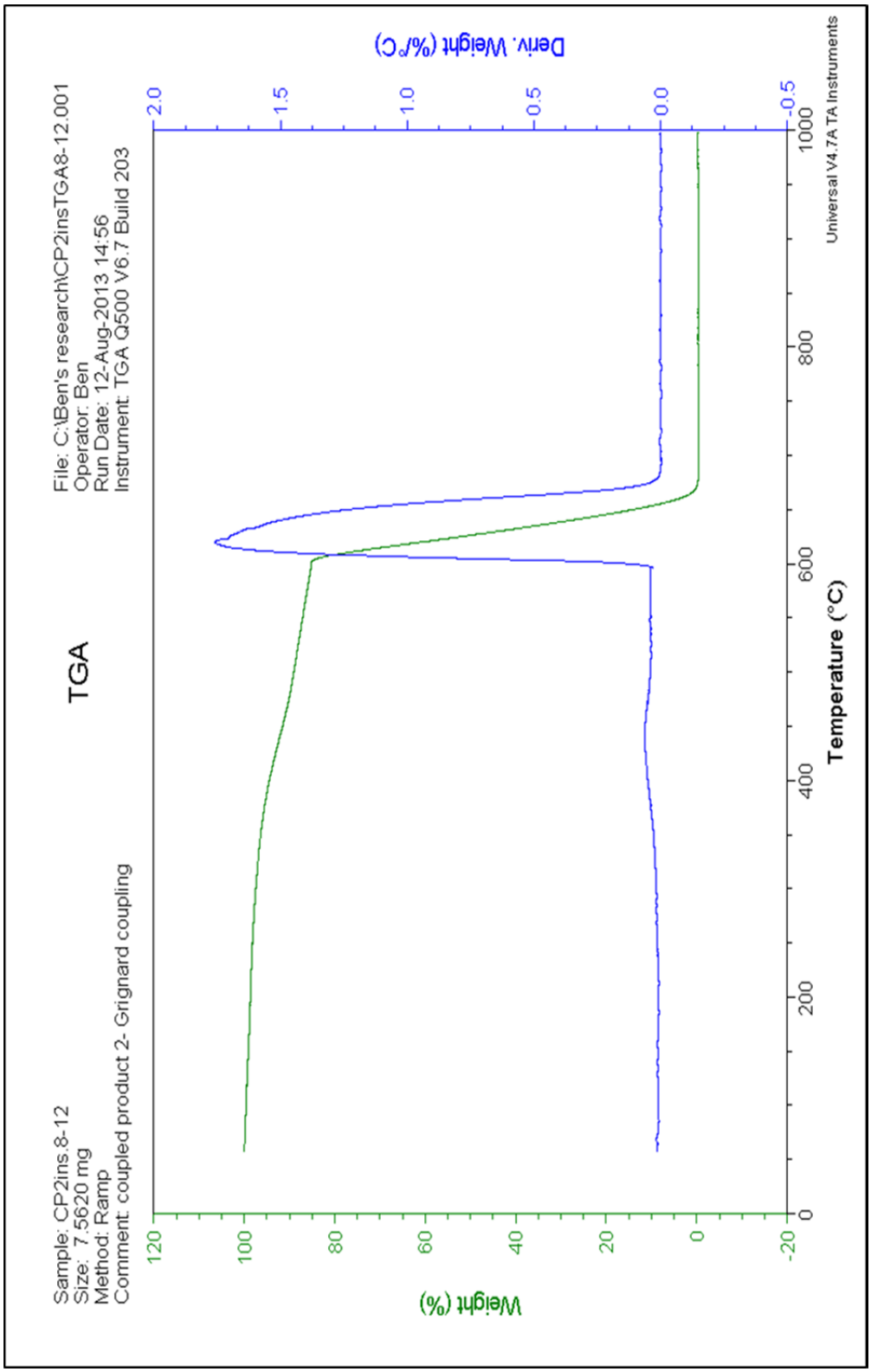

Figure 41. TGA thermogram of THF insoluble fraction of CP2 along with its derivative to better observe mass loss vs. temperature.

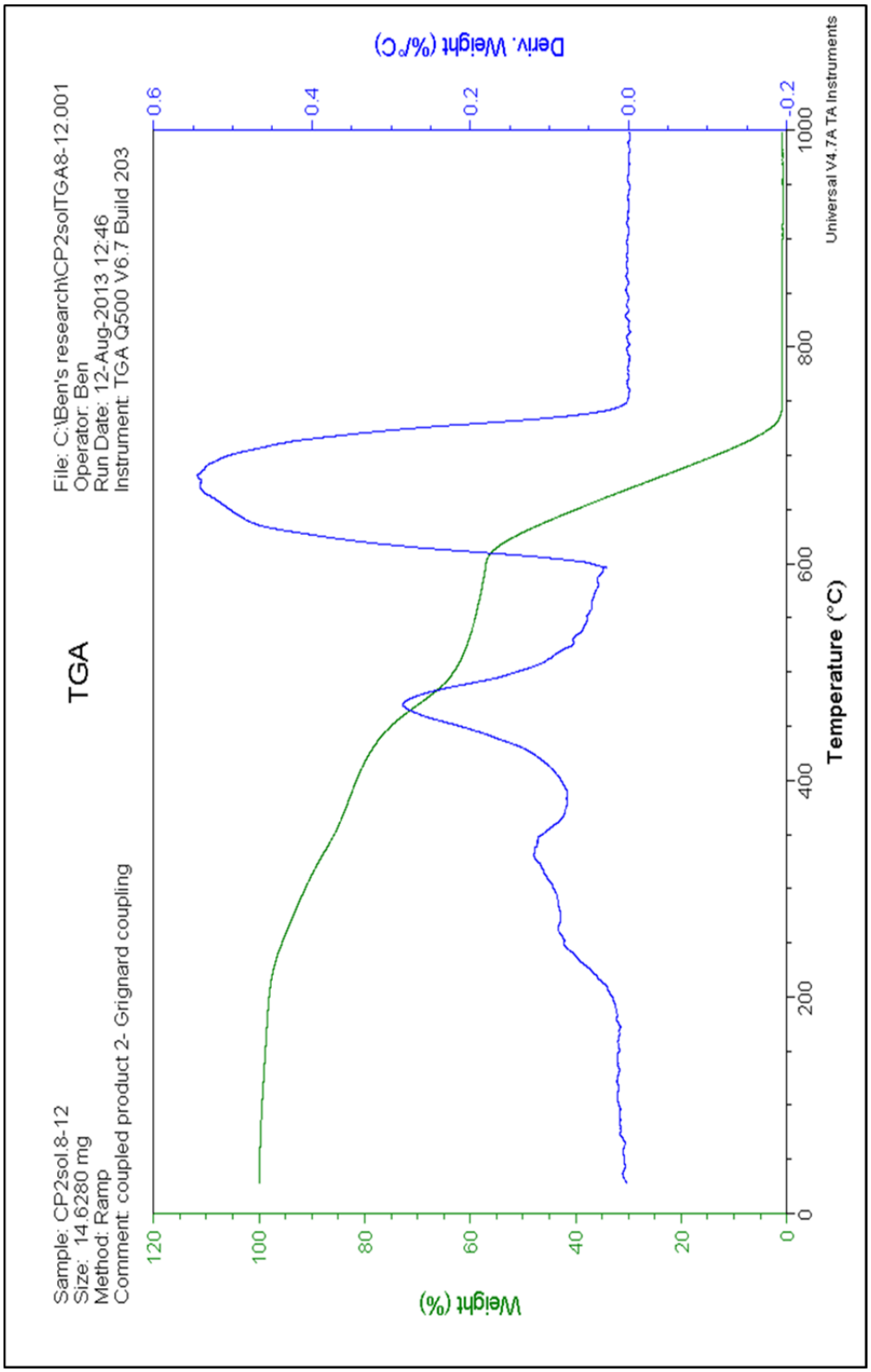

Figure 42. TGA thermogram of THF soluble fraction of CP2 along with its derivative to better observe mass loss vs. temperature.

to the CP1. The THF soluble CP2 loses 41.43% of its mass before 600 °C and 56.13% after 600 °C. If calculating based on the degradations of the lone P3HT and fullerene- C_{60}, the soluble CP2 would have 52% of its mass attributed to P3HT. A separation using THF seems imperative for product from Coupling Method 2 so that no low molecular mass species are used. Based on decomposition of the materials run on the TGA, a temperature of 275 °C was used as the upper limit for DSC analysis.

3.2.2 Differential Scanning Calorimetry

Differential Scanning Calorimetry (DSC) was performed on four systems: pure poly(3-hexylthiophene) (P3HT), P3HT mixed with the C_{60}-fullerene, P3HT mixed with the CP1, and P3HT mixed with the THF-soluble CP2. For each system, thermograms were collected for pre-thermal annealed and post-thermal annealed products, as seen in Figures 43 through 46. Data collected from the thermograms of the second pre-thermal annealing and both post-thermal annealings of all four systems were tabulated, shown in Table 6. Pre-thermal annealing run 1 was not tabulated due to its properties being dependent on how the mixture was initially processed. Seen in Figures 43, 44, and 46, the first post-thermal annealing run for each mixture had a small drop in the heat flow curve just to the left of the melting point peak. The change in heat capacity is believed to be a glass transition based on first derivative curves. The glass transition temperatures were 164.07 °C for the pure P3HT, 168.08 °C for the P3HT/C_{60} blend, and 167.32 °C for the P3HT/CP2 blend. All three runs had a ratio between the glass

transition temperature and onset melting temperature over 0.9, as seen in Table 6. The glass transition temperatures appear much closer to the melting phase than seen for most polymers. During thermal annealing the crystalline material is being reordered into higher crystalline perfection. The close proximity between the glass transition and melting is most likely due to a higher content of amorphous material being strained by the newly formed small crystals thus causing a shift of the glass transition to a much higher temperature.[35] A glass transition is not observed for the P3HT/CP1 blend due its low crystalline content and low strain on the amorphous material.

The pure P3HT system, seen in Figure 43, was run to be a reference in how the other materials affect the crystallization of P3HT at different stages. Referencing Table 6, the pre-thermal annealed P3HT had an onset melting temperature of 207.31 °C which rose slightly after thermal annealing. Looking at Figure 43, there is a shoulder on the right side of the melting endotherm due to differences in crystalline perfection of P3HT. To determine the maximum melting temperature of both species, a 2nd derivative of heat flow vs. temperature was analyzed to give temperatures of 218.24 °C for the first species and 225.28°C for the second species. The maximum melting temperature for the first species rose slightly after thermal annealing, but decreased after the second post run, shown in Table 6. The maximum melting temperature for the second species stayed fairly consistent for all three runs. The energy of transition decreased from 16.34 J/g to 15.00 J/g after thermal annealing of the P3HT, but increased to 15.86 J/g for the second post-thermal annealing run. Based on increases of melting temperatures and the energy

Table 6.
DSC Thermograms for Pure P3HT and Three Different Solar Cell Active Layer Mixtures

DSC Data for Pre and Post-Thermal Annealed Products								
Product Mixtures	Order of Run	Tg, Glass Transition (°C)	Onset of Melting Temperature (°C)	Maximum Melting Temperature (°C)	Tg/Onset Melt. Temp.	Energy of Transition (J/g)	Peak 1 Max. Melt. Temp. (°C)	Peak 2 Max. Melt. Temp. (°C)
P3HT only	Pre-thermal Annealed	N/A	207.31	217.63	N/A	16.34	218.24	225.28
	Post-thermal Annealed 1	164.07	208.98	218.21	0.91	15.00	218.61	225.29
	Post-thermal Annealed 2	N/A	208.16	217.34	N/A	15.86	217.71	225.33
P3HT/C_{60}	Pre-thermal Annealed	N/A	194.71	207.09	N/A	8.06	N/A	N/A
	Post-thermal Annealed 1	168.08	195.33	206.72	0.94	7.37	205.04	220.12
	Post-thermal Annealed 2	N/A	193.27	206.16	N/A	8.23	204.91	219.19
P3HT/CP1	Pre-thermal Annealed	N/A	157.28	191.78	N/A	2.56	N/A	N/A
	Post-thermal Annealed 1	N/A	161.01	172.03	N/A	3.05	N/A	N/A
	Post-thermal Annealed 2	N/A	153.14	182.54	N/A	1.66	N/A	N/A
P3HT/CP2	Pre-thermal Annealed	N/A	187.04	203.69	N/A	5.15	207.17	214.25
	Post-thermal Annealed 1	167.32	187.93	202.96	0.96	3.76	206.00	212.92
	Post-thermal Annealed 2	N/A	182.26	201.94	N/A	4.85	N/A	N/A

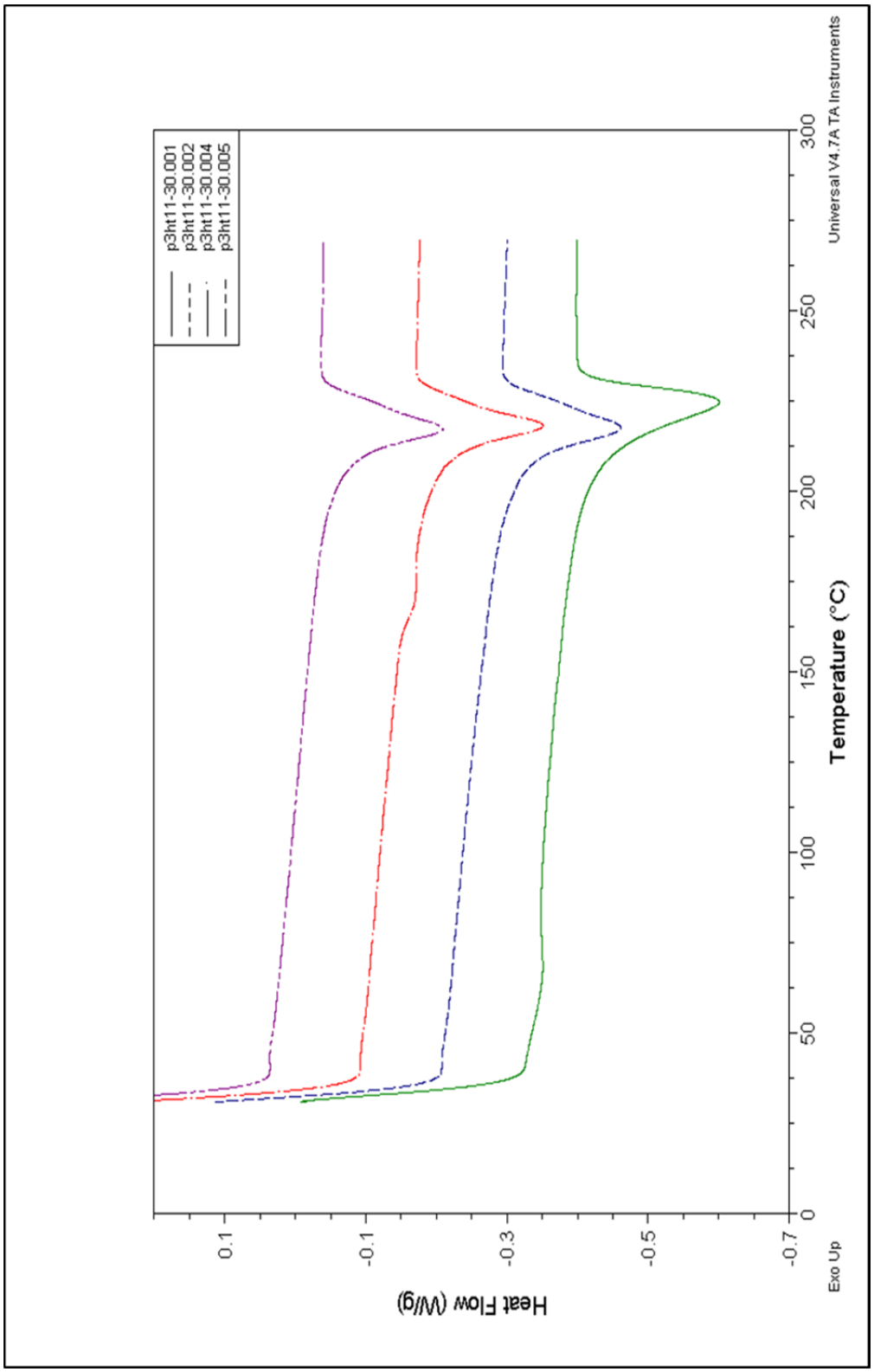

Figure 43. DSC thermograms for pre-thermal annealed P3HT run 1 (green), pre-thermal annealed P3HT run 2 (blue), post-thermal annealed P3HT run 1 (red), and post-thermal annealed P3HT run 2 (violet).

of transition, thermal annealing increases the perfection of the P3HT crystalline material, but there is a large portion of P3HT left in the amorphous phase.

Comparing the P3HT/C_{60} mixture to P3HT, the onset of melting was over 10 °C lower but followed a similar pattern, with a pre-thermal annealing onset melting temperature of 194.71 °C and post-thermal annealing onset melting temperatures of 195.33 °C, and 193.27 °C. A second derivative for the pre-thermal annealed P3HT/C_{60} blend did not show peaks, but the maximum melting point overall was 207.09 °C. Seen in Table 6 and Figure 44, the maximum melting temperatures after thermal annealing were around 205 °C and 220 °C. The first P3HT crystalline species had a 13 °C drop in its maximum melting point temperature and the second species had a 5 °C drop in its maximum melting point temperature in comparison to the pure P3HT. Table 6 also shows the energy of transition for P3HT decreases from values of 16.34 J/g, 15.00 J/g, and 15.86 for the pure P3HT to values of 8.06 J/g, 7.37 J/g, and 8.23 J/g for the P3HT/C_{60} blend. The fullerene-C_{60} addition results in a reduction of P3HT crystallinity. The energy of transitions followed a similar pattern for the P3HT/C_{60} mixture as the P3HT, showing a large content left in the amorphous phase after thermal annealing.

Seen in Figure 45, the P3HT/CP1 blend had an even further decrease in its onset of melting temperatures than the P3HT/C_{60} blend, dropping to temperatures of 157.28 °C, 161.01°C, and 153.14 °C. The P3HT/CP1 mixture did however show a similar pattern to the P3HT through the series of runs, increasing after thermal annealing and then

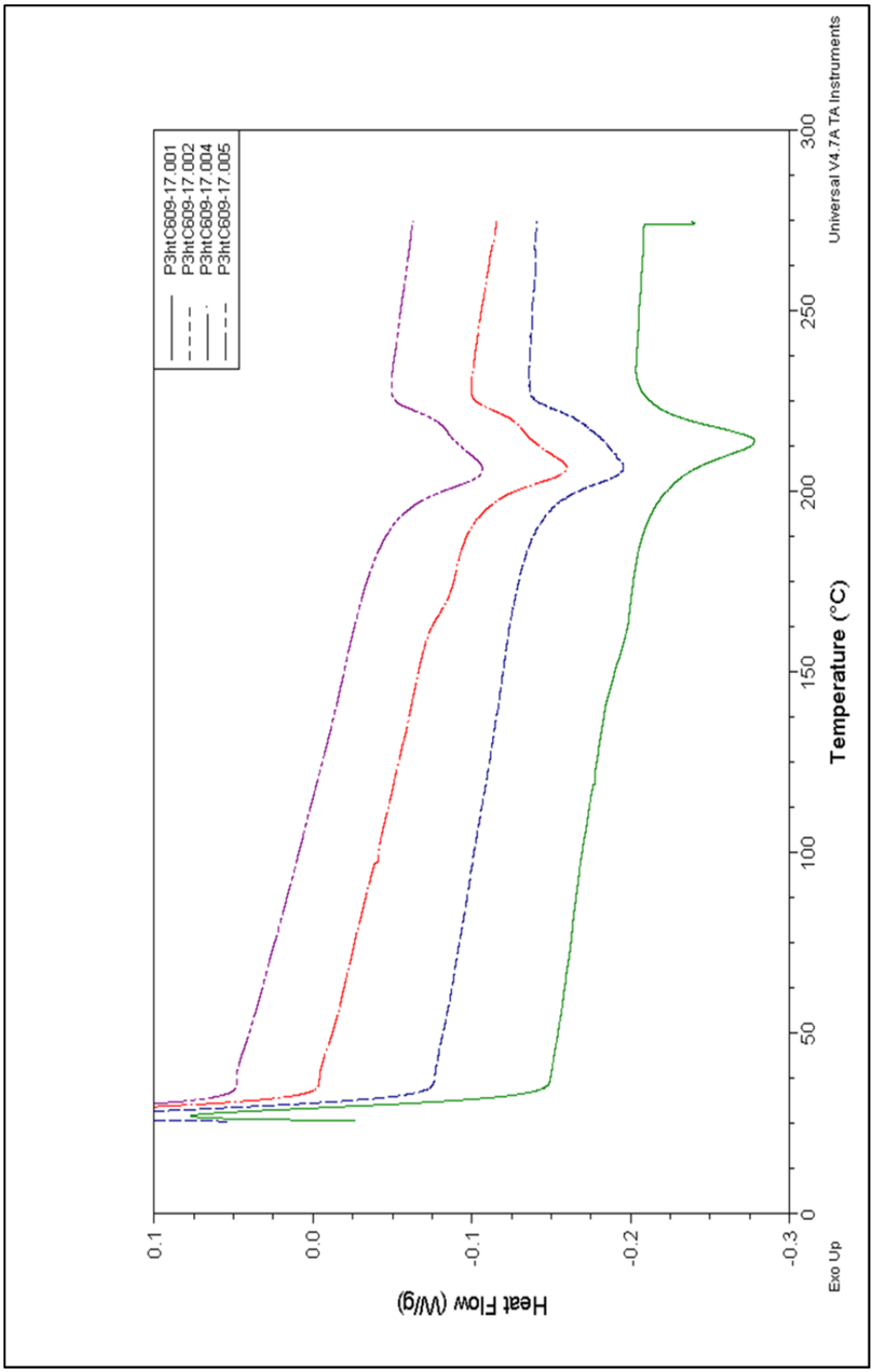

Figure 44. DSC thermograms for pre-thermal annealed P3HT/C_{60} blend run 1 (green), pre-thermal annealed P3HT/C_{60} blend run 2 (blue), post-thermal annealed P3HT/C_{60} blend run 1 (red), and post-thermal annealed P3HT/C_{60} blend run 2 (violet).

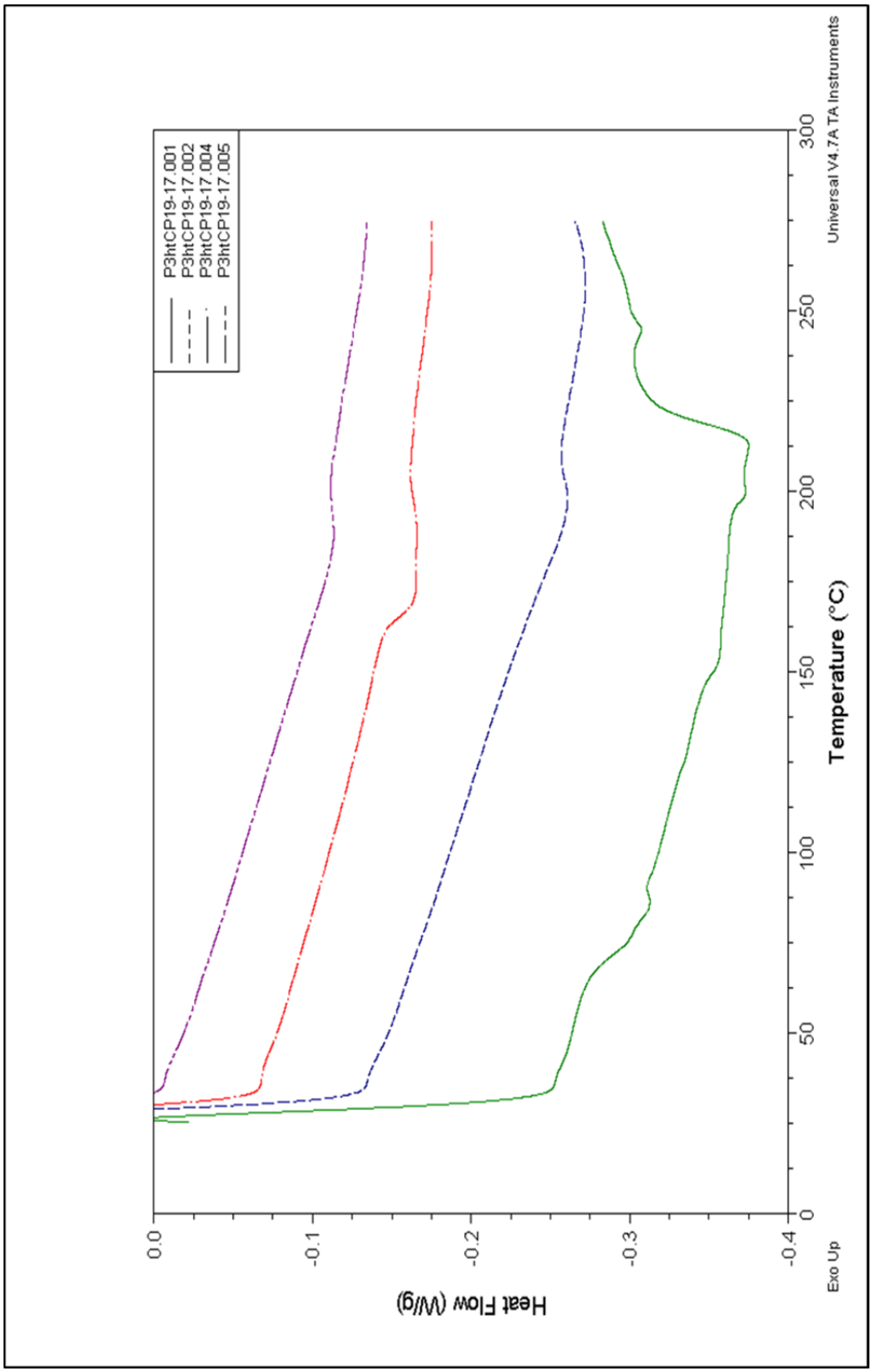

Figure 45. DSC thermograms for pre-thermal annealed P3HT/CP1 blend run 1 (green), pre-thermal annealed P3HT/CP 1 blend run 2 (blue), post-thermal annealed P3HT/CP1 blend run 1 (red), and post-thermal annealed P3HT/CP1 blend run 2 (violet).

decreasing on the final run. A second derivative for all the P3HT/CP1 mixture runs did not show peaks, but the overall maximum melting temperatures showed a drastic decrease from values of 217.63 °C, 218.21 °C, and 217.34 °C for the pure P3HT to temperatures of 191.78 °C, 172.03 °C, and 182.54 °C for the P3HT/CP1 blend. The energies of transition for the P3HT/CP1 blend were much lower in comparison to values of the pure P3HT and P3HT/C_{60} blend, with values of 2.56 J/g, 3.05 J/g, and 1.66 J/g. Other than the absence of a glass transition point, the P3HT/CP1 blend also differs from the other blends in that the energy of transition increases after thermal annealing. During thermal annealing for the P3HT/CP1 blend, polymer chains most likely reorder themselves quicker into a higher content of imperfect crystals.

The P3HT/CP2 blend, seen in Figure 46, had both higher onset of melting temperatures and maximum melting temperatures than the P3HT/CP1 blend, but was still lower than the P3HT/C_{60} blend and pure P3HT. Onset of melting for the P3HT/CP2 blend was at temperatures of 187.04 °C, 187.93 °C, and 182.26 °C and its maximum melting temperatures ranged from 201 °C to 204 °C, shown in Table 6. The energies of transition for the P3HT/CP2 blend, 5.15 J/g, 3.76 J/g, and 4.85 J/g, were 35 - 50% lower than the values for the P3HT/C_{60} blend and 65 - 75% lower than the values for the pure P3HT. The DSC thermograms shows that all blends have a negative effect on developing high crystalline P3HT material, with the coupled blends showing greater disruption to crystal formation. The thermograms also show that thermal annealing increases crystalline perfection, but due to insufficient amount of annealing time, most of the P3HT was left

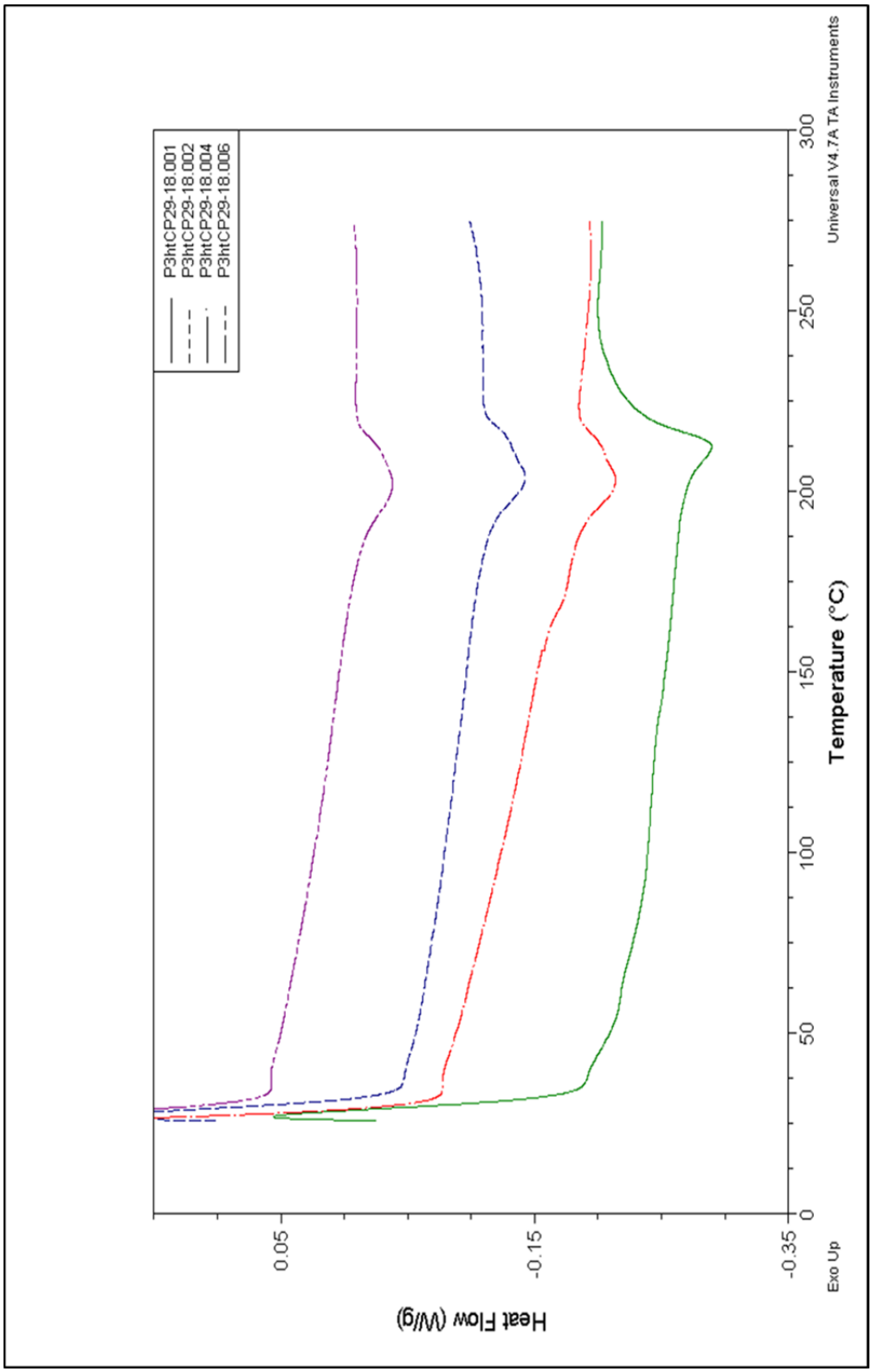

Figure 46. DSC thermograms for pre-thermal annealed P3HT/CP2 blend run 1 (green), pre-thermal annealed P3HT/CP 2 blend run 2 (blue), post-thermal annealed P3HT/CP2 blend run 1 (red), and post-thermal annealed P3HT/CP2 blend

in amorphous phase. In further studies, the coupling and thermal annealing processes will need to be optimized so that higher crystalline content and perfection can be achieved.

3.2.3 Transmission Electron Microscopy[36,37,38]

Transmission Electron Microscopy (TEM) was performed on purchased P3HT, a P3HT/C_{60} blend, and a P3HT/Coupled Product blend as well as their post-thermal annealed forms. Figures 47 through 52, show the images captured for all six materials. The poly(3-hexylthiophene) has a slight change after it has been thermally annealed. In Figure 48, the fibril material seen is an indication of P3HT chains packing together tighter and forming crystals as a result of the thermal annealing. The image of the pre-thermal annealed P3HT/C_{60} blend, seen in Figure 49, shows that the fullerene- C_{60} is evenly spread throughout the low crystalline P3HT material. After thermal-annealing, the P3HT forms spherulite crystals with areas of darker material around the edge, as seen in Figure 50. It is possible that the darker material surrounding the spherulites is fullerene-C_{60}, but it could also be due to variations in depth of the film. The P3HT/Coupled Product blend, as seen in Figure 51, shows dark areas of material thought to be clusters of fullerene-C_{60} coupled to the P3HT before thermal-annealing. After thermal-annealing, the dark areas are smaller and more spread throughout the film, as seen in Figure 52. Coupling the polymer to the fullerene-C_{60} appears to decrease segregation between electron donor and acceptor, but may have a negative effect on crystallization of P3HT.

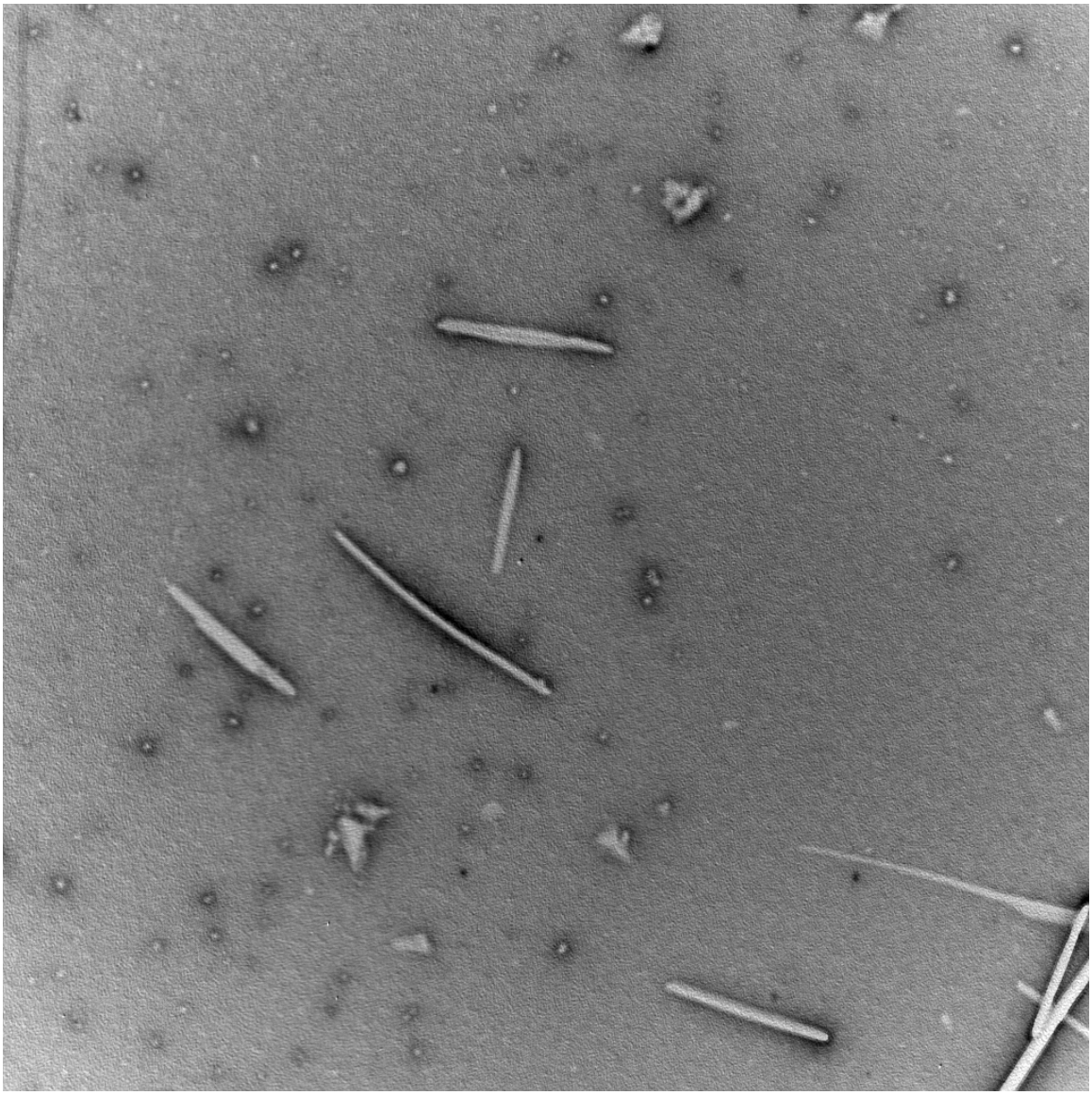

Figure 47. P3HT at 4000x magnification.

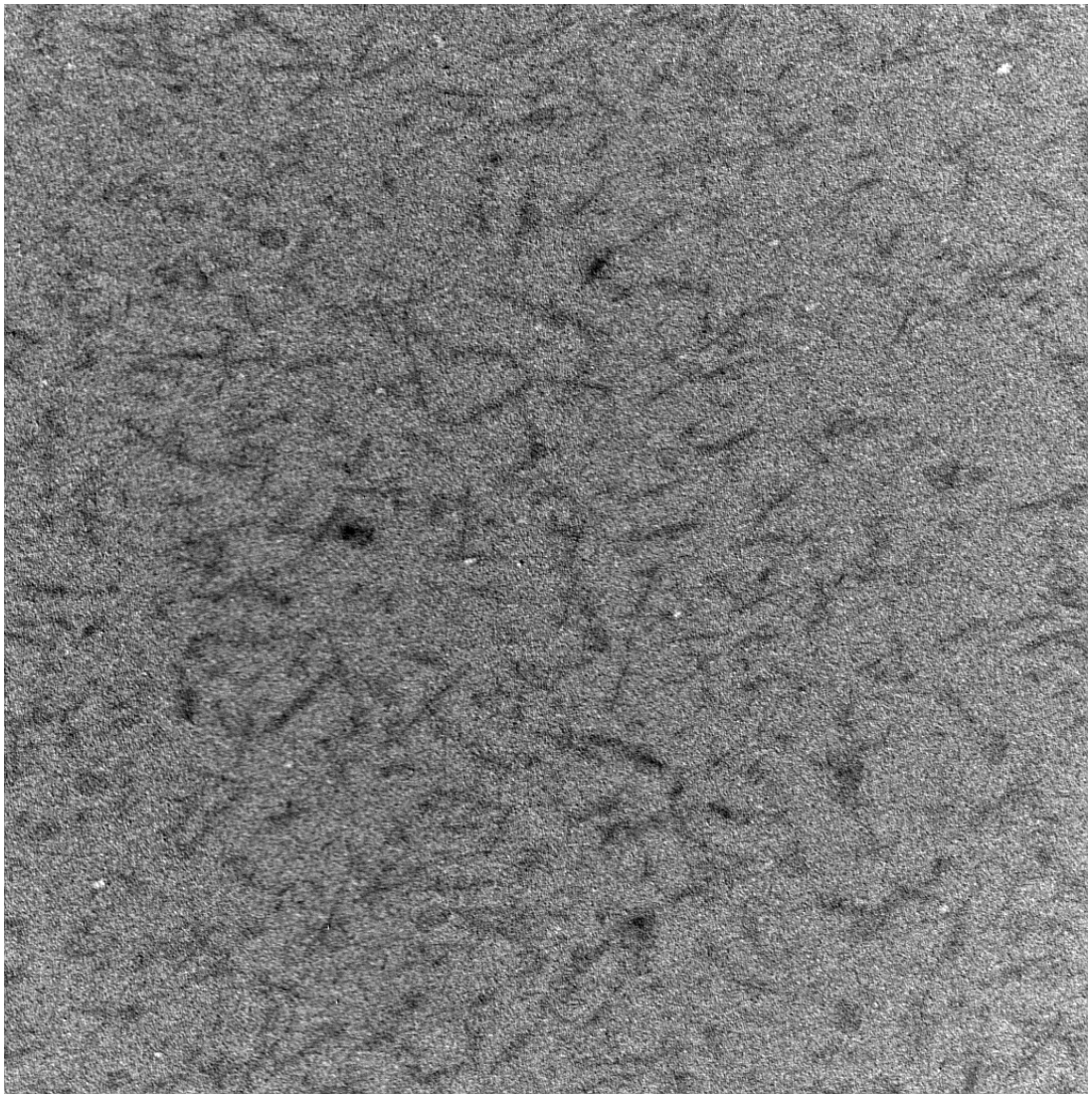

Figure 48. Thermally annealed (TA) P3HT at 15000x magnification.

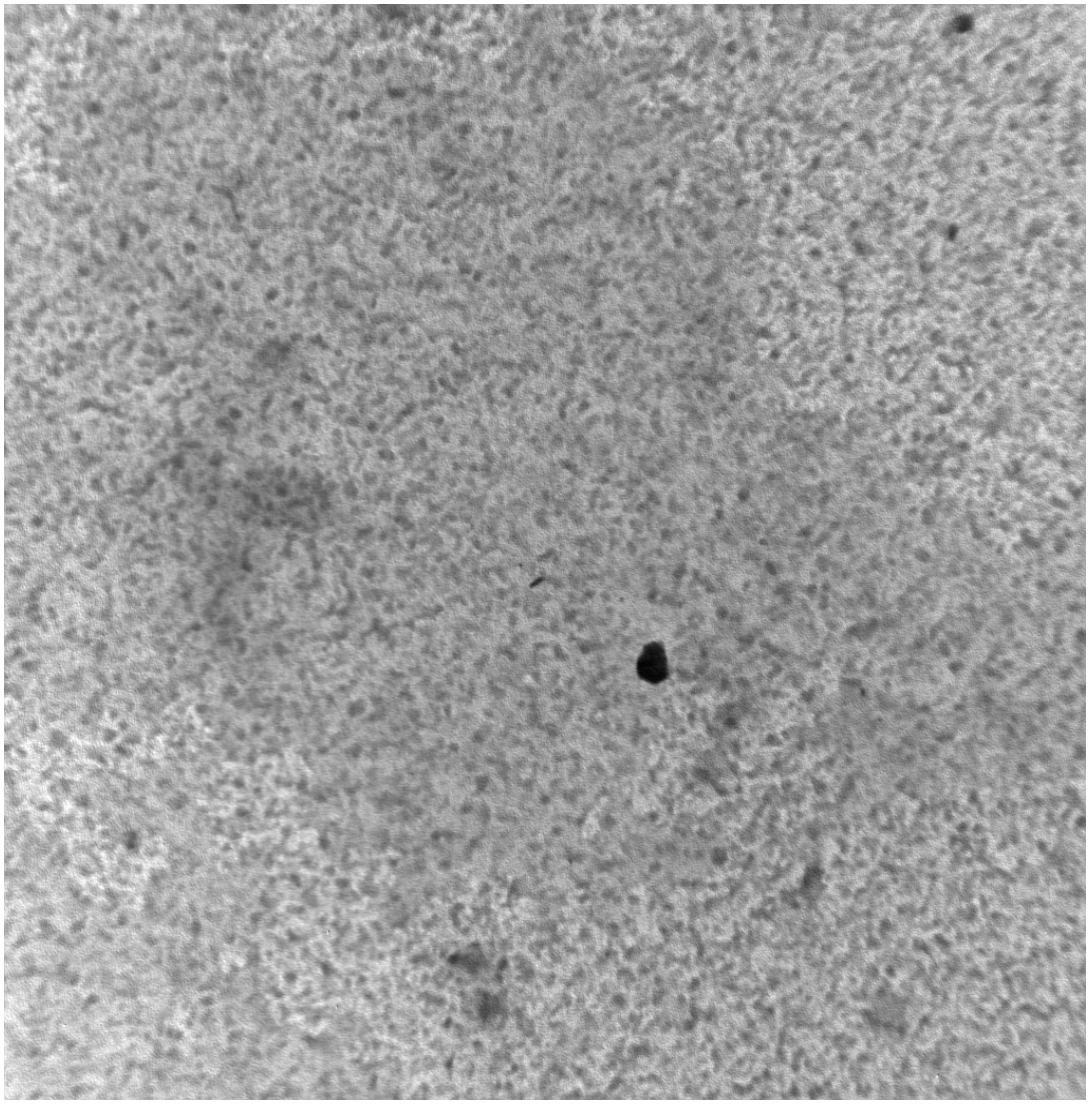

Figure 49. P3HT/C_{60} at 5000x magnification.

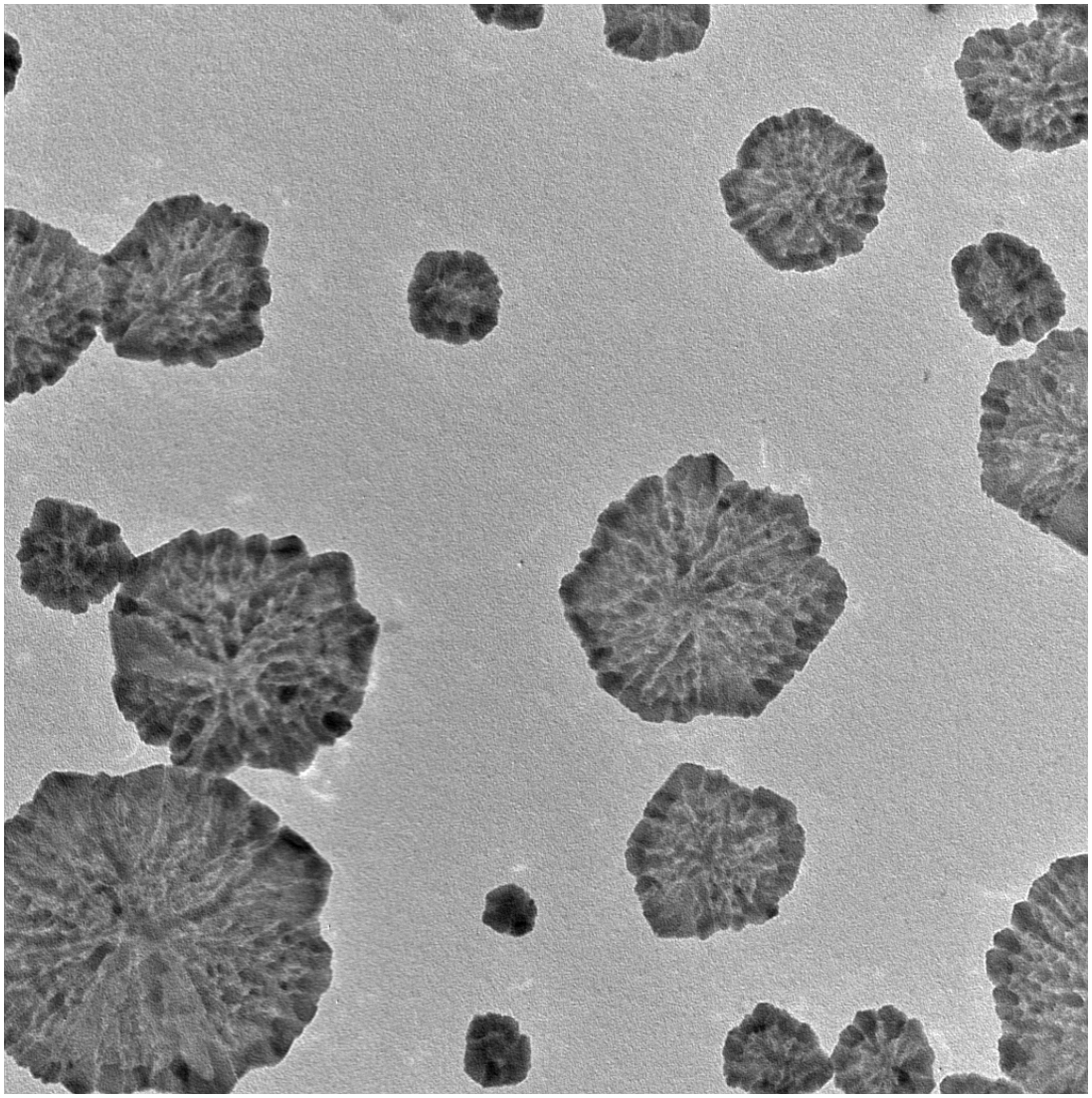

Figure 50. TA P3HT/C_{60} at 15000x magnification.

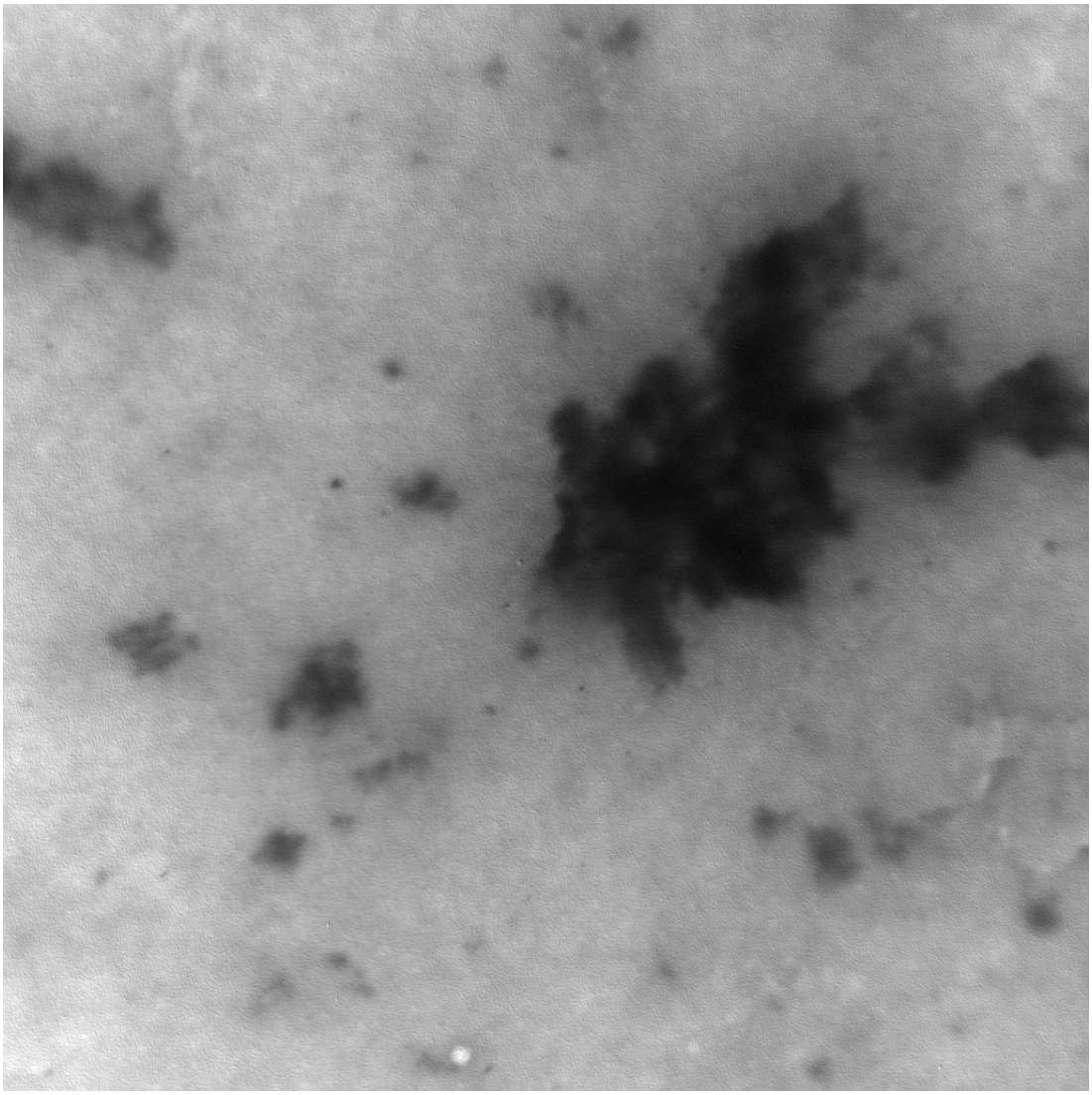

Figure 51. P3HT/Coupled at 4000x magnification.

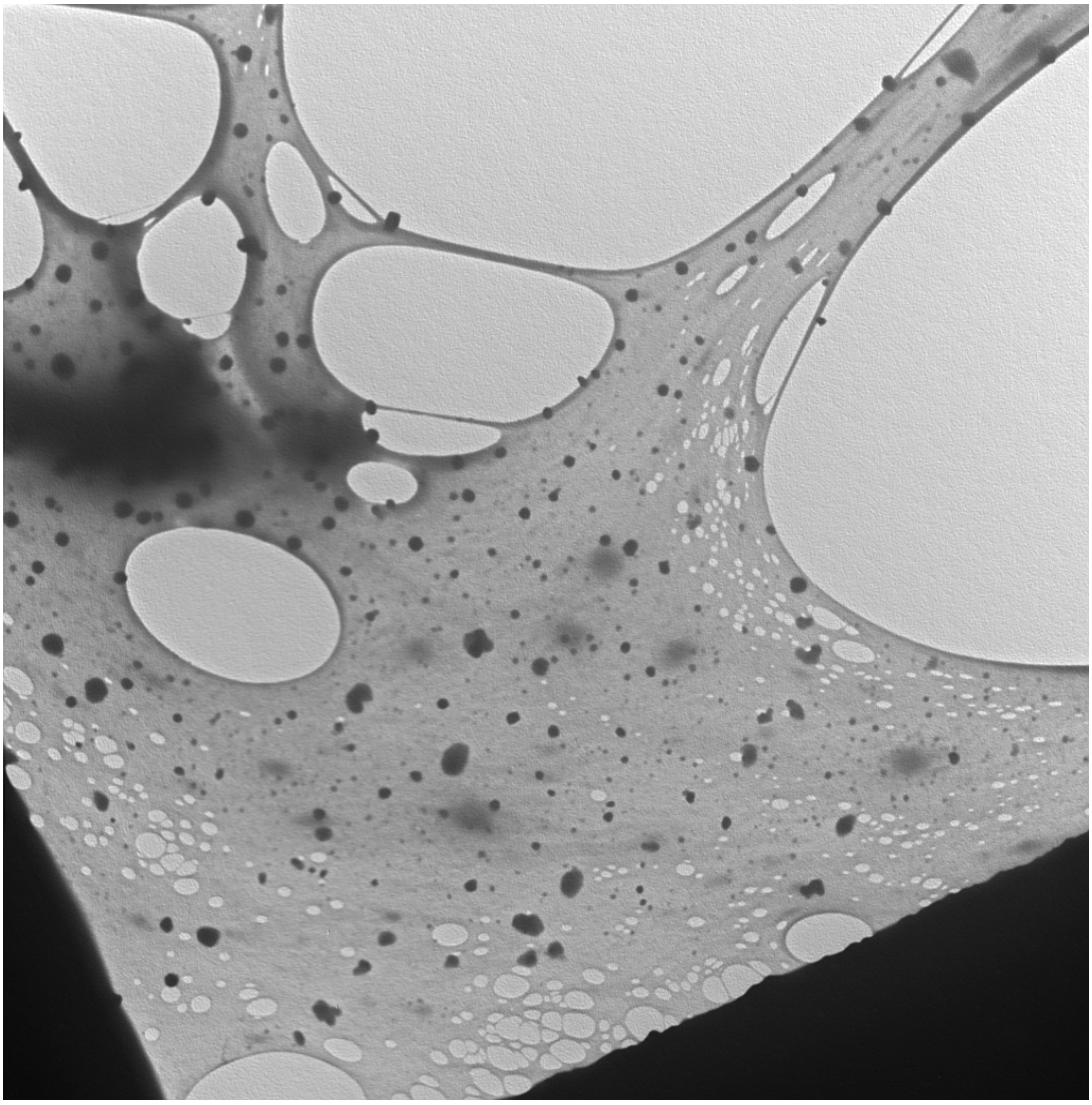

Figure 52. TA P3HT/Coupled at 4000x magnification.

3.3 Characterization of Solar Cells

3.3.1 Power Efficiency of Solar Cells

Solar cells representing both the non-coupled and coupled systems were fabricated by the same process, with the only difference being the active layer composition. I-V curves were obtained for solar cells representing the two different systems as seen in Figures 54 and 55. Using the curves obtained, the power efficiency was calculated by the formula $\eta = (P_m)/(E \times Ac)$, where P_m is the maximum power output of the device ($I \times V = P_m$), E is the input light, and Ac is the surface area of the fabricated solar cell. The percentages were calculated and tabulated, seen in Table 7. As seen in Figure 54 and Table 7, there were six solar cells fabricated with non-coupled system with five giving power conversion percentages and one showing no conductance. The low power conversion efficiency percentages can be due to several factors, with the most obvious being the use of fullerene-C_{60} over the more favorable PCBM found in more efficient solar cells.[9,10,11] Also processes within fabricating the solar cell, such as spin-coating of the layers or choices of the anode and cathode, could have had major effects on the efficiency of the solar cells. According to the study, however, all the failing factors for the solar cells with non-coupled active layers, were also repeated in the solar cells with the coupled systems. When comparing the two systems, there is only one difference that can affect the efficiency percentages between the two, coupling the electron donor to the electron acceptor. As seen in Figure 55 and Table 7, nine solar cells with coupled

Table 7
Power Efficiency of Fabricated Solar Cells (%)

Solar Cell Number	Non-coupled System	Coupled System
1	1.08×10^{-3}	No conductance
2	1.62×10^{-2}	3.46×10^{-12}
3	No conductance	No conductance
4	5.40×10^{-4}	No conductance
5	1.59×10^{-10}	No conductance
6	5.60×10^{-6}	4.12×10^{-12}
7	N/A	No conductance
8	N/A	No conductance
9	N/A	No conductance

systems were fabricated and tested for their power conversion efficiency, with the first six using CP2 material and the last three using CP1 coupled material. Only two out of the total nine solar cells showed any conductance across the solar cell. The two coupled solar cells that showed power conversion were at least 100 times less efficient than the least efficient non-coupled solar cell that had results. The results show a major disruption in the transport of charge in the active layer. From the DSC analysis and TEM images, it appears that the coupled material is more incorporated into the P3HT crystalline material but that there is a decrease in P3HT crystallinity. The decrease in crystallinity is due to the coupled material, but specifically it could be a result of the P3HT coupled to the fullerene-C_{60} having too low of molecular mass to allow high crystallinity. Further work will need to be done to optimize the procedures for

synthesizing P3HT and coupling it to fullerene-C_{60}. If using coupled material with long chain P3HT changes the result of the power conversion efficiency, then fabrication of the solar cells will be optimized to determine the limits of a solar cell with a coupled system.

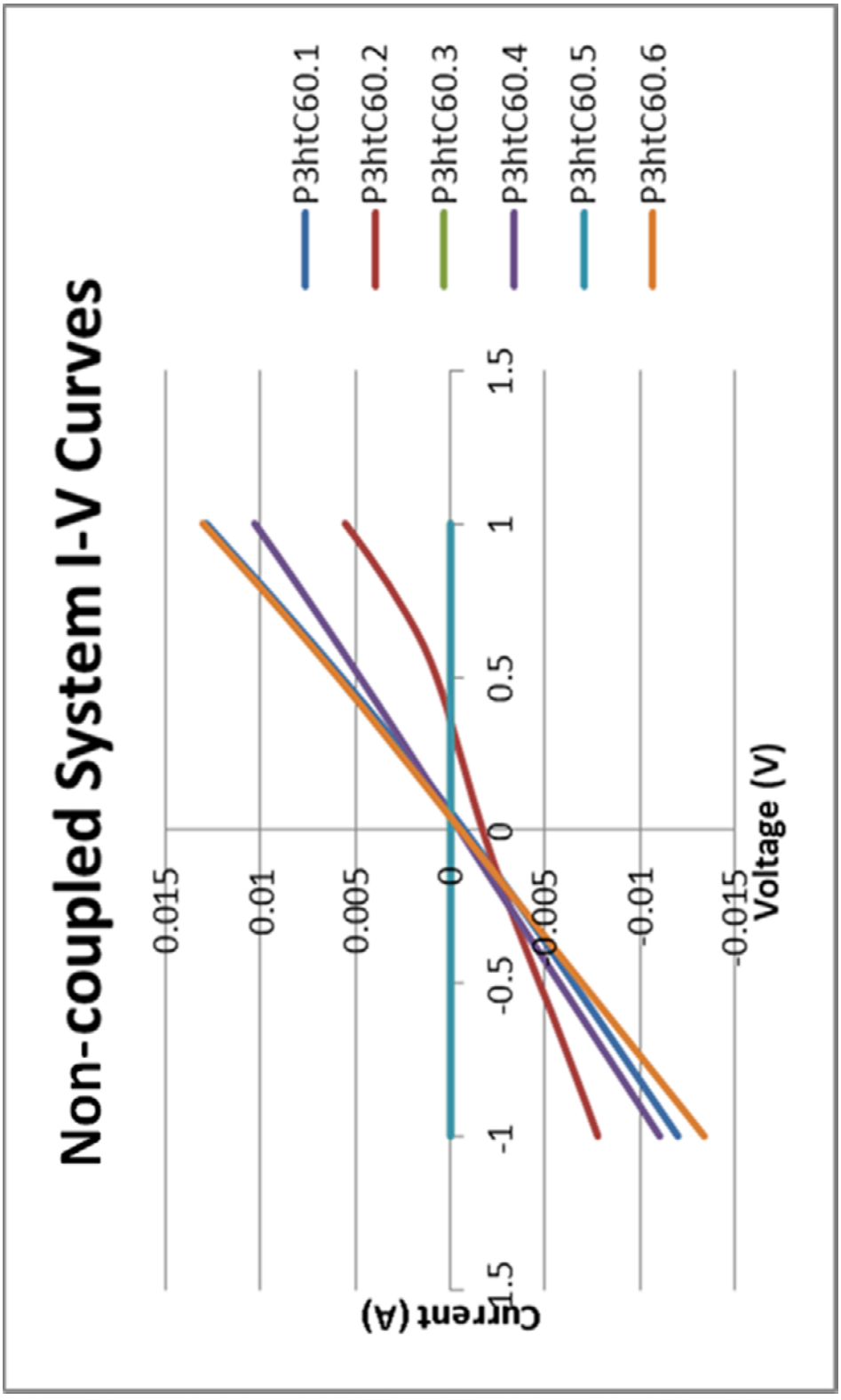

Figure 53. I-V curves for solar cells with non-coupled system (1-6).

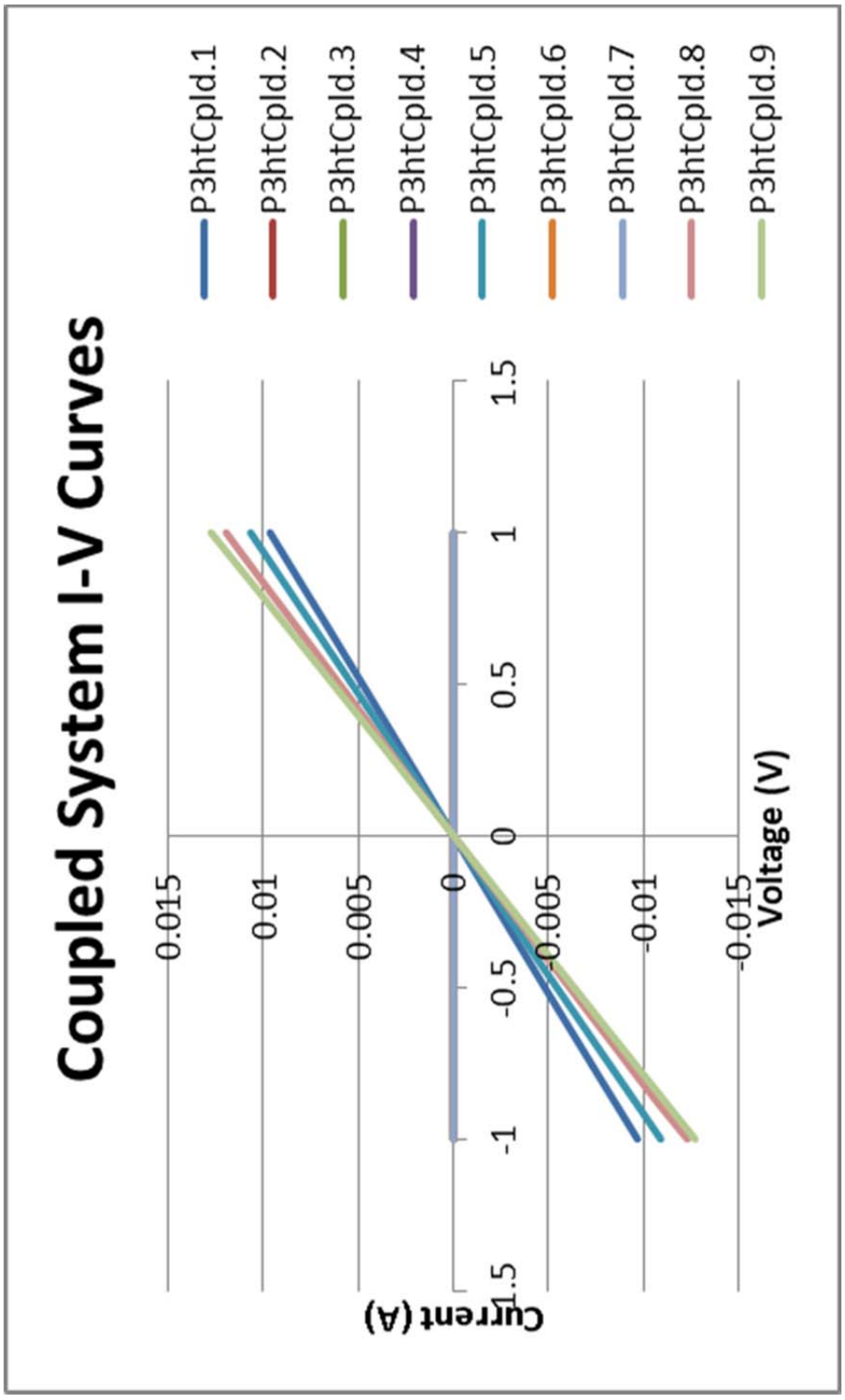

Figure 54. I-V curves for solar cells with coupled system (1-9).

4 CONCLUSIONS

In previous studies, thermal annealing has shown to increase light absorption and charge transport for organic solar cells with a heterogeneous blend of P3HT and PCBM (a derivative of C_{60}) for their active layer. Unfortunately, thermal annealing also causes segregation between the electron donor, P3HT, and the electron acceptor, PCBM, decreasing the efficiency of electron transport to the acceptor. To resolve the issue of transport between the donor and acceptor, it has been proposed to couple the electron donor to the acceptor to reduce segregation. In this study, a non-coupled system and a coupled system were created and their efficiencies compared. The non-coupled system had a heterogeneous mixture of P3HT and fullerene-C_{60} (substituted with PCBM for cost reasons) for its active layer and the coupled system had a heterogeneous mixture of P3HT and P3HT/C_{60} coupled material for its active layer. P3HT was synthesized and then coupled to fullerene-C_{60} using three coupling, with the electrosynthesis technique giving no results. The other two methods of coupling were by atom transfer radical addition (Method 1) and a Grignard addition (Method 2). The monomer, synthesized P3HT, and coupled products were characterized and compared to show the progression of the synthetic techniques. Characterization was also done on a coupled system and compared to a non-coupled system, as well as, pure P3HT to determine the effect coupling the electron donor and acceptor would have on the crystallinity of P3HT. The fabricated solar cells were studied as a final test to compare the two systems.

GC/MS results showed a major peak at retention time 12.1 min which had a mass of 373 Daltons (Da), the formula weight of the desired product 2-bromo-3-hexyl-5-iodothiophene. The only other peak gave a molecular mass of 326 Da from the mass spectrometry results, which was 2,5-bromo-3-hexylthiophene, also an applicable product for the synthesis of P3HT. The FTIR spectrum, gave peaks of 2953 cm^{-1}, 2925 cm^{-1}, and 2855 cm^{-1} for C-H stretching of the aliphatic hexyl group and 3081 cm^{-1} for vinyl C-H stretching of the lone aromatic group on the thiophene. A peak of 1460 cm^{-1} was seen as a result of C-H bending for the hexyl group. The ^{1}H NMR spectrum of the monomer product had four peaks in the aliphatic region, a triplet at 0.88 ppm, a septuplet of 1.30 ppm, a quintuplet at 1.54 ppm, and a triplet at 2.51 ppm which were all a result of the aliphatic hydrogen atoms on the hexyl group. There was only one peak in the aromatic region, a singlet at 6.96 ppm the result of the lone aromatic hydrogen on the C-4 position of the thiophene. The other two aromatic carbons, at the C-2 and C-5 positions, were substituted with the halogens, iodine and bromine. Substitutions at the C-2 and C-5 position were confirmed by ^{13}C NMR spectroscopy. Six peaks were seen in the aliphatic region of the ^{13}C NMR spectra due to the hexyl group. Four other peaks were seen in the spectra at shifts of 71.0 ppm, 111.7 ppm, 137.9 ppm, and 144.2 ppm. The two latter peaks were a result of the carbon adjacent to the hexyl group (C-3) and the carbon adjacent to the hydrogen (C-4). The peak at 111.7 ppm was due to the carbon substituted with bromine and the peak at 71.07 ppm was due to the carbon substituted with iodine. The halogens shield the nuclei of the aromatic carbons causing them to shift

upfield. The monomer was determined to be 2-bromo-3-hexyl-5-iodothiophene and used in the synthesis of poly(3-hexylthiophene) (P3HT).

The synthesized P3HT was washed with different solvents to remove low molecular mass P3HT. HPLC data for the high molecular mass fraction showed molecular masses of 60780 Da, 3250 Da, and 650 Da, with 69% of the total product having a molecular mass of 3250 Da. A molecular mass below 10,000 Da for P3HT has been shown to give poor crystallinity,[31] however two comparable studies used P3HT with molecular masses of 5400 Da and 6000 Da.[20,21] Although low molecular mass P3HT has been used, the synthesized P3HT would not be used as the non-coupled P3HT material in the two active layer systems. P3HT purchased through Sigma-Aldrich was used for the non-coupled P3HT in the two active layer systems due to its molecular weight of 87,000.[39] The FTIR spectrum of the synthesized P3HT is very similar to the purchased P3HT and only differs from the monomer due to peaks resulting from unsymmetrical C=C stretching of a conjugated system. Results from ^{1}H NMR spectroscopy for the synthesized P3HT are different than the monomer in the aliphatic region due to effects seen by polymers and due to areas of regioregular and regiorandom chains. The peaks have broadened due to the polymer's anisotropic tumbling, mentioned in Section 3.1.5, and no longer show splitting. There are also extra peaks found in the aliphatic region for the P3HT in comparison to the monomer, as a result of areas of regioregular and regiorandom material. Regioregular material is shifted downfield while regiorandom material is shifted similar to what is observed for the aliphatic protons in the monomer's spectra.

As mentioned in Section 3.1.5, the peaks at 2.7 ppm and 2.5 ppm for the synthesized P3HT, indicates the ratio between regioregular and regiorandom species. The synthesized P3HT is calculated to have 79.6% regioregularity, which is less than the 91.0% calculated for the purchased P3HT. In the aromatic region there was only one peak at 6.95 ppm, similar to the monomer, but with broadening. The only noticeable difference between the ^{13}C NMR spectroscopy results of the synthesized P3HT and the monomer was a shift made by the carbon bonded to the iodine. As predicted, the iodine end group was replaced by a hydrogen atom and the other end group of bromine remained for the coupling, confirmed by the presence of a peak at 108.8 ppm. The P3HT synthesized had both a lower molecular mass and regioregularity than the purchased P3HT. The synthesized P3HT did however have the predicted end groups to be used for CP1.

Both CP1 and CP2 were analyzed by HPLC and shown to have over 75% of the product with molecular masses under 3000 Da, too low to crystallize efficiently independent of non-coupled P3HT. CP1 did have a P3HT with molecular masses of 109800 Da (3%) and 23175 Da (21%), which are more desired than the low molecular mass species. The FTIR spectra of both coupled materials is similar to the synthesized P3HT, except for two sharp peaks at 1181 cm^{-1} and 1428 cm^{-1} which are seen in the spectra of the fullerene-C_{60}. Similar peaks appear in the FTIR spectra of a another P3HT/C_{60} coupled product in a comparable study after the coupling procedures, confirming the coupling of P3HT to C_{60}.[21] ^{1}H NMR spectroscopy results for CP1 and CP2 show that both materials have

lower percentages of high conjugated material than the synthesized P3HT due to the steric hindrance of the fullerene-C_{60} distorting the chains and throwing them out of coplanarity. CP1 has even further distortion to its backbone due to coupling at the C-2 position. CP2 has 37% of highly conjugated material based on the ratio between the peaks at 2.7 ppm and 2.5 ppm. CP1 appears to have no highly conjugated material based on the fact there is only a peak at 2.5 ppm. In the two comparable studies,[20,21] there is only highly conjugated product indicated by a peak at around 2.7 ppm and the absence of the peak around 2.5 ppm. The difference in the coupled product in this study compared to the other two studies could be the lack of spacing between the P3HT and C_{60}, as well as, P3HT with lower regioregularity. In the aromatic region, CP2 has a peak at 6.92 ppm similar to the peaks found for the monomer, synthesized P3HT, and purchased P3HT, but also has peaks at 7.16 ppm and 7.40 ppm due to species of low conjugation. The CP1 spectrum does not have a peak around 6.9 ppm, seen for the other materials, but has peaks at 7.20 ppm and 7.45 ppm for the lower conjugated species. ^{13}C NMR spectra for the coupled materials are similar to the monomer, synthesized P3HT, and purchased P3HT with one exception, a strong peak at 143 ppm. Also observed in the spectra of $HBrC_{60}$, this peak confirms the coupling of P3HT to fullerene-C_{60}. Analysis using TGA confirmed the coupling of P3HT to fullerene-C_{60} and was used to estimate the composition of the coupled material. Runs with pure P3HT and fullerene-C_{60} are compared to the runs of coupled products. Seventy percent of pure P3HT decomposed before the gas switch over at 600 °C while 95% of the pure fullerene-

C_{60} decomposed after the gas switch over at 600 °C, seen in Table 5. The thermogram for CP2 shows 38.54% decomposition before 600 °C and 52.92% after 600 °C. Comparing the thermogram of CP2 to the thermograms of pure P3HT and fullerene-C_{60}, the composition of the material is determined to be 49% P3HT based on the assumption that the coupled materials decompose in similar patterns to their pure counterparts. The same comparison shows that the CP2 had a high percentage of C_{60} before the THF soluble and insoluble are separated. The THF soluble CP2 lost 41.43% of its mass before 600 °C compared to only 22.10% by the pre-separated CP2. Assuming the coupled materials decompose in similar patterns to the pure materials, the THF soluble coupled product is composed of 52% P3HT and 48% fullerene-C_{60}. Based on TGA thermograms for insoluble and soluble CP2, it is imperative to use THF to separate out the soluble higher molecular mass product from the insoluble lower molecular mass material. Both coupling methods appear to be effective in coupling, but steric hindrance caused by fullerene-C_{60} causes the coupled products to have lower conjugation than pure P3HT. The low molecular mass of the coupled P3HT and the reduced conjugation could be detrimental to the production of high crystalline P3HT in the solar cells.

Results from DSC show the coupled product blend has a reduced melting point in comparison to the non-coupled system and pure P3HT, which is also observed in one of the comparable studies.[21] Thermal annealing raised the onset of melting temperatures for all four samples slightly, but only raised the maximum melting point for the pure P3HT sample. Thermal annealing also lowered the energy of transition for all samples

except the blend of P3HT/CP1, which had an increase from 2.56 J/g to 3.05 J/g after thermal annealing. Post-thermal annealing thermograms for the pure P3HT, P3HT/C_{60}, and P3HT/CP2 samples showed a glass transition point, which was closer to the melting phase than seen for most studies of polymers. The parameters used for the thermal annealing in the study result in a loss of crystallinity over the whole material. During the thermal annealing process the P3HT chains are reordering themselves into higher crystalline perfection, but due to the short annealing time most of the P3HT material is left in an amorphous state. To give higher perfection and crystallinity, the thermal annealing process needs to be optimized. TEM images of pre-thermal annealed and post-thermal annealed products of pure P3HT and a P3HT/C_{60} blend show the addition of fullerene-C_{60} changes the shape of how crystals form after thermal annealing, from a rod shape to a spherical shape. The substitution of coupled product for fullerene-C_{60} seems to reduce segregation of the donor and acceptor for post-thermal annealed product, but produces poor crystalline material.

Comparing the power efficiency of fabricated solar cells with a coupled active layer to those with a non-coupled active layer, a negative effect is observed for solar cell efficiency. Solar cells with a coupled active layer gave either no conductance across the cell or were exponentially less efficient than the cells with a non-coupled active layer. The results do not match the comparable study where C_{60}-end capped P3HT was incorporated into a P3HT/PCBM blend, which gave an almost equal efficiency to the P3HT/PCBM blend with a power efficiency of 3.76%.[21] It is expected that there will be a

lower efficiency in this study due to the replacement of PCBM with non-derivatized fullerene-C_{60}, but the coupled system in this study does not even approach the efficiency found in the non-coupled system. The results show that there is a problem with charge transport across the active layer of the coupled system solar cell. Either charge separation and mobility across the P3HT backbone or electron transport to the fullerene-C_{60} has been affected negatively, inhibiting charge transport to the anode and cathode. DSC and TEM results show that the coupled product decreases P3HT's ability to crystallize beyond the effect caused by non-coupled fullerene-C_{60}. There is no longer segregation between the electron donor and acceptor, but the formation of high crystalline material is disrupted due to the coupled product. The low molecular mass and conjugation of the coupled P3HT could be the reason for disruption of crystal formation. As mentioned before in Section 3.1.2 and 3.1.3, the molecular mass of the coupled P3HT and its conjugation are too low to form good crystalline material. Its inability to form high crystalline perfection causes disruption to crystal formation as it is incorporated into the non-coupled P3HT matrix. Low crystallinity by the non-coupled P3HT causes poor charge separation and mobility throughout the P3HT material. Electron transport to the fullerene-C_{60} could also be a reason for the low or no conductance of the coupled system solar cells. The electron withdrawing ability of the fullerene-C_{60} has been shown to decrease as it reaches a certain level of saturation.[40] If there are too many P3HT chains coupled to the fullerene-C_{60} it loses its ability to withdraw electrons from the donor, allowing for recombination of the exciton and

therefore inhibiting charge transport to the cathode. Three factors need to be optimized to determine the true effects of coupling the donor and acceptor: production of high molecular mass, regioregular P3HT for coupling, spacing between the P3HT chain and the fullerene, and substitution of the fullerene acceptor group. Production of high molecular mass, regioregular P3HT coupled to the fullerene should increase incorporation of the coupled material into the non-coupled P3HT crystalline matrix and decrease disruption to the formation of high crystalline material. Optimizing the spacing between the donor and acceptor during coupling is important for lowering steric hindrance caused by the fullerene end group while reducing segregation between the two after thermal annealing. Developing coupled material with a 1:1 ratio of P3HT to fullerene-C_{60} will limit saturation of the fullerene and allow the fullerene to retain its electron withdrawing ability. Until these factors can be addressed, coupling the donor to the acceptor appears to add no benefits and can even be problematic.

REFERENCES

1. Freund, Michael S. *Self-Doped Conducting Polymers,* 1st ed.; John Wiley & Sons, Ltd: West Sussex, **2007**.

2. Introduction to Polymer Characterization. *Edward N. Peters Comprehensive Desk Reference of Polymer Characterization and Analysis,* 1st ed.; American Chemical Society: Washington, D. C., **2003**; pp 3-29.

3. Handbook of Conducting Polymers*;* Skotheim, T. A.; Elsenbaumer, R. L.; Reynolds, J. R., Ed.; Marcel Dekker, Inc: New York, **1998**.

4. Hadziioannou, G.; Malliaras, G. G. Semiconducting Polymers*,* Vol. 2; Wiley-VCH: Veinheim, 2007.

5. Hadziioannou, G.; Malliaras, G. G. Semiconducting Polymers*,* Vol. 1; Wiley-VCH: Veinheim, 2007.

6. Kumar, N.; Vadera, S. R.; Singh J.; Das, G.; Negi, S. C.; Aparna, P.; Tuli, A. Conducting Polymers: Emerging Commercial Materials. *Defence Science J.* **1996**, 46, 91-104.

7. International Energy Agency. *World Energy Outlook 2009;* Paris, France, 2009.

8. Spanggaard, H.; Krebs, F. C. A Brief History of the Development of Organic and Polymeric Photovoltaics. *Solar Energy Materials & Solar Cells* **2004**, *83*, 125-146.

9. Gunes, S.; Neugebauer, H.; Sariciftci, N. S. Conjugated Polymer-Based Organic Solar Cells. *Chem. Rev*. **2007**, *107*, 1324-1338.

10. You, J.; Chen, C.; Hong, Z.; Yoshimura, K.; Ohya, K.; Xu, R.; Ye, S.; Gao, J.; Li, G.; Yang, Y. 10.2% Power Conversion Efficiency Polymer Tandem Solar Cells Consisting of Two Identical Sub-Cells. *Adv. Mater.* **2013**, *25*, 3973-3978.

11. You, J.; Dou, L.; Yoshimura, K.; Kato, T.; Ohya, K.;Moriarity, T.; Emery, K.; Chen, CC.; Gao, J.; Li, G.; Yang, Y. A Polymer Tandem Solar Cell with 10.6% Power Conversion Efficiency. *Nature Comm.* **2013**, *4*, 1-10.

12. Springborg, M. The Electronic Properties of Polythiophene. *J. Phys.: Condens. Matter.* **1992**, *4*, 101-120.

13. Somanathan, N.; Radhakrishnan, S. Optical Properties of Functionalized Polythiophenes. *Inter. J. of Mod. Phys. B* **2005**, *19,* 4645-4676.

14. Roncali, J. Conjugated Poly(thiophenes): Synthesis, Functionalization, and Applications. *Chem. Rev.* **1992,** *92*, 711-738.

15. Hou, J.; Yang, C.; Li, Y. Synthesis of Regioregular Side-chain Conjugated Polythiophene and its Application in Photovoltaic Solar Cells. *Syn. Met.* **2005**, *153*, 93-96.

16. Chochos, C.; Economopoulos, S.; Deimede, V.; Gregoriou, V.; Lloyd, M.; Malliaras, G.; Kallitsis, J. Synthesis of a Soluble n-Type Cyano Substituted Polythiophene Derivative: A Potential Electron Acceptor in Polymeric Solar Cells. *J. Phys. Chem.* C **2007**, *111*, 10732-10740.

17. Huang, Y.; Wang, Y.; Sang, G.; Zhou, E.; Huo, L.; Liu, Y.; Li, Y. Polythiophene Derivative with the Simplest Conjugated-Side-Chain of Alkenyl: Synthesis and Applications in Polymer Solar Cells and Field-Effect Transistors. *J. Phys. Chem. B* **2008**, *112*, 13476-13482.

18. Chang, Y.; Hsu, S.; Su, M.; Wei, K. Intramolecular Donor-Acceptor Regioregular Poly(hexylphenanthrenyl-imidazole thiophene) Exhibits Enhanced Hole Mobility for Heterojunction Solar Cell Applications. *Adv. Mater.* **2009**, *21*, 2093–2097.

19. Clarke, T.M.; Ballantyne, A.M.; Nelson, J.; Bradley, D.; Durant, J.R. Free Energy Control of Charge Photogeneration in Polythiophene/Fullerene Solar Cells: The Influence of Thermal Annealing on P3HT/PCBM Blends. *Adv. Funct. Mater.* **2008**, *18*, 4029-4035.

20. Boudouris, B.W.; Molins, F.; Blank, D.A.; Frisbie, C. D.; Hillmyer, M.A. Synthesis, Optical Properties, and Microstructure of a Fullerene-Terminated Poly(3-hexylthiophene). *Macromolecules* **2009**, *42*, 4118-4126.

21. Lee, J.U.; Jung, J.W.; Emrick, T.; Russell, T.P.; Jo, W.H. Synthesis of C_{60}-end Capped P3HT and its Application for High Performance of P3HT/PCBM Bulk Heterojunction Solar Cells. *J. Mater. Chem.* **2010**, *20*, 3287-3294.

22. Loewe, R. S.; Ewbank, P. C.; Liu, J.; Zhai, L.; McCullough, R. D. Regioregular, Head-to-Tail Coupled Poly(3-alkylthiophenes) Made Easy by GRIM Method: Investigation of the Reaction and the Origin of Regioselectivity. *Macromolecules* **2001**, *34*, 4324-4333.

23. Yokoyama, A.; Miyakoshi, R.; Yokozawa, T. Chain-Growth Polymerization for Poly(3-hexylthiophene) with a Defined Molecular Weight and a Low Polydispersity. *Macromolecules* **2004**, *37*, 1169-1171.

24. Chen, X.; Han, X.; Vamvounis, G.; Holdcroft, S. Rod-Coil Graft Copolymers from Poly(3-hexylthioophene) Precursors. *Polymer Preprints (American Chemical Society, Division of Polymer Chemistry)* **2007**, *48*, 102-103.

25. Eckenhoff, W. T.; Biernesser, A. B.; Pintauer, T. Kinetic and Mechanistic Aspects of Atom Transfer Radical Addition (ATRA) Catalyzed by Copper Complexes with Tris(2-pyridylmethyl)amine. *Inorganic Chemistry* **2012**, *51*, 11917-11929.

26. Wang, J.; Matyjaszewski, K. Controlled/"Living" Radical Polymerization. Halogen Atom Transfer Radical Polymerization Promoted by a Cu(I)/Cu(II) Redox Process. *Macromolecules* **1995**, *28*, 7901-7910.

27. Kvarnstrom, C.; Kulovaara, H.; Damlin, P.; Vuorinen, T.; Lemmetyinen, H.; Ivaska, A. Electrosynthesis of a Copolymer Containing C_{60} in the Main Chain. *Syn. Metals* **2005**, *149*, 39-45.

28. Baek, W.; Yang, H.; Yoon, T.; Kang, C. J.; Lee, H. H.; Kim, Y. Effect of P3HT:PCBM Concentration in Solvent on Performances of Organic Solar Cells. *Sol. Energy Mat. & Sol. Cells* **2009**, *93*, 1263-1267.

29. Kingsley, J. W.; Green, A.; Lidzey, D. G. Fabrication and Optimization of P3HT:PCBM Organic Photovoltaic Devices. *Org. Photovoltaics X*. **2009**, *7416*.

30. Origin 8.1; OriginLab Corporation: Northampton, MA, 2009; (accessed Nov 19, 2013).

31. Liu, J.; Arif, M.; Zou, J.; Khondaker, S. I.; Zhai, L. Controlling Poly(3-hexylthiophene) Crystal Dimension: Nanowhiskers and Nanoribbons. *Macromolecules*. **2009**, *42*, 9390-9393.

32. Silverstein, R. M.; Webster, F. X.; Kiemle, D. J. *Spectrometric Identification of Organic Compounds*; John Wiley & Sons, Inc.; New Jersey, 2005.

33. Kuzmany, H.; Winkler, R.; Pichler, T. Infrared Spectroscopy of Fullerenes. *J. Phys.: Condens. Matter*. **1995**, *7*, 6601-6624.

34. Pappenfus, T. M.; Hermanson, D. L.; Kohl, S. G.; Melby, J. H.; Thoma, L. M.; Carpenter, N. E. Regiochemistry of Poly(3-hexylthiophene): Synthesis and Investigation of a Conducting Polymer. *J Chem. Educ.* **2010**, *87*, 522-525.

35. Wunderlich, B. *Thermal Analysis of Polymeric Materials*; Springer; Berlin Heidelberg, 2005.

36. Liu, J.; Shao, S.; Wang, H.; Zhao, K.; Xue, L.; Gao, X.; Xie, Z.; Han, Y. The Mechanisms for Introduction of n-dodecylthiol to Modify the P3HT/PCBM Morphology. *Org. Electr.* **2010**, *11*, 775-783.

37. Vanlaeke, P.; Swinnen, A.; Haeldermans, I.; Vanhoyland, G.; Aernouts, T.; Cheyns, D.; Deibel, C.; D'Haen, J.; Heremans, P.; Poortmans, J.; Manca, J.V. P3HT/PCBM Bulk Heterojunction Solar Cells: Relation Between Morphology and Electro-optical Characteristics. *Sol. En. Mater. & Sol. Cells*. **2006**, *90*, 2150-2158.

38. Lee, J. U.; Jung, J. W.; Emrick, T.; Russell, T.P.; Jo, W. H. Synthesis of C_{60}-end Capped P3HT and Its Application for High Performance of P3HT/PCBM Bulk Heterojunction Solar Cells. *J. of Mater. Chem.* **2010**.

39. Sigma-Aldrich. FAQs. http://sigma-aldrich.custhelp.com/app/answers/detail/a_id/591/p/129,179 (accessed Nov. 25, 2013).

40. Lenes, M; Shelton, S.; Sieval, A.; Kronholm, D.; Hummelen, J.; Blom, P. Electron Trapping in Higher Adduct Fullerene-Based Solar Cells. *Adv. Funct. Mater.* **2009**, 19, 1-6.